



**Technische Universität Wien**  
**Faculty of Technical Chemistry**  
**Research Group for Cell Chip**

**Material Characterization**  
**and**  
**Printer Classification**  
**to establish**  
**3D printed Reagent Storage and Release Solutions**

**Under the supervision of:**  
**Univ. Prof. Dipl.-Ing. Dr. Peter Ertl**  
**Univ.Ass. Martin Frauenlob, PhD**  
**Univ.Ass.in Dipl.-Ing.in Dr.in techn. Silvia Schobesberger**

**Submitted by**  
**Philipp Schlossgangl**  
**Matr. Nr.: 0160475**

---

(Place, Date)

---

(Signature)

---

## Declaration of Authorship

Hereby, I declare that I have composed the presented paper independently on my own and without any other resources than the ones indicated. All thoughts taken directly or indirectly from external sources are properly denoted as such.

---

(Place, Date)

---

(Signature)

---

## Acknowledgements

I would like to thank Univ.Prof. Dipl.-Ing. Dr. Peter Ertl for giving me the opportunity to be part of the CellChipGroup.

I am especially grateful to my supervisor, Univ.Ass.in Dipl.-Ing.in Dr.in techn. Silvia Schobesberger, for providing me with the topic of my master's thesis, establishing a clear timeline and structure for the project, and continuously offering invaluable help and support.

I also want to extend my sincere thanks to Univ. Ass. Martin Frauenlob for his openness and willingness to help whenever questions arose.

Special thanks to Florian Selinger, who was always there to assist with technical issues and machine troubleshooting, and to Max Schimpf, for his invaluable tips on organizing my work and using helpful tools effectively.

I am deeply appreciative of all the members of the CellChipGroup, who were not only supportive on the technical side but also made me feel welcome on a personal level. Being part of such a great team has been very enjoyable.

I would also like to thank my family, particularly my parents, for supporting me — both mentally and financially — throughout my master's journey.

My heartfelt thanks go to my girlfriend, who has always been there for me, offering any kind of support whenever she could, and most importantly, for her patience and understanding.

Finally, I want to thank my friends for their mental support and for always being there when I needed them. Reflecting on challenges together helped me immensely.

I am grateful to everyone who has played a role in my life and supported me on my journey toward becoming a 'Diplomingenieur'.

---

## Abstract

Microfluidic devices equipped with reagent storage and release units are crucial components in the development of point-of-care (PoC) diagnostic devices, which are important in medical diagnostics, chemical analysis, and biological research. Traditionally, the fabrication of these devices has been a time-consuming and expensive process, often involving complex manufacturing techniques. The integration of additive manufacturing, specifically resin-based 3D printing, with microfluidics has the potential to revolutionize the creation of ready-to-use 3D-printed microfluidic devices. This innovative approach simplifies the manufacturing process by eliminating the need for additional steps such as casting, bonding, or drilling, thereby enhancing efficiency and precision. 3D printing offers a rapid and cost-effective alternative, allowing for the creation of highly detailed and customizable microfluidic channels and components. This shift not only accelerates the development cycle but also creates new possibilities for innovation in design and functionality. However, a critical aspect of this technology is the evaluation of print quality to ensure design specifications are met, as well as the optimization of print settings for high printing accuracy.

A cornerstone of this thesis was the development and optimization of protocols for the additive manufacturing of resins that lack predefined parameters using a digital light processing (DLP) printer. Thereby, precise control over printing conditions was aimed to achieve accurate microfluidic device fabrication. The DLP printer's capabilities in terms of resolution were investigated with selected resins by evaluating printed geometries relevant for microfluidic devices. The optimized settings were applied in the development of effective reagent storage and release mechanisms for point-of-care (PoC) diagnostic devices. Effective reagent storage and controlled release are critical components in the functionality of these devices. The interplay between these areas - '3D printing in microfluidics' and 'reagent storage and release' - hold the potential to advance the development and functionality of microfluidic and PoC devices for various applications.

---

## Kurzfassung

Mikrofluidische Apparate, die mit Reagenzienlagerungs- und Freisetzungseinheiten ausgestattet sind, sind entscheidende Komponenten in der Entwicklung von Point-of-Care (PoC)-Diagnosegeräten, die in der medizinischen Diagnostik, chemischen Analyse und biologischen Forschung von großer Bedeutung sind. Traditionell war die Herstellung dieser Geräte ein zeitaufwändiger und teurer Prozess, der oft komplexe Fertigungstechniken erforderte. Die Integration der additiven Fertigung, insbesondere des harzbasierten 3D-Drucks, mit der Mikrofluidik hat das Potenzial, die Herstellung einsatzbereiter, 3D-gedruckter mikrofluidischer Geräte zu revolutionieren. Dieser innovative Ansatz vereinfacht den Herstellungsprozess, indem zusätzliche Schritte wie Gießen, Bonden oder Bohren entfallen, was die Effizienz und Präzision erhöht. Der 3D-Druck bietet eine schnelle und kostengünstige Alternative und ermöglicht die Erstellung hochdetaillierter und anpassbarer mikrofluidischer Kanäle und Komponenten. Dieser Wandel beschleunigt nicht nur den Entwicklungszyklus, sondern schafft auch neue Möglichkeiten für Innovationen in Design und Funktionalität. Ein kritischer Aspekt dieser Technologie ist jedoch die Bewertung der Druckqualität, um sicherzustellen, dass die Konstruktionspezifikationen eingehalten werden, sowie die Optimierung der Druckeinstellungen für eine hohe Druckgenauigkeit. Ein Eckpfeiler dieser Arbeit war die Entwicklung und Optimierung von Protokollen für die additive Fertigung von Harzen, die keine vordefinierten Parameter aufweisen, unter Verwendung eines Digital Light Processing (DLP)-Druckers. Dabei wurde eine präzise Kontrolle der Druckbedingungen angestrebt, um eine genaue Herstellung mikrofluidischer Geräte zu erreichen. Die Fähigkeiten des DLP-Druckers in Bezug auf die Auflösung wurden mit ausgewählten Harzen untersucht, indem gedruckte Geometrien bewertet wurden, die für mikrofluidische Chips relevant sind. Die optimierten Einstellungen wurden bei der Entwicklung effektiver Reagenzienlagerungs- und Freisetzungsmechanismen für Point-of-Care (PoC)-Diagnosevorrichtungen angewendet. Eine effektive Reagenzienlagerung und kontrollierte Freisetzung sind entscheidende Komponenten für die Funktionalität dieser Apparate. Das Zusammenspiel dieser Bereiche – "3D-Druck in der Mikrofluidik" und "Reagenzienlagerung und -freisetzung" – birgt das Potenzial, die Entwicklung und Funktionalität mikrofluidischer und PoC-Geräte für verschiedene Anwendungen voranzutreiben.

---

# Contents

<b>1</b>	<b>Introduction</b>	<b>1</b>
1.1	3D-printing for fabrication . . . . .	1
1.1.1	Additive manufacturing compared to conventional manufacturing . . . . .	2
1.1.2	3D-printing methods . . . . .	3
1.1.2.1	Overview . . . . .	3
1.1.2.2	Fused Deposition Modeling . . . . .	7
1.1.2.3	Digital Light Processing . . . . .	8
1.1.3	3D printing for microfluidic Rapid Prototyping . . . . .	11
1.1.4	3D-Printing: State of the Art in Microfluidics . . . . .	12
1.2	3D-printing for Point-of-Care devices . . . . .	14
1.2.1	Point-of-Care Testing . . . . .	14
1.2.2	Reagent-Storage and -Release in PoC . . . . .	14
1.2.3	State of the Art '3D-printing in PoC' . . . . .	17
<b>2</b>	<b>Aim of this thesis</b>	<b>18</b>
<b>3</b>	<b>Materials and Methods</b>	<b>19</b>
3.1	3D printers . . . . .	19
3.2	3D printing resins . . . . .	20
3.3	Characterization of NanoClear Resin . . . . .	20
3.3.1	Experimental Determination of Curing Table Data . . . . .	21
3.3.2	Creation of .ini-file . . . . .	25
3.3.3	Storage of the .ini-file . . . . .	26
3.3.4	Experimental Determination of Offset-value . . . . .	26
3.3.5	Post-Processing of 3D-prints . . . . .	26
3.3.6	Experimental Determination of XY-plane correction factor . . . . .	27
3.3.7	Creation of XY-curing table . . . . .	28
3.3.8	Testing of determined print settings . . . . .	29
3.4	Classification of ASIGA 3D-Printer . . . . .	30
3.4.1	Geometry Assessment . . . . .	30
3.4.2	Height Assessment . . . . .	30
3.4.3	Partial Walls Assessment . . . . .	31
3.4.4	Build Tray for Microfluidics . . . . .	32
3.4.5	Pillars Assessment . . . . .	32
3.4.6	Channels Assessment . . . . .	33
3.4.7	PDMS casting with NanoClear . . . . .	34
3.5	Reagent Storage and Release . . . . .	35

---

3.5.1	3D printed holder . . . . .	35
3.5.2	3D printed microfluidic devices . . . . .	35
3.5.3	AuNP - conjugate pad . . . . .	36
3.5.4	Empty blister packs . . . . .	37
3.5.5	Blister preparation and device assembly . . . . .	37
3.6	Software and Equipment . . . . .	39
3.6.1	Software . . . . .	39
3.6.2	Microscopes . . . . .	39
3.6.3	AI tools . . . . .	39
3.7	Helper Objects and other 3D printed objects . . . . .	40
<b>4</b>	<b>Results and Discussion</b>	<b>42</b>
4.1	Characterization of NanoClear Resin . . . . .	42
4.1.1	Z-calibration curve . . . . .	42
4.1.2	Offset value . . . . .	42
4.1.3	XY curing parameters . . . . .	44
4.1.4	Testing of determined print settings . . . . .	44
4.2	Classification of ASIGA 3D-Printer . . . . .	46
4.2.1	Geometry Assessment . . . . .	46
4.2.2	Height Assessment . . . . .	49
4.2.3	Partial Walls Assessment . . . . .	50
4.2.4	Pillars Assessment . . . . .	53
4.2.5	Channels Assessment . . . . .	56
4.2.6	PDMS casting with NanoClear . . . . .	63
4.3	Reagent-Storage and -Release . . . . .	65
4.3.1	AuNP-pad: on-chip storage and release . . . . .	65
4.3.2	Blister-Mechanism . . . . .	69
4.3.3	Combination: AuNP and Blister . . . . .	70
<b>5</b>	<b>Conclusion</b>	<b>72</b>
5.1	Principal Findings . . . . .	72
5.2	Outlook for future research . . . . .	73
5.3	Final thoughts . . . . .	73
	<b>References</b>	<b>74</b>
	<b>Appendix</b>	<b>82</b>

# List of Figures

1	Additive Manufacturing, Layer-by-Layer formation. [4] . . . . .	1
2	SLA printing mechanism schematic. [17] . . . . .	3
3	Selective Laser Sintering illustration. [19] . . . . .	4
4	Material Jetting illustration. [20] . . . . .	5
5	EBM printing illustration. [22] . . . . .	5
6	Xolography printing illustration. Reprinted with permission from C. Dakres-Burkey and R. F. Shepherd [26], Nature. . . . .	6
7	FDM printing mechanism schematic. [29] . . . . .	7
8	DLP printing mechanism schematic. Reprinted with permission from Ge et al. [36], Elsevier. . . . .	9
9	Left: Prusa MK3S [71], Right: Asiga Max X43 UV [72] . . . . .	19
10	Necessary equipment for material file generation. . . . .	22
11	Left: centered container. Right: resin sample. . . . .	22
12	Container filled with resin and sealed with Play-Doh . . . . .	23
13	Left: filling of container. Right: placing container inside the printer. . . . .	23
14	Left: UV spot visualized with paper. Right: washing off excess resin from cured spot. . . . .	23
15	Left: dial gauge setup. Right: cured spot. . . . .	24
16	Left: measuring spot. Right: measuring reference value. . . . .	24
17	3D printed device for inspecting layer adhesion. . . . .	26
18	”Stairs” layout on build platform. . . . .	27
19	Left: FunToDo calibration object. Right: CCG fluid router CAD file. . . . .	29
20	Geometry CAD-file with sunken features. . . . .	30
21	Distribution of cuboids across build platform. . . . .	31
22	Partial Walls CAD file. . . . .	32
23	Pillars CAD file. Layout for different layer heights. Top row: negative. Bottom row: positive. . . . .	33
24	Layout for rectangular channel inspection. . . . .	33
25	Round channels. Smallest channel: 20 $\mu$ m. Increment: 20 $\mu$ m. Biggest channel: 480 $\mu$ m. . . . .	33
26	Round channels. Printing alignment, flat and upright. . . . .	34
27	Left: PDMS mold lofted. Right: PDMS mold sunken. . . . .	34
28	Left: 3D printed holder. Right: 0.5mL Eppendorf tube. [77] . . . . .	35
29	Left: Device for AuNP-pad. Right: Device for blister mechanism. . . . .	35
30	Combined device for AuNP and blister storage, CAD render. Left: variant I). Right: variant II). . . . .	36
31	AuNP conjugate pads. From left to right: OD6, OD3, OD1.5. . . . .	36

---

32	Empty blister packs. Left: GeloMyrtol. [78] Right: Vitamin D3. [79] . . .	37
33	Preparation for combined device (AuNP + blister). . . . .	38
34	Roland GS24 cutter plotter. [80] . . . . .	38
35	Centering device for "material-test". . . . .	40
36	Anti-spillage lid for build tray containing NanoClear resin. . . . .	41
37	Left: Capillaries "negative". Right: capillaries "positive". . . . .	41
38	Z-Calibration curve for $7.05 \text{ mW/cm}^2$ . . . . .	42
39	Left: Undercuring of the resin, indicated by the cavities (pointed at with red arrows). Right: Overcuring of the resin, indicated by bulky segments between the layers, marked with red ellipses. . . . .	43
40	Side-view of layers with the chosen print parameters. . . . .	43
41	FunToDo Calibration Object. Printed with a layer height of $50\mu\text{m}$ . . . . .	45
42	CCG shaped fluid router. Left: Filled channels. Right: Filling of the channels with pipette tips. . . . .	45
43	Lofted features, $25\mu\text{m}$ layer height. Material: PlasClear. The left scalebar accounts for image columns 1, 2 and 3. The right scalebar accounts for image columns 4 and 5. . . . .	46
44	Sunken features, $25\mu\text{m}$ layer height. Material: NanoClear. . . . .	46
45	Actual over nominal sidelength of squared, lofted features. Printed with PlasClear, observed via brightfield microscopy (measurements form individual features, $n=3$ ), dotted line represents the nominal sidelength. . . . .	47
46	Actual over nominal sidelength of squared, lofted features. Printed with NanoClear, observed via brightfield microscopy (measurements form individual features, $n=3$ ), dotted line represents the nominal sidelength. . . . .	47
47	Actual over nominal sidelength of squared, sunken features. Printed with PlasClear, observed via brightfield microscopy (measurements form individual features, $n=3$ ), dotted line represents the nominal sidelength. . . . .	48
48	Actual over nominal sidelength of squared, sunken features. Printed with NanoClear, observed via brightfield microscopy (measurements form individual features, $n=3$ ), dotted line represents the nominal sidelength. . . . .	48
49	Build plate skewness effect. Left: before calibration. Right: after calibration.	49
50	Actual over nominal thickness of lofted walls. Printed with PlasClear, observed via brightfield microscopy (measurements form individual walls, $n=4$ ), dotted line represents the nominal sidelength. . . . .	51
51	Actual over nominal thickness of lofted walls. Printed with NanoClear, observed via brightfield microscopy (measurements form individual walls, $n=4$ ), dotted line represents the nominal sidelength. . . . .	51

52	Actual over nominal thickness of sunken "walls". Printed with PlasClear, observed via brightfield microscopy (measurements form individual walls, n=4), dotted line represents the nominal sidelength. . . . .	52
53	Actual over nominal thickness of sunken "walls". Printed with NanoClear, observed via brightfield microscopy (measurements form individual walls, n=4), dotted line represents the nominal sidelength. . . . .	52
54	Pillars, printed with NanoClear. Top: lofted. Bottom: sunken. Size: from left to right: 215 $\mu\text{m}$ , 172 $\mu\text{m}$ , 129 $\mu\text{m}$ , 86 $\mu\text{m}$ and 43 $\mu\text{m}$ . . . . .	53
55	PlasClear, actual vs. nominal pillar diameter, lofted. Observed via brightfield microscopy (measurements form individual pillars, n=5), dotted line: nominal diameter. . . . .	53
56	NanoClear, actual vs. nominal pillar diameter, lofted, Universal tray. Observed via brightfield microscopy (measurements form individual pillars, n=5), dotted line: nominal diameter. . . . .	54
57	NanoClear, actual vs. nominal pillar diameter, lofted. LowForce tray. Observed via brightfield microscopy (measurements form individual pillars, n=5), dotted line: nominal diameter. . . . .	54
58	NanoClear, actual vs. nominal pillar diameter, sunken, Universal tray. Observed via brightfield microscopy (measurements form individual pillars, n=5), dotted line: nominal diameter. . . . .	55
59	NanoClear, actual vs. nominal pillar diameter, sunken, LowForce tray. Observed via brightfield microscopy (measurements form individual pillars, n=5), dotted line: nominal diameter. . . . .	55
60	Schematic of trapped resin in a microfluidic channel. . . . .	56
61	Emerging structure at channel "lid". Image acquired with optical microscope Olympus IX83. . . . .	57
62	Scanning Electron Microscope image of a rectangular channel. . . . .	57
63	Curing dynamics: Difference between the border and the inside of channels. A-A indicates a sectional view of the inside of a channel. The emerging structure is visualized in blue. On the inside of the channel, the pillary structure reaches the bottom of the channel, subsequently blocking it, whereas on the sides, the channel remains free. . . . .	58
64	Topview. a) 100 $\mu\text{m}$ layer height, nominal value of narrowest non-clogged channel: 300 $\mu\text{m}$ . b) 50 $\mu\text{m}$ layer height, nominal value of narrowest non-clogged channel: 350 $\mu\text{m}$ . c) 25 $\mu\text{m}$ layer height, nominal value of narrowest non-clogged channel: 250 $\mu\text{m}$ , d) layer height 25 $\mu\text{m}$ , adaptation with reduced fill-exposure, nominal value of narrowest non-clogged channel: 150 $\mu\text{m}$ , e) layer height 25 $\mu\text{m}$ , adaptation with build manipulation, nominal value of narrowest non-clogged channel: 125 $\mu\text{m}$ . . . . .	58

---

65	Evaluated channel heights. Material: NanoClear. Rectangular channels. Print layout: horizontal. 100µm layer height. . . . .	59
66	Evaluated channel heights. Material: NanoClear. Rectangular channels. Print layout: horizontal. 50µm layer height. . . . .	59
67	Evaluated channel heights. Material: NanoClear. Rectangular channels. Print layout: horizontal. 25µm layer height. . . . .	60
68	Circular channels, printed horizontally ("flat"). . . . .	61
69	Circular channels, printed vertically ("upright"). . . . .	62
70	Effect of different printing orientations. Left: Channels printed flat. Right: Channels printed upright. Channel diameter (both): 480µm. . . . .	63
71	PDMS mold (left) and PDMS chip (middle) inspected under a microscope. Right: magnified (mag.) PDMS features (wall/channel). . . . .	64
72	Timeline of design iterations for Gold-Nanoparticle release. . . . .	65
73	Multiplexing device for AuNP release evaluation. The outer dimensions are 26.9 mm x 21.9 mm. . . . .	66
74	AuNP-pads soaked in Eppendorf-tube for 1 and 5 minutes. . . . .	67
75	AuNP-pads: soaked for 1 minute versus flushed within microfluidic chip. . . . .	67
76	Initial design with loaded AuNP-pad and hydrostatic reservoir, leading to AuNPs being trapped inside the channel. . . . .	68
77	Successful experiment with loaded AuNP-pad and hydrostatic reservoir. . . . .	68
78	Timeline of design iterations for blister mechanism. . . . .	69
79	3D-printed spikes, inspected under a microscope. . . . .	69
80	Blister, filled with food-colored water. . . . .	70
81	Tin foil, close-up image of punctures from 3D printed spikes. Left: 4 spikes. Right: Array of spikes for higher flow rate. . . . .	70
82	Combination of AuNP and blister device. Left: Variant I). Right: Variant II). . . . .	71
83	Experiment with combined device (AuNP + blister). . . . .	71
84	Excel sheet for determination of XY-curing parameters . . . . .	84
85	Z-Calibration curve for $3mW/cm^2$ . . . . .	84

---

## List of Tables

1	AM methods overview in chronological order, adapted from [11]. . . . .	3
2	ELEGOO printer comparison used by Shafique et al. [52] . . . . .	13
3	Specifications of utilized 3D printers. . . . .	19
4	Specifications of utilized 3D printing resins. [73], [74] . . . . .	20
5	Exemplary results of material test at a light intensity of $7.05 \text{ mW/cm}^2$ , M (M1, M2, M3) signifies measurement. . . . .	25
6	Geometry assessment parameters. . . . .	30
7	Partial Walls feature size. . . . .	32
8	Pillars assessment parameters. . . . .	32
9	XY-stairs evaluation. Before and after application of XY correction factor. . . . .	44
10	Z-axis calibration effect on cuboid thickness. . . . .	49
11	PlasClear, evaluated feature height. . . . .	50
12	Accuracy in z-direction for NanoClear. . . . .	50
13	Deviation from nominal channel height for different channels . . . . .	60
14	PDMS-Channel and -Wall actual measured dimensions. Nominal wal- l/channel width: $150\mu\text{m}$ . . . . .	64
15	PlasClear "Geometry". Complete data table. . . . .	85
16	NanoClear "Geometry". Complete data table. . . . .	86

---

## List of abbreviations

<b>ABS:</b>	Acrylonitrile Butadiene Styrene
<b>AM:</b>	Additive Manufacturing
<b>AuNP:</b>	Gold Nanoparticles
<b>CAD:</b>	Computer Aided Design
<b>CCG:</b>	Cell Chip Group
<b>CNC:</b>	Computer Numerical Control
<b>DLP:</b>	Digital Light Processing
<b>DMD:</b>	Digital Mirror Device
<b>DMLS:</b>	Direct Metal Laser Sintering
<b>EBM:</b>	Electron Beam Melting
<b>FDM:</b>	Fused Deposition Modeling
<b>FEP:</b>	Fluorinated Ethylene Propylene
<b>LCD:</b>	Liquid Crystal Display
<b>LED:</b>	Light Emitting Diode
<b>LH:</b>	Layer Height
<b>OD:</b>	Optical Density
<b>PBS:</b>	Phosphate-Buffered Saline
<b>PDMS:</b>	Polydimethylsiloxane
<b>PETG:</b>	Polyethylene Terephthalate Glycol
<b>PLA:</b>	Polylactic Acid
<b>PoC(T):</b>	Point-of-Care, Point-of-Care-Testing
<b>SLA:</b>	Stereolithography
<b>SLM:</b>	Selective Laser Melting
<b>SLS:</b>	Selective Laser Sintering
<b>STL:</b>	Standard Tessellation Language
<b>TPU:</b>	Thermoplastic Polyurethane
<b>UV:</b>	Ultraviolet

# 1 Introduction

*Imagine a future where microfluidics and additive manufacturing unite to create a world of ready-to-use 3D-printed devices. By creating the device virtually and then directly printing it, the need for additional manufacturing steps is mediated. A simpler and more efficient microfluidic world would emerge.*

*Coupled with finding a solution for a reagent-storage and -release mechanism, those objectives will form the cornerstone of this thesis.*

## 1.1 3D-printing for fabrication

3D printing, also known as additive manufacturing, is a technology that allows for the creation of three-dimensional objects from a digital file. This process involves layering materials, such as plastics, composites, or biomaterials, to construct objects layer-by-layer. Each layer is a thinly sliced, horizontal cross section of the eventual object, which is created by curing and bonding materials like a liquid photopolymer with ultraviolet light, melting polymer filaments or fusing powder grains. [1], [2], [3]

There are several methods of 3D printing, but the core principle remains the same: building objects from the bottom up, layer-by-layer. This fabrication technique offers a high degree of design flexibility and can produce objects that range in shape, size, rigidity, and color. [1]

### Workflow:

The desired object is created with a computer aided design (CAD) software. Then the object is transformed into a suitable file-format (.stl, .obj, .ply, .amf, .3mf) and uploaded into the so-called "slicer" software. Within the slicer, the object is sliced into layers (see Figure 1). The sliced object is then transformed into a file-format which is read- and executable by the 3D-printer (e.g. g-code, cws, .print), and uploaded to the printer. The printer will then create the sliced object, layer-by-layer.

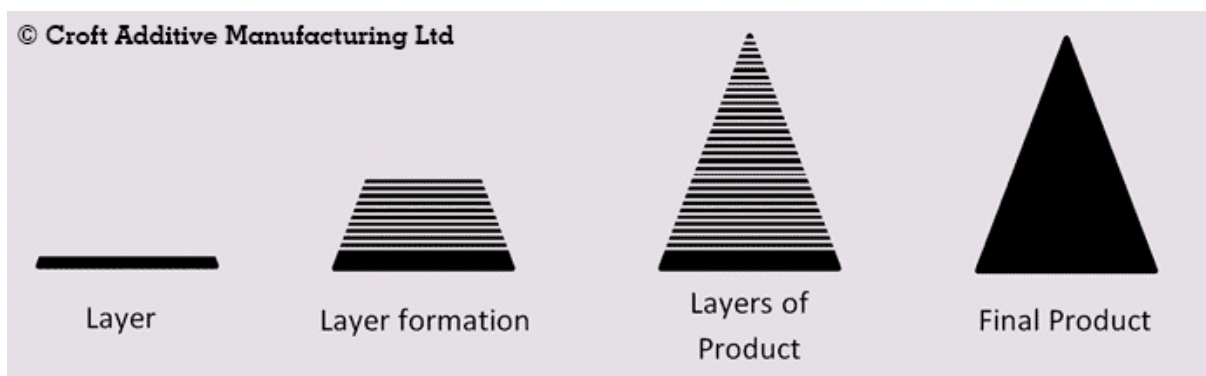


Figure 1: Additive Manufacturing, Layer-by-Layer formation. [4]

### 1.1.1 Additive manufacturing compared to conventional manufacturing

Conventional methods such as casting, forging, machining, stamping, and coating have been in use for many decades and are still widely used today. However, additive manufacturing has several benefits (+) over these traditional manufacturing techniques, but also comes with limitations (-). (+) **Cost:** Manufacturing costs are independent of the quantity of the produced part. For conventional manufacturing, the produced part becomes cheaper with mass production and is often necessary to make it economically sustainable in the first place. For 3D-printing, any quantity can be produced without the need for tooling etc., so even one single object can be produced without driving up the costs. [5], [6], [7]

(+) **Speed:** For small and medium-sized objects, 3D-printing is faster because it eliminates the need for tools, casts and molds like in conventional manufacturing. [5], [6]

(+) **Quality:** Complex designs with high quality can be produced at no additional costs. Intricate details, that would be impossible or at least very costly with conventional methods, can be produced. [5]

(+) **Impact:** Since little waste is generated, and only the material that is needed is produced, 3D-printing is considered to have less environmental impact. [5]

(+) **Innovation:** Without the constraints from conventional manufacturing, designs can be varied in complexity and adapted rapidly, which opens up the field of rapid prototyping. [5]

( - ) **Size constraints:** The AM machine usually needs to be bigger than the part it can produce. For conventional manufacturing, machines can also be smaller than the produced part. Examples would be continuous feeding systems or CNC milling, where the tool can be significantly smaller than the produced part. [5]

( - ) **Post-processing requirements:** There are various post-processing steps to improve surface finish, dimensional accuracy, and mechanical properties of AM parts. While some methods need post-processing (sintering, UV curing, cleaing), not all AM methods need post-processing (e.g. FDM). [8], [9]

( - ) **Material limitations:** Almost every material is processable with conventional manufacturing, whereas AM has a limited selection of materials available, and widely used plastics (such as polystyrol) can not be used. [6]

( - ) **Equipment cost:** High-end AM machines can be very expensive, but 3D printers have a relatively wide price-range, from a few hundred dollars to several thousand. [10]

( - ) **Mechanical properties of produced parts:** Parts produced by additive manufacturing may have different mechanical properties compared to those made by traditional methods. For instance, they might have anisotropic properties, where strength and durability vary depending on the direction of the layers. The weak link is often the interface between layers. [8], [9]

## 1.1.2 3D-printing methods

### 1.1.2.1 Overview

Over the years, several different 3D printing techniques have emerged. In Table 1, commonly used printing methods are listed in chronological order of their introduction to the market and their inventor. [11] The history of 3D printing dates back to the 1980s, when technologies such as SLA or DLP, among others, emerged. [12]

Table 1: AM methods overview in chronological order, adapted from [11].

Year	Technology	Inventor
1980s	Stereolithography	Chuck W. Hull
1980s	Selective Laser Sintering	Carl Deckard & Joe Beaman
1980s	Fused Deposition Modeling	S. Scott Crump
1980s	Digital Light Processing	Larry Hornbeck
1990s	Electron Beam Melting	Arcam
1990s	Binder Jetting	MIT
1990s	Material Jetting	Stratasys et al.
1990s	Selective Laser Melting	EOS
2020s	Xolography	Martin Regehly, Stefan Hecht [13]

- **Stereolithography (SLA):**

Stereolithography was the first ever concept of 3D-printing, established by Chuck W. Hull. He applied his patent [14], on the 8th of August, 1984. [15] SLA is a technology that uses an ultraviolet (UV) laser to selectively cure liquid photopolymer resin. The laser triggers photopolymerization and subsequent solidification of the material locally. The desired object is formed in a layer-by-layer fashion, and the laser must sweep across the whole layer before moving on to the next one. [16]

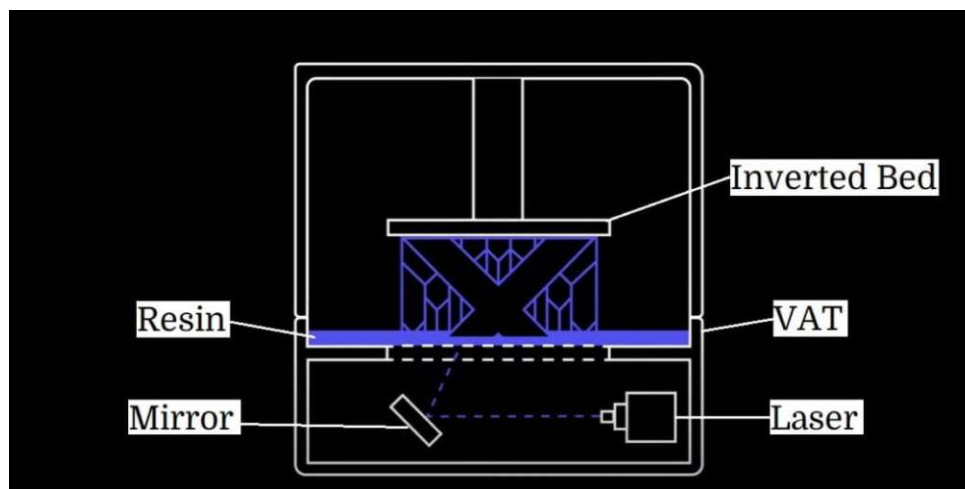


Figure 2: SLA printing mechanism schematic. [17]

- **Selective Laser Sintering (SLS):**

SLS uses a laser to sinter powdered material layer-by-layer. After a CO<sub>2</sub>-laser fuses polymer powder particles together, the print stage moves down in z-direction. After each layer, a new layer of powder gets distributed evenly at the top by roller. The part grows from bottom to top inside the build chamber. Thereby, highly dense objects with a high resolution can be manufactured. In addition, no support structures are needed and unused powder can be reused. Post-processing for SLS includes, among others: tumbling, dyeing, spray paint and (metal)-coatings. [18]

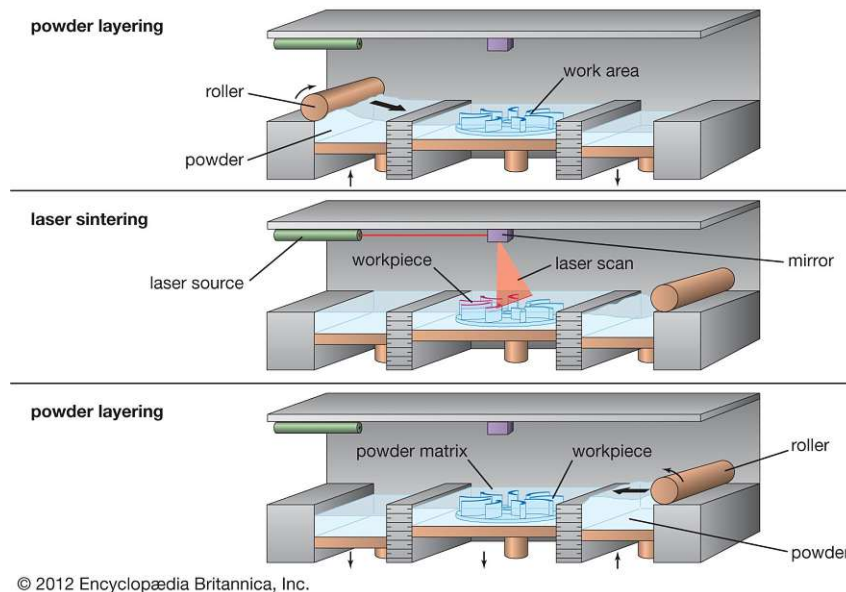


Figure 3: Selective Laser Sintering illustration. [19]

- **Binder Jetting:**

Binder Jetting is an AM process where powdered material is selectively bound together using a liquid binder. It is similar to the process of SLS, but instead of a laser, an inkjet printing head (as it can be found in office printers) deposits a liquid binder onto the powder. Compared to FDM, SLA or DLP, no support structures are needed, since the powder bed acts as support for free-hanging structures and features. Post-processing steps are necessary, such as sintering or infiltration. [12]

- **Material Jetting:**

Material Jetting uses multiple printheads (see Figure 4) to deposit droplets of material (usually photopolymers) onto a printing plate. The resin is then cured by UV light. It allows for combining different materials or colors. [12]



- **Selective Laser Melting (SLM):**

SLM, also called Direct Metal Laser Sintering (DMLS), uses a laser to selectively melt metal powder layer-by-layer. The powder is fully melted, creating dense and strong parts. Metals like titanium, steel or aluminum can be processed. It is used in automotice and aerospace. [23]

A special form of selective laser melting, called Direct Energy Deposition, was created and patented by the company "Relativity Space". A laser is used to melt metals, and the material is being fed from a spool in filament form. [24]

- **Xolography (Volume 3D-printing):**

Xolography is based on holography, a technology invented in 1946 by Dennis Gabor. Xolography uses dual-color photoinitiators, molecules that respond to two different wavelengths of light. The process involves intersecting two light beams within a vat of resin. One beam creates a "light sheet", while the other projects an image onto this sheet. Unlike traditional layer-by-layer 3D printing methods, xolography can create objects in a volumetric fashion, meaning that the entire object can be printed all in one. [25]

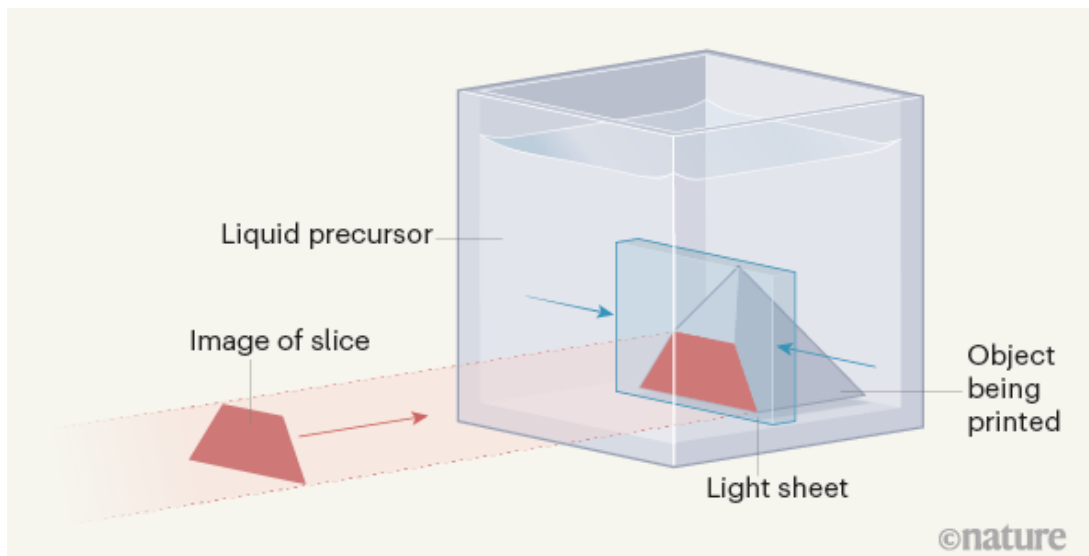


Figure 6: Xolography printing illustration. Reprinted with permission from C. Dakres-Burkey and R. F. Shepherd [26], Nature.

### 1.1.2.2 Fused Deposition Modeling

FDM, also called Fused Filament Fabrication (FFF) produces objects using a heated extrusion nozzle that deposits semi-molten thermoplastic filaments onto a build platform. The material is heated  $\sim 0.5^\circ\text{C}$  above melting point and solidifies instantly post-extrusion. Layer by layer, the objects grows from the bottom to the top. After extrusion, the filament quickly solidifies again, creating a rigid structure. After each layer, the printhead moves an increment in z-direction (or the printbed moves, depending on the type of printer), called the **layer height**. The path of the nozzle is determined by the so called g-code (computer numerical control programming language). Typical materials for FDM printing, naming only a few, are PLA, ABS, PETG, TPU, ASA and Nylon. [27]

In industrial applications, it is mainly used for rapid prototyping, due to its low production cost, ease to create complex parts and the speed of creating a prototype. [28]

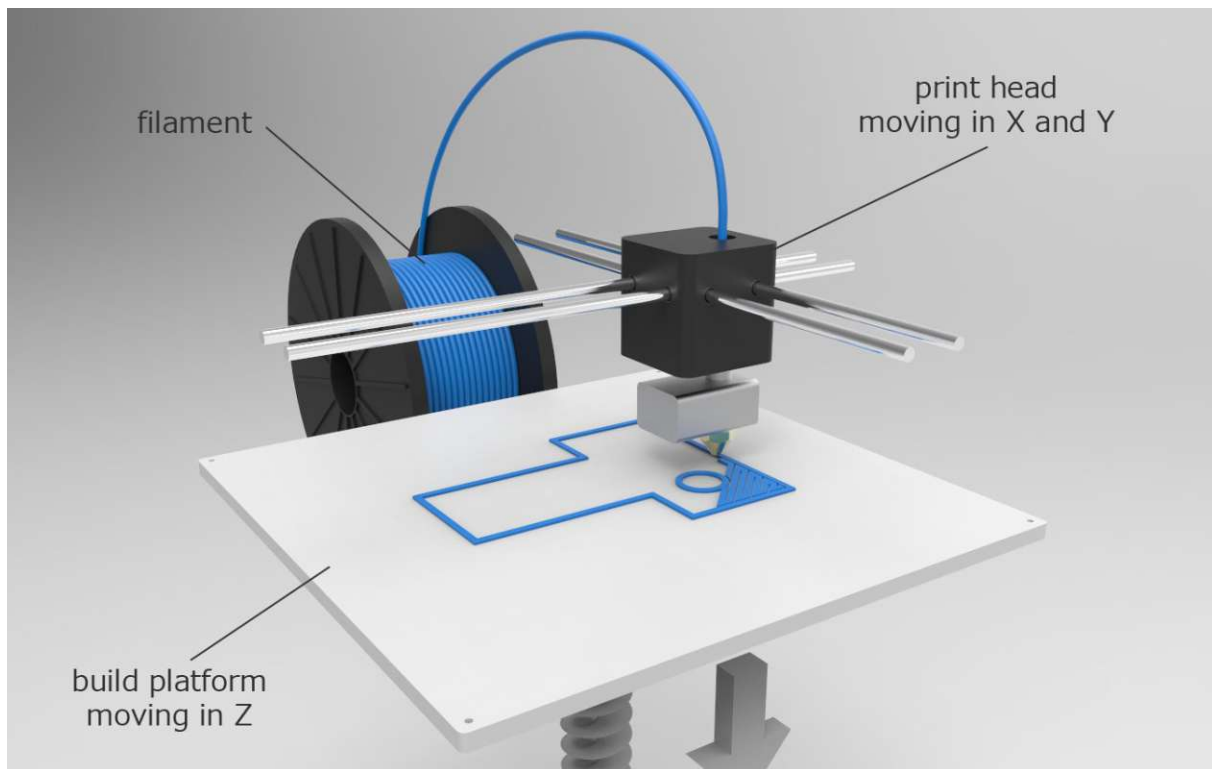


Figure 7: FDM printing mechanism schematic. [29]

### 1.1.2.3 Digital Light Processing

**Vat photopolymerization:** SLA and DLP both are vat photopolymerization techniques, widely used in various industries due to their high resolution and smooth surface finish. Common industries include automotive, aerospace [30], healthcare and consumer products. For example, in the medical sector, dental models, anatomical models, surgical aids, and custom-fit prosthetics are produced. In the jewelry industry, molds for casting metal are created by 3D-printing. [31]

**LCD Printers:** LCD 3D printing, also called mSLA (masked SLA) printing, is very similar to DLP-printing (see section 1.1.2.3), but instead the light-source is an array of UV-LEDs and the masking is done via the LCD (liquid-crystal display) screen. As in DLP-printing, complete layers are flashed at the resin tank. The relatively low-cost LCD printers are popular among hobbyists, because they come at the same price-range as FDM printers but with a higher accuracy. [32], [33]

**Technology:** Vat photopolymerization makes use of photopolymerization of photo-sensitive photopolymers. A chain-reaction, triggered by the energy of short wavelength UV light (usually around 400nm), solidifies resin inside a vat. In the simplest form, photopolymers (e.g. acrylates or urethanes) are mixed with a photoinitiator. Upon receiving energy from the UV light source, the photoinitiator forms free radicals, initiating the polymeric chain reaction, creating a solid network of the polymers present. [16] The light source is usually sitting below the vat, below a glass plate, and the bottom of the vat typically consists of a transparent membrane. The build platform, to which the object will stick, dips into the liquid resin and moves closely to the bottom of the vat, usually at a distance of 5-100 $\mu$ m. This distance is referred to as **layer height**. The layers are created before initiating the print by "slicing" the object (see Figure 1) with 3D printing software. After that, the sliced object can be uploaded to the printer, and the print can be started. For SLA, a laser travels along the path of the layer that is being produced at the moment, redirected by a mirror. For DLP, the whole layer is flashed upon the vat at once. After the solidification of the layer by the UV source, the build platform moves up (in z-direction) to detach from the membrane of the vat, and then moving down again to prepare for the solidification of the next layer. Thereby, the objects is being "pulled out" of the vat layer-by-layer. [16] Also worth mentioning is this context is the file type used for 3D printing. Chuck Hull, the inventor of 3D printing, also invented the STL file type, which is still commonly used in 3D-printing, although new file-types have emerged in recent years (.obj, .ply, .amf, .3mf). STL (short for Standard Tessellation Language) files encode the geometry of a CAD-file. Tessellation refers to splitting a surface or object into geometric shapes (e.g. triangles) so that no overlaps are occurring. It is important to note that STL-files do not store information about colour or texture. [34]

**Digital Light Processing:** DLP 3D printing is often considered a derivative or "sibling" technology to SLA, sharing many similarities but with some distinct differences. While SLA uses a UV laser to cure liquid resin layer-by-layer, DLP uses a digital light projector to flash an entire image of a layer at once, speeding up the printing process. DLP itself was developed by Texas Instruments in 1987, and is used in cinematographic projectors, automotive industry (screens) and lithography. [35]

Liquid resin solidifies via photopolymerization upon receiving energy from a UV light-source. For DLP printing, usually a digital projector screen is used to flash a single image of each layer across the bottom of the vat. This image is made up of square pixels. The pixel size of the printer's projector determine the printer's XY resolution: smaller pixels indicate a higher resolution and vice versa. The area of the layer is then illuminated, and solidifies between the build platform and the vat membrane. This solid layer then sticks to both, to the build platform and the transparent membrane of the vat. When the build platform then moves upwards, the layer/object detaches from the vat membrane, while still sticking to the build platform. After the detachment, the build platform then dips into the vat again and moves closely to the vat membrane, to form the next layer. This process is repeated, layer-by-layer, until the whole object is formed. [28]

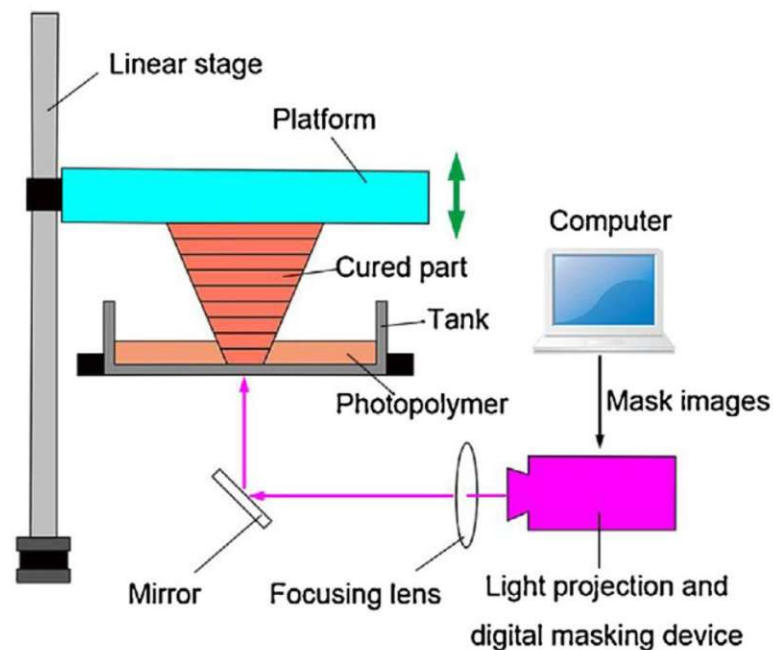


Figure 8: DLP printing mechanism schematic. Reprinted with permission from Ge et al. [36], Elsevier.

### Crucial components of a DLP 3D Printer:

- **Projector:** The projector illuminates a sequence of images, representing each layer of the 3D model, into the gap between the bottom of the resin vat and the build platform. The projector can use various light sources, typically LEDs or UV lamps, to cure the photopolymer resin. The resolution of the 3D print is directly influenced by the projector's pixel resolution. Higher pixel density leads to finer details and smoother surfaces in the printed object. High-end DLP printers reach XY resolutions of less than 50 microns. [37]
- **Vat:** The vat is a container that holds the photopolymer resin. It has a transparent bottom, usually made of glass or acrylic, which allows the projected light to pass through and cure the resin. [38]
- **Build Plate:** The build plate is the surface on which the printed object is formed. It moves vertically, lowering into the vat to start the print and gradually rising as each layer is cured. [39] A precisely leveled and adjustable build plate is crucial for accurate layer formation and adhesion. [40]
- **Light Source:** The light source, typically a UV LED or lamp, is positioned within the projector and provides the necessary energy to initiate the photopolymerization process. [41] The specific wavelength of the light source must match the photoinitiator in the resin for effective curing. [42]
- **Mirror System:** DLP printers use a mirror system to direct the projected light onto both the build platform and the resin inside the vat, enhancing precision and uniformity. The build platform is positioned close to the bottom of the vat, leaving a small gap filled with resin. [43] A Digital Mirror Device (DMD) is a chip with many microscopic mirrors, that can be rotated electronically. It is used to focus the UV-light onto the build plate. [31]

### Resin constituents and characteristics:

A resin consists of polymer molecules combined with various additives. Monomers or oligomers are the fundamental building blocks, acrylates and urethanes are amongst the most commonly used. [37] To start the photopolymerization chain-reaction, a photoinitiator is added. Other compounds found in resins can be photoabsorbers or photoblockers, which inhibit the polymerization process at sites where no UV light is present. Additives such as particles (e.g. ceramic) or plasticisers can be added to enhance or modify the material. [44]

DLP printing offers different material types. **Polycarbonate-like** materials provide excellent strength and thermal resistance while maintaining a translucent or clear appearance. **Acrylonitrile butadiene styrene-like** resins are known for their excellent toughness and stiffness, and they feature minimal shrinkage. **Polypropylene-like** resin produces a durable, impact-resistant material. It can be used for snap joints and living hinges. **Photo elastomers** provide high elongation at break and excellent impact resistance. **Filled** resins include ceramic or glass particles suspended in the liquid. They exhibit good creep resistance and high heat deflection temperatures. [31]

### 1.1.3 3D printing for microfluidic Rapid Prototyping

Another benefit of 3D printing is the ability to rapidly prototype 3D constructs, especially valuable in the development of microfluidic chips.

”Rapid prototyping is a provocateur of innovation; it provides reductions in cost and time. When producing one iteration or a limited run of a product, it is very costly to use traditional manufacturing, thus AM is a far cheaper and also faster approach.” [5]

In the past few years, the advances in additive manufacturing led to the usage of 3D-printers in the field of microfluidics. Especially resin-based 3D-printing, where very delicate structures can be printed, became of interest. The possibility of printing a fully functional device mitigates the need of additional manufacturing steps, such as casting, bonding or drilling. Coupled with the possibilities of various 3D-printed structures, such as closed channels, valves, ports, pillars, walls, etc., additive manufacturing is a promising way to push the boundaries of microfluidics. Especially in prototyping and concept development, this technology can be utilized in various ways. [45]

#### Importance of Classification and Characterization

The actual printed dimensions deviate from the nominal ones within a certain range, therefore it is necessary to evaluate the geometric discrepancy between design and print. This is referred to as ”classification”. To take countermeasures or to be able to compensate the deviations, it is necessary to profoundly know about the limitations of the printer. Equally important is to know about its strengths to select the most suitable printer for the design to be printed. [46]

Another important aspect of 3D-printing is the resin. There are various resins on the market, with attributes like (non)-transparent, ultra-durable, flexible and biocompatible, among others. [47] Especially in microfluidics, low-viscosity resins are beneficial, because excess resin, remaining within the tiny channels after printing, needs to be removed. High-viscose, honey-like resins are often problematic in this field, since the desired structures might get printed, but the channels simply cannot be freed of the excess resin. [48] Such low-viscose materials are often produced by third-party manufacturers, and therefore need to be characterized in order to know how the material behaves upon printing.

### 1.1.4 3D-Printing: State of the Art in Microfluidics

Su et al. reviewed recent advancements in 3D printing strategies for microfluidic devices, highlighting the improvements of new materials and design approaches have improved the structural and functional integration of these devices. Below, applications of 3D printed microfluidic devices are highlighted and summarized. [49]

- **PDMS and Silicone-Based Inks:** PDMS and other silicone-based inks are commonly used in 3D printing due to their biocompatibility, flexibility, and ease of use. These materials are ideal for creating microfluidic devices that require precise control over fluid dynamics and mechanical properties.
- **Micro Sensing:** Sensors can be integrated into 3D-printed microfluidic devices. Thereby various parameters such as temperature, pressure, and chemical composition can be monitored, providing real-time data for applications in biomedical diagnostics and environmental monitoring.
- **”LEGO®” based Approach:** In this approach, modular microfluidic components that can be assembled like LEGO bricks. 3D printing facilitates the production of these standardized, interchangeable parts, allowing for easy customization and reconfiguration of microfluidic systems.
- **3D Printed Microfluidic Components (Valves, Pumps, Mixers)** Essential components such as valves, pumps, and mixers can be produced using 3D printing. This allows for the creation of integrated systems with complex geometries that can precisely control fluid flow, mixing, and other functions within microfluidic devices.
- **3D Printed Conformal Devices** Conformal devices can adhere to and function on irregular surfaces. 3D printing enables the fabrication of microfluidic devices that can conform to non-planar surfaces, expanding their application to wearable sensors and implants that require close contact with biological tissues.
- **3D Printed Droplet Maker** Microfluidic devices can be used to create droplets with precise control over their size and composition. 3D printing these devices allows for the integration of complex channel designs, which can produce uniform droplets for applications in drug delivery, diagnostics, and chemical reactions.
- **3D Printed PoC Devices** 3D printing allows for the rapid and cost-effective production of PoC devices. These devices can be customized for specific diagnostic tests and produced on-demand, making healthcare more accessible, especially in remote or resource-limited settings.
- **Soft Robotics with 3D Printed Microfluidics** Soft robotics leverages flexible materials to create robots that can mimic natural movements. 3D printed microfluidics can be integrated into soft robotic systems to control fluid flow, which in turn manipulates the robot’s movements, enhancing its functionality and adaptability.

Zhiming et al. demonstrated the fabrication of microfluidic chips with cross-sectional channel dimensions of  $20\ \mu\text{m} \times 20\ \mu\text{m}$  by using the DLP printer from Boston Micro Fabrication, one of the most precise printers on the market. The tiny channels were achieved by mathematically calculating a critical energy dose for the so-called "roof" or "lid" of a microfluidic channel, essentially a mechanism which was named "dosing- and zoning-controlled vat photopolymerization" (DZC-VPP). Keeping UV-exposure below this critical energy dose will prevent UV light from penetrating into the channel, eliminating a problem that stems from the nature of 3D-printing itself. [50]

Shafique et al. used low-cost LCD resin printers (150-600\$) to create a micromixer, microvalves, capillary circuits and organ-on-a-chip devices. Additionally, a 3D-printer ink with a very low viscosity was developed by the researchers. The ink is based on the monomer Poly(ethylenglycol)diacrylat (Pegda-250), with Triphenylphosphine Oxide (TPO) as photoinitiator, Isopropylthioxanthone (ITX) as photoabsorber, and Pentaerythritol tetraacrylate (PETTA) as crosslinker. Shafique et al. found that low-cost photopolymerization LCD 3D printing could achieve high-resolution fabrication of complex microfluidic devices, including microchannels, thin membranes, and organ-on-chip devices, with the potential for mass production of over 10,000 units in 24 hours using a single printer. Table 2 shows the used LCD printers and their XY- and z-resolution. [51]

Table 2: ELEGOO printer comparison used by Shafique et al. [52]

Manufacturer: ELEGOO		
Model:	XY Resolution	Layer Thickness
Mars 3 Pro	$35\ \mu\text{m} \times 35\ \mu\text{m}$	0.01-0.2mm
Mars 4 Ultra	$18\ \mu\text{m} \times 18\ \mu\text{m}$	0.01-0.2mm
Saturn 2	$28.5\ \mu\text{m} \times 28.5\ \mu\text{m}$	0.01-0.2mm
Saturn 3 Ultra	$19\ \mu\text{m} \times 24\ \mu\text{m}$	0.01-0.2mm

## 1.2 3D-printing for Point-of-Care devices

### 1.2.1 Point-of-Care Testing

Point-of-Care Testing (POCT) refers to the application of laboratory diagnostic procedures in immediate proximity to the patient. It represents a modern alternative approach to traditional laboratory testing, driven by the need for timely determination of vital parameters. The key conceptual features are the elimination of sample transportation to the central laboratory, the absence of sample preparation, and the immediate availability of results directly at the patient's side, or by the patients themselves. [53] PoC devices are transforming medicine from a symptom/diagnosis/treatment model to a monitoring/prediction/prevention paradigm. Additionally, they are particularly beneficial in remote or resource-limited settings. They are used for a wide range of applications, including the detection of viruses, biomarkers associated with cancer or pregnancy-tests. They are used in hospitals and clinics, but also for environmental monitoring, food safety and drug discovery. [54], [55], [56], [57] The advent of 3D printing technology has enabled the fabrication of microfluidic PoC devices. These devices are now being designed with complex features that were previously difficult to achieve, allowing for rapid prototyping and tailored solutions for specific diagnostic needs. Examples include 3D-printed devices for anemia diagnosis and self-heating microfluidic devices for disease detection. [58], [59]

### 1.2.2 Reagent-Storage and -Release in PoC

Point-of-Care (PoC) diagnostic devices often require the integration of various reagents for sample preparation and analysis. Effective reagent storage and release mechanisms are crucial for the functionality of these devices.

**Reagent Storage:** Reagents in PoC devices need to be stored in conditions that prevent degradation, contamination or environmental impacts. For instance, some reagents may require airtight containers to prevent oxidation, while others might need to be kept in dark, cool places to retain their reactive properties. [60], [61]

**Reagent Release:** PoC devices need to have mechanisms that enable reagent release when needed. The release mechanism must be precise and controlled, as the timing and quantity of reagent release can be critical to the success of an experiment or diagnostic test. [62] Techniques for release include manual methods, such as pipetting, or automated systems that deliver the reagent by pushing a button or triggering a sensor. [60], [63]

Blister pouches, for example, have been implemented as an effective solution for liquid reagent storage and release, providing a low-cost and integrated approach suitable for various PoC diagnostic applications. [64]

## Storage Methods:

- Liquid Storage
  - Liquid Reservoirs:  
Reagents can be directly stored on-chip, with a flexible thermoplastic elastomer membrane acting as a seal. [62]
  - PDMS - sponge  
A porous, sponge-like material made from PDMS can be used as reservoir-free storage solution. [62]
  - Centrifugal microfluidic platforms:  
A centrifugal microfluidic platform is a technology that uses centrifugal forces to manipulate fluids in microscale devices. It enables the automation of processes such as mixing and transfer of reagents and sample solutions. [62]
  - Blisters:  
Blister pouches consist of the main body, usually dome-shaped, defining the volume and shape, and a thin film or foil to enclose the reagents. They can be pierced and/or compressed to empty their content, while usually maintaining their required shape and volume. [60]
  - Stick-packs:  
In the packaging industry, stick packs are used to store solids and liquids for a long time. Reagents can be stored without significant losses and interactions with the surrounding environment, and on-demand release is also implementable. [61]
- Dry Storage
  - Adsorption  
Physical (Van-der-Waals forces) or chemical (covalent bonds) adsorption is used to immobilize reagents via adhesion to surfaces. The immobilization of reagents is used in, for example, in  $\mu$ PADs. [62]
  - Lypophilization-based Storage  
Vacuum and low-temperatures are used to remove water, it is also referred to as freeze-drying of reagents. The freeze-dried reagents can be stored directly on the chip. [62]
  - Nanocarriers  
Nanocarriers, e.g. Gold-Nanoparticles (AuNP), are used in lateral flow assays for the immobilization of detection antibody and the colorimetric readout. Thereby, the conjugated AuNPs are dried within a conjugate pad and are released as soon as the sample enters the pad. [62]
- Hydrogel Storage:  
Hydrogels are a network of polymer chains that have the ability to swell and absorb a large amount of water, often containing over 90% of water. Since hydrogels have the ability to preserve bioactive substances, they can be useful in storage- and release-applications. [62]

Release Methods:

- Liquids Release
  - Liquid reservoirs:  
An integrated membrane will deflect upon applied pressure and subsequently release the stored reagents. [62]
  - PDMS - sponge  
The reagents in the sponge can be release passively, by a fluid running through the sponge, or actively by manually compressing it release the stored liquids or reagents. [62]
  - Centrifugal force liquid release  
The reagents are being pushed towards the target upon centrifugal forces. [62]
  - Blister / Stick-packs  
Application of pressure or the controlled perforation of the sealing membrane are used to release reagents stored in blisters or stick-packs.
  - Pumping mechanisms  
Pumps can be used to handle and move stored reagents. Syringe pumps, peristaltic pumps, piezoelectric pumps or capillary pumps are among the most commonly used pumps in microfluidics. Also hand-powered or self-designed pumps can be used. [65]
  - Valves for controlled release:  
Valves can be used to actively control and handle reagents. For example Burst-valves or Quake-valves are among the most commonly used. [66], [67]
- Dry Release  
Solid reagents need to be released into liquid phase before usage. For example, dissolution and capillary force-based movement of reagents are used in lateral flow assays. [62]
- Stimulus-based Release  
Physical or chemical stimuli are used for controlled reagents release. Thermoresponsive polymers can be used for temperature-based stimulus. But also special substances can be used as stimulus for release, for example the mechanism of hydrogel shrinking upon contact with NaOH was realized by Deng et al. [62]

### 1.2.3 State of the Art '3D-printing in PoC'

In the review from Yang et al., several 3D printed devices and auxiliary equipment are stated. A i) nucleic acid amplification reactor for infectious diseases was printed with a stereolithographic printer (Manufacturer: FormLabs, Model: Form2). The reactor was printed with clear, methacrylate based resin (Formlabs, FLGPCL02). The fully 3D printed microfluidic reactor array is capable of carrying out extraction, concentration and isothermal amplification of nucleic acids in a variety of fluids. Another device was a ii) 3D printed centrifuge for manual blood separation. The "3D-fuges" are based on the concept of a previously established "paperfuge", which separates blood in a paper-based microfluidic device. The 3D printed device can reach angular speeds of 10.000 rpm and weighs less than 20 grams. Another "3D-fuge" achieved iii) nucleotide extraction with a handheld, 3D printed centrifuge. Requiring a sample volume of 2mL. Device iv) performed hemoglobin concentration measurements by using a monolithic microfluidic chip, printed with the D3 ProJet 1200, with a resolution of 30µm. [68]

Ordutowski et al. developed a proof-of-concept enzyme-linked immunosorbent assay (ELISA) for immunoglobulin E (IgE) detection. For fabrication, the technology of binder jetting with a powder bed 3D printer was utilized (Manufacturer: 3DSYSTEMS, Model: Z650). The printer creates layers by sintering PMMA beads with solvent-based binders. Discs for microtiter plate wells, beams to be incorporated into a PDMS channel, microfluidic channels, and one-way valves for reagents storage were 3D printed with PMMA. [69]

Dalvand et al. developed a device to detect uric acid in urinary samples. A 3D printer that is based on the PolyJet technology was used. The microfluidic chip was directly printed with transparent photopolymer resin, and consisted of two 35µL chambers that were connected via a porous membrane. One side was then loaded with the urinary sample and detection was performed by colorimetric analysis in ImageJ. [70]

## 2 Aim of this thesis

By utilizing additive manufacturing, new possibilities emerge to create microfluidic chips at relatively low-cost. In addition, complex parts can be created without the need for a production line, molds or additional manufacturing steps. Thereby ideas, considerations and designs can be tested quickly and efficiently, giving new possibilities in terms of chip development. The purpose of this study was to investigate the capabilities of a digital light processing 3D printer for microfluidic applications.

The second part of this thesis addressed the field of "Reagent Storage and Release". By using the benefits of additive manufacturing, the aim was to design and produce a fully 3D-printed microfluidic chip. Different storage and release methods were tested, and subsequently merged into a single chip.

### Thesis Statement and Research Questions

This project made use of the capabilities of a resin-based Digital Light Processing 3D-printer in the field of microfluidics. The findings were then used to create a functional microfluidic chip that incorporated a storage- and release mechanism. The following points laid the foundation for this project:

- Material characterization: preparation of a third-party resin for printability
- Document and assess the capabilities and limitations of the 3D printer with emphasis on microfluidic chips and features
- Development of mechanisms that can be easily integrated into PoC devices.

## 3 Materials and Methods

### 3.1 3D printers

The specifications of the FDM printer and the DLP printer can be found in Table 3.

#### FDM printer:

The FDM printer was used for holders and custom-made devices to aid chip-manufacturing.

#### DLP printer:

The DLP printer was used for the creation of microfluidic chips and PDMS-molds. The printer is highly valuable since it offers multi-range printing and a has huge variety of parameters to adjust. In resin 3d-printing, typically the layer height is fixed before printing (e.g. 100 $\mu$ m). This printer is capable of printing with variable layer heights within a single print. It can print bulk material with larger layer heights to save time, while fine details can be printed with smaller layer heights for higher precision. It is open for 3rd-party resins, which makes it attractive for microfluidic applications, where low-viscosity resins can be beneficial.

Table 3: Specifications of utilized 3D printers.

	<b>FDM printer</b>	<b>DLP printer</b>
Manufacturer	Prusa	ASIGA
Model	i3 MK3S	MAX X43 UV
Resolution	Nozzle: 0.4mm	Pixel: 43x43 $\mu$ m
Minimum z-step	50 $\mu$ m	1 $\mu$ m

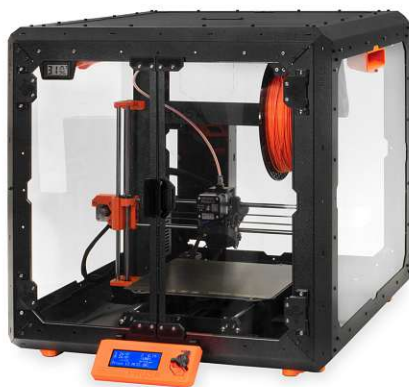


Figure 9: Left: Prusa MK3S [71], Right: Asiga Max X43 UV [72]

## 3.2 3D printing resins

Two transparent (clear) resins were used to fabricate the 3D prints. PlasClear by Asiga was available and ready to use. NanoClear by the manufacturer FunToDo is a third-party resin that can be used with the Asiga DLP printer, but only after creating the so-called material file first. The process of creating the material file will be described in section 3.3.

Table 4: Specifications of utilized 3D printing resins. [73], [74]

	PlasClear (Asiga)	NanoClear (FunToDo)
Appearance:	Clear	Clear
Viscosity:	342 mPa·s	83 mPa·s
Hardness Shore D:	79	85
Shrinkage:	-	<0.2%
Z-axis resolution:	-	2 to 200 $\mu\text{m}$
UV-cure wavelength:	-	225 to 415 nm

## 3.3 Characterization of NanoClear Resin

**General:** Asiga has developed a platform that allows the use of any photocurable resin, regardless of whether the resin is produced by Asiga or by third-party manufacturers. However, the printer needs certain parameters of the material to be able to print it. The dynamics of the material upon being exposed to UV light determine the printing parameters.

**Requirements:** For the layer-by-layer printing, the cured layer needs to have enough strength to withstand viscous- and separation forces, and it also needs to be thick enough to bond to the previous layer. The optimal exposure time of a layer is influenced by the light intensity and the light-curing properties of the material.

Consequently, the printer needs two main parameters:

- the currently set light intensity of the UV-lamp
- the "Curing-Table" for the material currently used

Both, the set light intensity and the curing table, are stored within the so-called "material file". This file, with appendix ".ini", which stands for "initialisation", is a textfile that is being accessed by the software of the printer. All the information within this file are being sent to the printer before a print. If this file does not exist, because it is a third-party material with no material file available, it can be created manually.

### 3.3.1 Experimental Determination of Curing Table Data

To create a z-curing table, which will act as calibration data for the printer, the following parameters are to be experimentally determined:

- UV light intensity
- Exposure time
- Thickness of the material being exposed to UV-light

#### **Required equipment:**

- 3D printer (Asiga Max X43 UV)
- Material to be tested
- FEP film
- Calipers
- Isopropanol
- Protective gloves
- UV protective eyewear
- Calculator
- Pencil and Paper / Laptop to document measurements
- Empty build tray
- glass beaker for small sample of resin
- 3D-printed container to retain liquid resin
- Play-Doh as sealant for 3D-printed container
- Dial-Gauge for precise measurement of layer thickness
- Dial-Gauge holder
- Metal plate to secure Dial-Gauge holder
- Glass-slide
- 3D-printed centering for positioning of 3D-printed container

Before starting to measure, everything should be prepared properly and each of the above mentioned items should be at hand (see Figure 10). The glass plate within the printer must be clean, an empty build tray should be installed, and the build plate needs to be removed. As a last step, the light intensity must be set to the desired value at the printer directly (Maintenance → LED → Power Level).



Figure 10: Necessary equipment for material file generation.



Figure 11: Left: centered container. Right: resin sample.

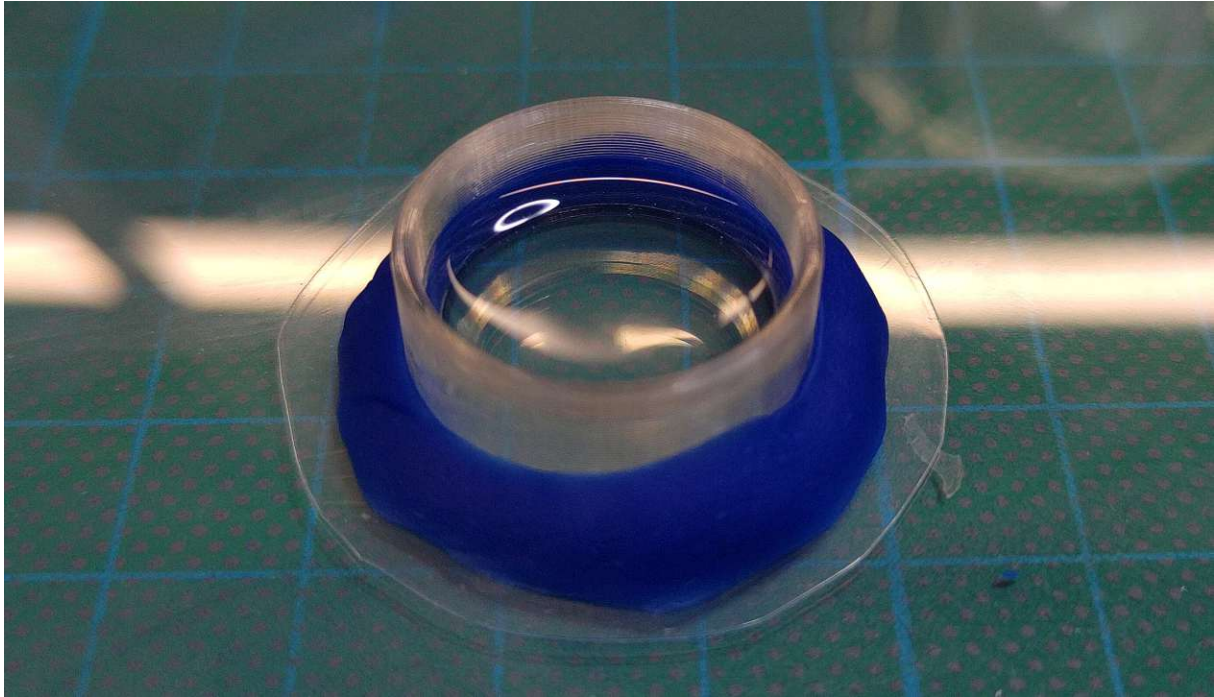


Figure 12: Container filled with resin and sealed with Play-Doh

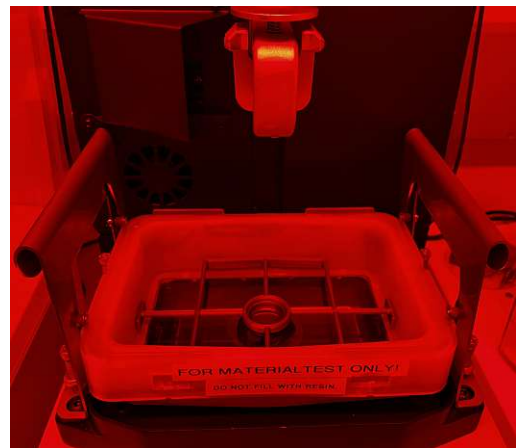


Figure 13: Left: filling of container. Right: placing container inside the printer.

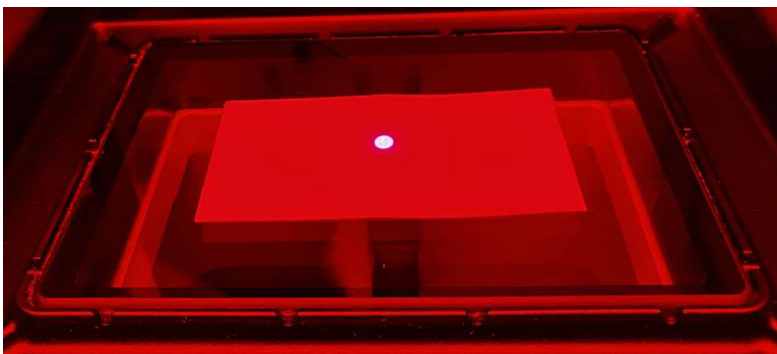


Figure 14: Left: UV spot visualized with paper. Right: washing off excess resin from cured spot.

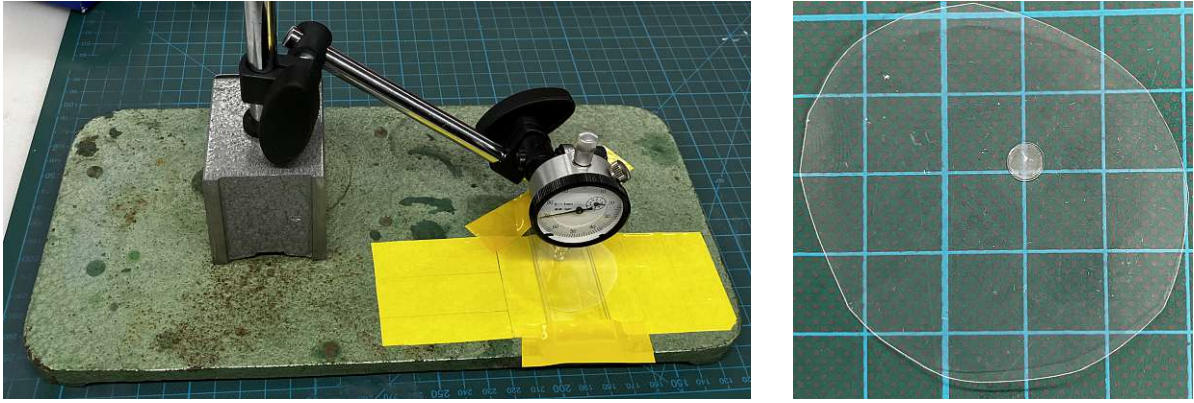


Figure 15: Left: dial gauge setup. Right: cured spot.



Figure 16: Left: measuring spot. Right: measuring reference value.

**Brief overview of the proceedings:**

- 1): choose a light intensity.
- 2): place batch of resin into an empty tray.
- 3): illuminate the material with a spot of UV light for x seconds.  
(Maintenance → SPOT TIMER)
- 4): measure the cured spot.
- 5): jot down every measurement. (exposure time and thickness)

**Detailed description of the experimental procedure:**

Figure 11 on the left shows the empty build tray with centering device and empty container placed in the middle, Figure 11 on the right shows a batch of resin sample used for filling

the container. Figure 12 shows the container placed on top of a piece of FEP film, filled with resin, sealed by Play-Doh. Figure 13 on the left shows the filling of the container with liquid resin, before placing it into the 3D printer (Figure 13 on the right). Figure 14 on the left demonstrates the illuminated UV spot when activating the spot timer, visualized by placing a strip of paper onto the glass plate. By activating the spot timer, the UV spot will be illuminated upon the container, and will result in cured resin at the site of the UV spot. Figure 14 on the right shows the removal of resin from the sample, the cured resin will then stick to the FEP film (see Figure 15 on the right). After the resin removal, the illuminated spot needs to be measured. Therefore, a dial gauge with an accuracy of 1µm was used (see Figure 15 on the left). Figure 16 shows the measurement of the cured spot with the dial gauge. The measured value will then be documented, and the next resin sample can be cured. All the measured data needs to be documented, and an exemplary table can be found in Table 5.

Table 5: Exemplary results of material test at a light intensity of 7.05 mW/cm<sup>2</sup>, M (M1, M2, M3) signifies measurement.

Measurement	Time (s)	M1 (mm)	M2(mm)	M3(mm)
#1	0.5	0.035	-	-
#2	1	0.080	0.77	0.78
#3	2	0.126	0.127	-
#4	3	0.152	0.149	-
#5	5	0.190	0.189	-
#6	8	0.216	2.13	2.19
#7	10	0.235	-	-
#8	25	0.316	-	-
#9	50	0.377	0.378	0.373
#10	100	0.509	-	-

### 3.3.2 Creation of .ini-file

To create the ".ini" material file, the acquired data needs to have the format:

$Z = [\text{energy, thickness, intensity}]$

intensity = set light intensity, in  $[\frac{\text{mW}}{\text{cm}^2}]$

thickness = measured, in [mm]

energy = intensity\*time, in  $[\frac{\text{mW}}{\text{cm}^2} \cdot \text{s}]$

In the curing table, the curing energy needs to be placed in the first column, followed by measured thickness and UV light intensity. In order to get the values in the format of  $Z = [\text{energy, thickness, intensity}]$ , an excel-sheet with the experimental data was created first. Then this excel sheet was processed with MATLAB. The MATLAB script automatically creates a text file in the specified way ( $Z = \dots$ ). The code can be found in 5.3. It is important to state that the z-curing table can be created in any way, as long as it has the specified format ( $Z = \dots$ ).

### 3.3.3 Storage of the .ini-file

A new .ini file can be created by copying an existing file, which can be found in the following system folder:

`C:\Program Files\Asiga\Composer\Materials`

It is important to note that the existing file needs to be copied into a local folder temporarily, because only there it can be manipulated. After copying the file to a local folder, it was renamed, the content deleted and new data inserted. When finished, the newly created file needs to be copied again into `C:\Program Files\Asiga\Composer\Materials`. After that, the new material-file will show up in the "Composer" software (by Asiga).

### 3.3.4 Experimental Determination of Offset-value

After parameter variation of 1) light intensity, and 2) offset-value, the prints were evaluated under the microscope. By designing a holder that places the prints in a way that the layers can be inspected from the side, the layers could be inspected.

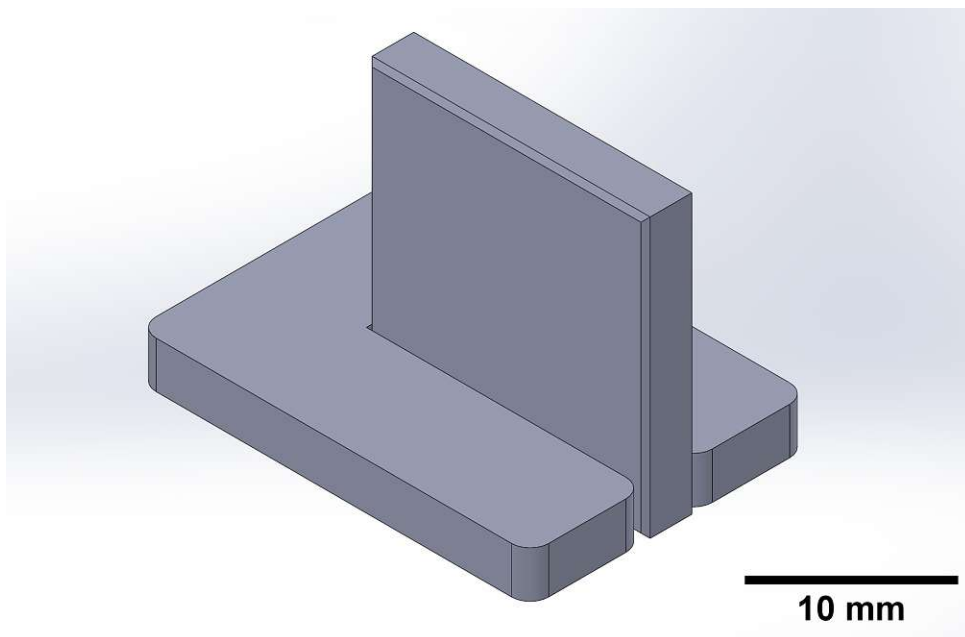


Figure 17: 3D printed device for inspecting layer adhesion.

### 3.3.5 Post-Processing of 3D-prints

Detrimental for resin 3D-printing is post-processing of green-parts. A detailed description was published by FunToDo. [75] In short: 1) wash the print thoroughly with isopropanol and/or put it into an ultrasonic bath. 2) Free the part of isopropanol either with compressed air or put it in an oven. 3) Cure the part inside a curing station or under the sun. [75] The curing station (Manufacturer: FormLabs, Model: FormCure) has 13 LEDs, operates at a wavelength of 405nm and has a radiant power output of 9100 mW. [76]

### 3.3.6 Experimental Determination of XY-plane correction factor

To ensure geometric accuracy, two factors need to be taken into account:

- XY growth  
... is an effect that causes the perimeter of a part to grow by a fixed thickness.
- XY shrinkage  
... is an effect that causes the entire part to shrink by a certain fraction.

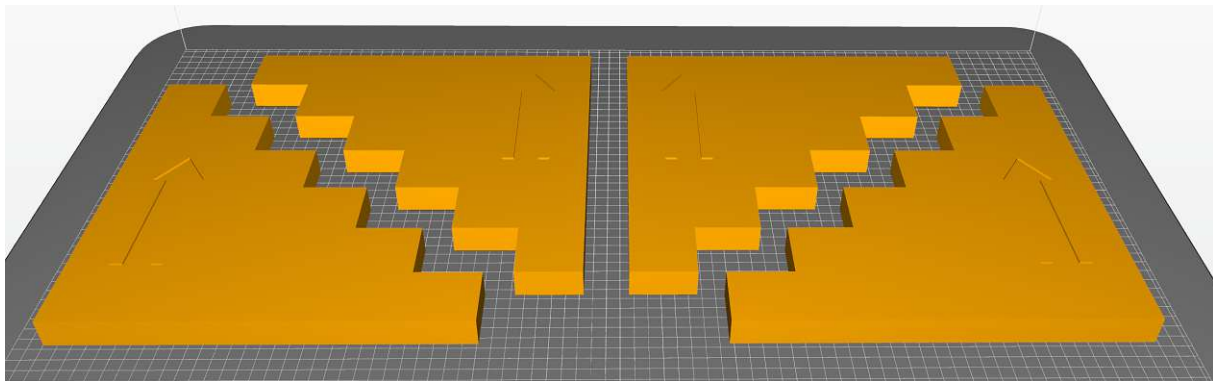


Figure 18: "Stairs" layout on build platform.

To determine XY growth and XY shrinkage, the stairs need to be printed, and then measured with callipers. To ensure this counts for different layer height, the stairs need to be printed with different layer height. The chosen values were: 100µm, 50µm, 25µm and 10µm. It is very important to note that XY growth will be different for each layer thickness. The material file allows to add the XY growth value for each layer height separately.

The XY shrinkage will also be different for each layer thickness, but, as opposed to the XY growth, the material file does not allow for a separate XY shrinkage value for each layer thickness. Instead, one value needs to be chosen, which will scale all layers by the chosen factor within the composer software. This might result in dimensional inaccuracies for some layer heights, depending on the material. In this work, the four layer heights' (100µm, 50µm, 25µm, 10µm) average shrinkage value was taken, resulting in parts being slightly smaller when printing with high layer height values, and parts being slightly bigger when printing with small layer heights.

$$ActualPrintSize = (ImageSize + 2 \cdot XY_{Growth}) \cdot XY_{Shrinkage} \quad (1)$$

Formula (1) calculates the actual print size. It can be seen that the gradient of the graph will be the XY shrinkage. The Y-intercept divided by the gradient, then divided by 2, will be the XY growth. Asiga provided an Excel sheet as well as CAD files for determination of above mentioned parameters. The CAD-files are stairs, with a step height of 5mm, starting from 5mm and ending at 30mm (6 steps in total). The actual values are then plotted, and calculated in excel based on the above mentioned formula.

### 3.3.7 Creation of XY-curing table

To create the XY-curing table, Asiga prepared an Excel sheet, where the actual values of the "XY-stairs" could be inserted. Then, as mentioned above, the slope and the intercept were calculated, which were then used to calculate XY-growth and XY-shrinkage. To minimize measurement errors, the sheet was adapted in the following way: 4 stairs were printed per layer, and distributed throughout the build platform. Then the values of all 4 stairs were taken and the median was calculated. This was done for 4 layer heights in total: 10 $\mu$ m, 25 $\mu$ m, 50 $\mu$ m and 100 $\mu$ m. For the XY-shrinkage values, the shrinkage values of all 4 layer heights were taken, and the mean was calculated (see section ??). For the XY-growth, the individual values for each layer were taken, and the "XY curing table" was created.

#### Exemplary XY curing table:

"," imposes a comment.

XY-growth values:

XY = [curing energy from z-curing table, value to add/subtract in mm]

Positive values within the curing table will get subtracted and vice versa, depending on the outcome of the measurements. Some parts grow more than they shrink and vice versa, so both options are possible.

The value for the curing energy is taken from the z-curing table for each specific layer height. To get the exact energy value at the desired layer height, interpolation might be required.

XY=[2.2063, 0.00962] ; 10 $\mu$ m layer height

XY=[2.7316, 0.008548] ; 25 $\mu$ m layer height

XY=[4.4520, 0.00646] ; 50 $\mu$ m layer height

XY=[9.4265, 0.017625] ; 100 $\mu$ m layer height

XY-shrinkage values:

Scale = [factor in x-direction, factor in y-direction, factor in z-direction]

Scale= [1.009847946, 1.009847946, 1.000]

### 3.3.8 Testing of determined print settings

#### FunToDo Calibration Object

On the website of FunToDo, a calibration object with numerous features that allows to inspect the print quality and capabilities of the printer/material is provided. Overhangs from  $15^\circ$  to  $75^\circ$ , walls, channels, bridges, a sphere, spikes, tunnels, pillars and holes are on this object.

#### CCG shaped fluid router

To showcase the ease of fabricating microfluidic channels, a fluid router with intertwining channels was printed. The channels were assembled in a way that resemble the letters "CCG" for CellChipGroup. The channels had a diameter of 0.8mm.

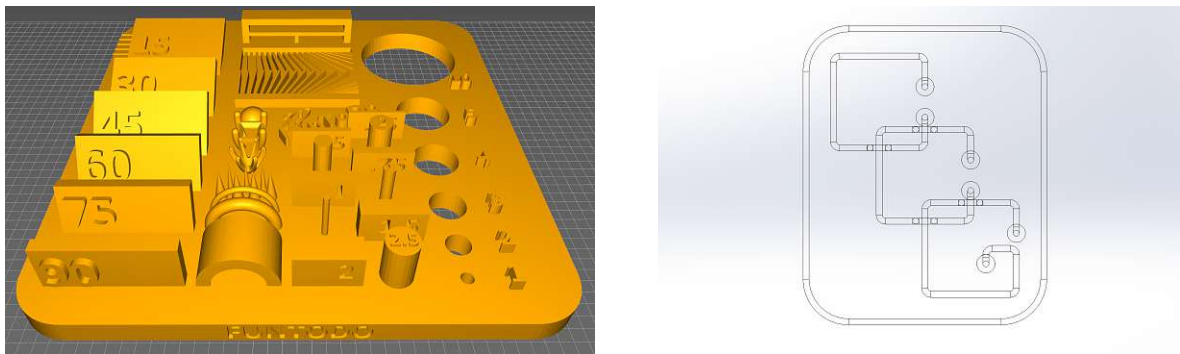


Figure 19: Left: FunToDo calibration object. Right: CCG fluid router CAD file.

## 3.4 Classification of ASIGA 3D-Printer

### 3.4.1 Geometry Assessment

To evaluate the dimensional accuracy of the 3D printer across different size scales (Table 6), an array of circles, squares, and triangles was printed.

Table 6: Geometry assessment parameters.

Materials: PlasClear, NanoClear		
Layer Heights [ $\mu\text{m}$ ]: 100, 50, 25, 10, 5		
Circle Diameter [ $\mu\text{m}$ ]	Square Sidelength [ $\mu\text{m}$ ]	Triangle Sidelength [ $\mu\text{m}$ ]
2000	1000	1732
1000	500	866
500	250	433
250	125	216.5
125	62.5	108.25



Figure 20: Geometry CAD-file with sunken features.

### 3.4.2 Height Assessment

According to Asiga, the Max X43 UV has a dimensional accuracy in z-direction of up to  $1\mu\text{m}$  (material dependent). The smallest layer height tested was  $5\mu\text{m}$ . Decreasing layer heights result in significantly longer print times. The process of assessing the total print height, as well as feature height, was refined progressively. To first assess the height of printed features, a bar was created with multiple circles on it. The print was analyzed under the microscope by turning the bar  $90^\circ$ . After that, the first assessment was discarded, due to reasons later discussed in section 4.2.2. For the second height assessment, cuboids were distributed across the build platform, as it is showcased in Figure 21.

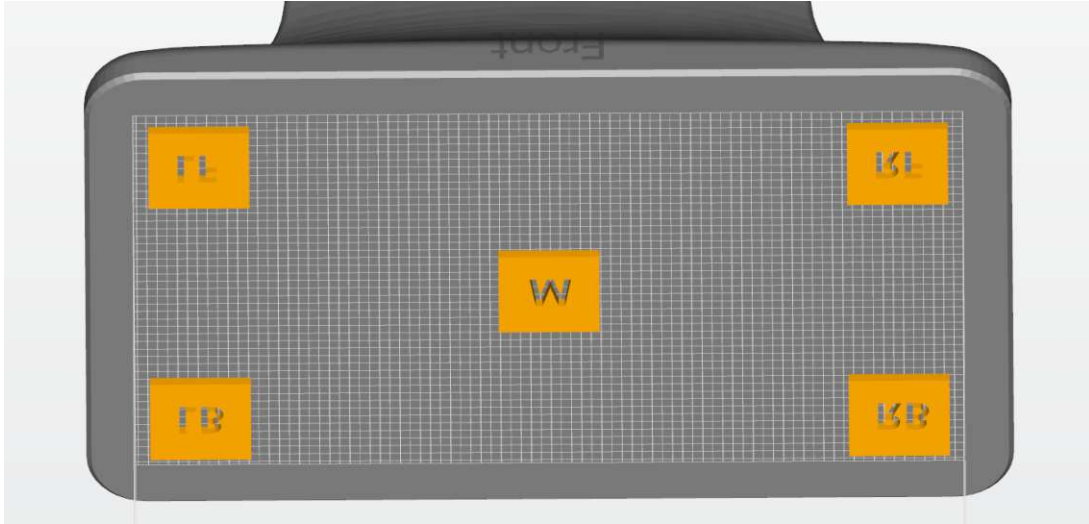


Figure 21: Distribution of cuboids across build platform.

### Corrective measures for ensuring dimensional accuracy in z-direction

The z-axis calibration needs to be performed as described by Asiga (cite), but additionally, when tightening the build platform screw, a second person should push down the build platform to ensure that the platform does not tilt due to the applied torque when tightening the screw.

### Local (features) height evaluation

To assess the size of features, the rod was discarded, since the printed parts were too thin and distortions due to a warping effect would influence the measured thickness. Instead, the prints from the section (insert section channels) were analyzed. To get information about the z-direction accuracy, the different layers were imaged and analyzed with a microscope. The parts had dimensions that would eliminate warping effects.

### 3.4.3 Partial Walls Assessment

Since the partial walls already count as detail, the assessed layer heights were not printed with 100 $\mu\text{m}$  layer height (range only from 5 to 50  $\mu\text{m}$ ).

The walls started with a thickness of 50 $\mu\text{m}$  and incremented by 10 $\mu\text{m}$  for each wall, reaching 190 $\mu\text{m}$  at the end.

As for the geometrical assessment, the partial walls were also printed as positive and negative features.

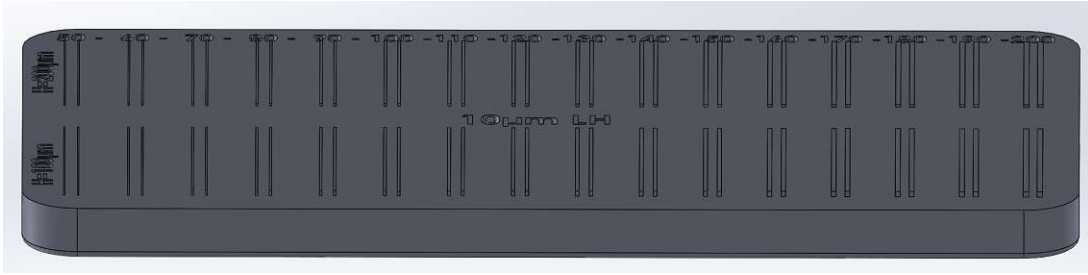


Figure 22: Partial Walls CAD file.

The values for the wall thickness were chosen 1) due to the limitations of the printer ( $43\mu\text{m}$  pixel size) and 2) due to the size of partial walls being used in the field of microfluidics.

Table 7: Partial Walls feature size.

Materials: PlasClear, NanoClear		
Layer Heights [ $\mu\text{m}$ ]: 50, 25, 10, 5		
Wall height	Wall thickness	Wall length
100 $\mu\text{m}$	50-200 $\mu\text{m}$	7.1mm
200 $\mu\text{m}$	50-200 $\mu\text{m}$	7.1mm

### 3.4.4 Build Tray for Microfluidics

The 'LowForce' build tray (Asiga) has a special membrane that should facilitate the release of the print from the release liner on the bottom of the vat, therefore especially suitable for microfluidic prints, and was compared with the 'Universal' and 'UltraGloss' (both Asiga) build trays.

### 3.4.5 Pillars Assessment

For this assessment, although the pixels of the printer are quadratic, only circular pillars were chosen, to 1) check to abilities of the printer and 2) since round pillars are commonly used in microfluidics. The dimensions of the pillars are listed in Table 8, they were printed again with four different layer heights ( $5\mu\text{m}$ ,  $10\mu\text{m}$ ,  $25\mu\text{m}$ ,  $50\mu\text{m}$ ) and with a one-pixel increment, starting with  $43\mu\text{m}$  (minimal pixel size), incrementing by  $43\mu\text{m}$  for 5 times until reaching a diameter of  $215\mu\text{m}$ .

Table 8: Pillars assessment parameters.

Materials: PlasClear, NanoClear	
Layer Heights [ $\mu\text{m}$ ]: 50, 25, 10, 5	
Build Trays:	UltraGloss, Universal, LowForce
Pillar Dimensions [ $\mu\text{m}$ ]:	43, 86, 129, 172, 215

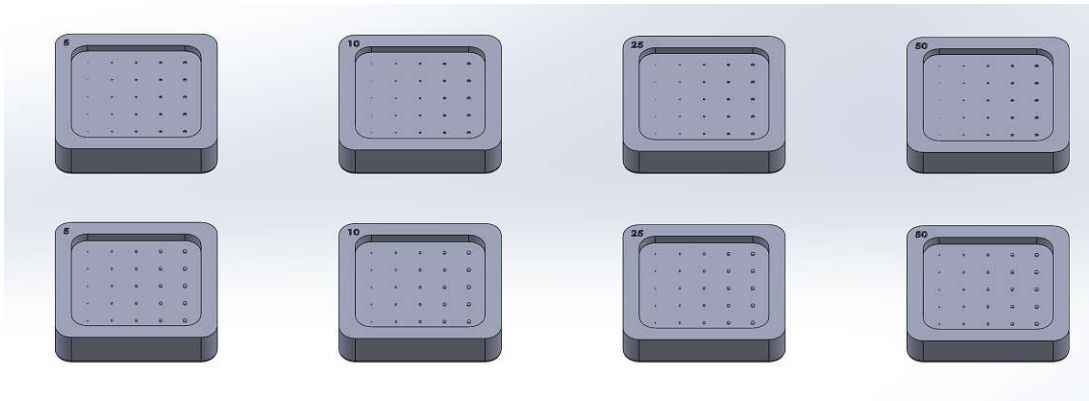


Figure 23: Pillars CAD file. Layout for different layer heights. Top row: negative. Bottom row: positive.

### 3.4.6 Channels Assessment

Since channels are essential in microfluidic applications, the printers capabilities of producing them were assessed.

The following versions were printed, tested and evaluated:

- rectangular channels, printed flat
- circular channels, printed flat
- circular channels, printed upright (channel direction = z-direction)

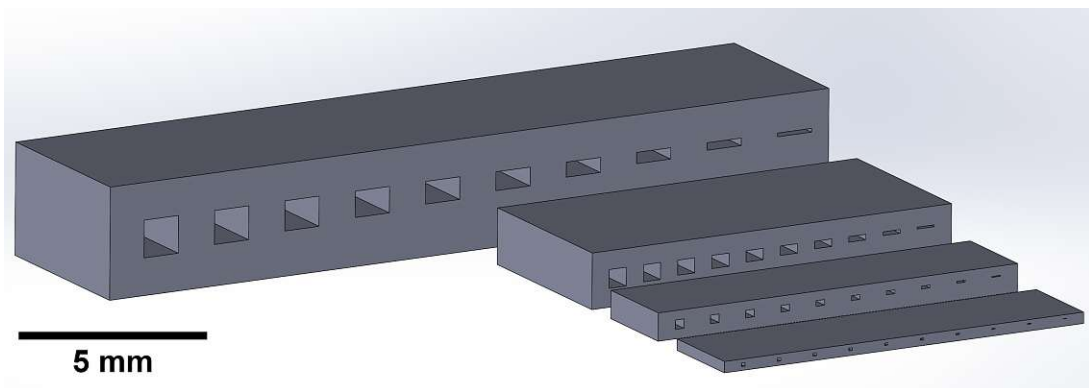


Figure 24: Layout for rectangular channel inspection.

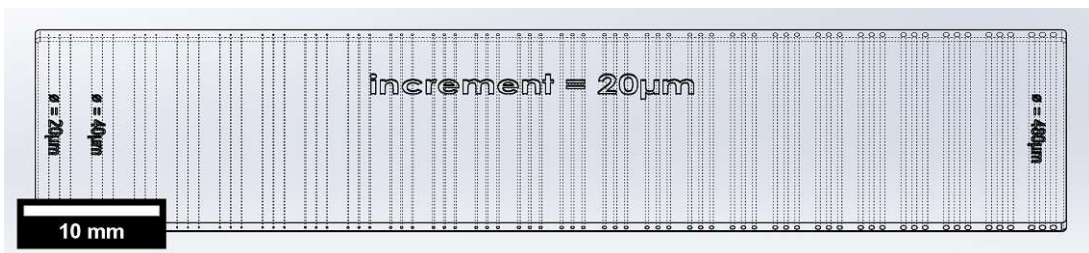


Figure 25: Round channels. Smallest channel: 20 $\mu$ m. Increment: 20 $\mu$ m. Biggest channel: 480 $\mu$ m.

After printing the channels, they were analyzed with different microscopes: Scanning Electron Microscope (SEM) and light microscopes (Olympus IX83 and Olympus IX71).

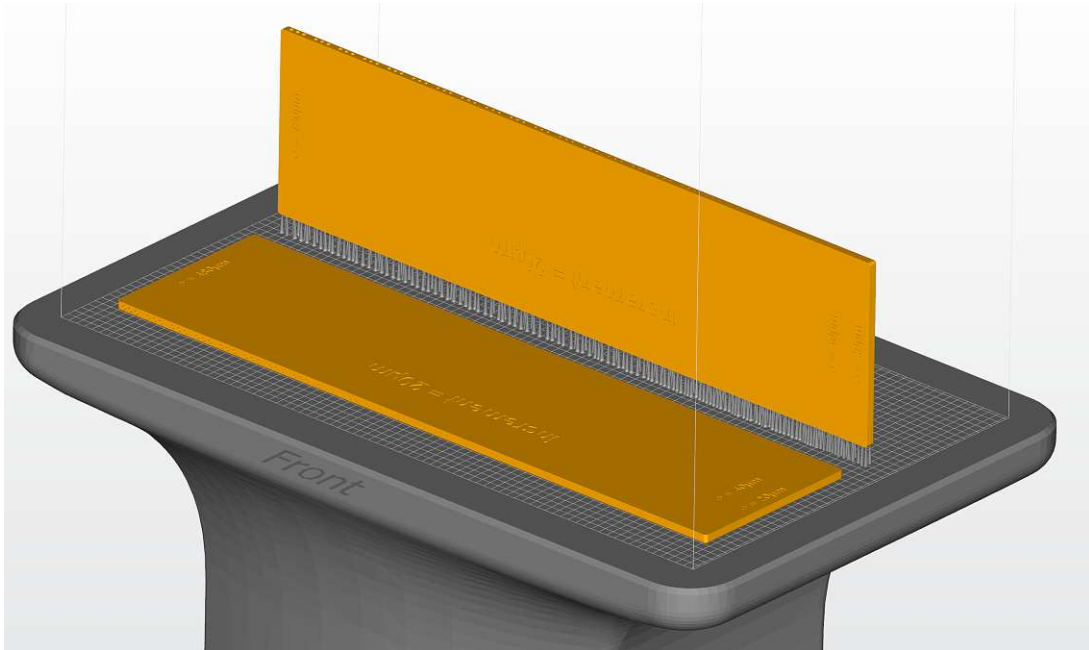


Figure 26: Round channels. Printing alignment, flat and upright.

### 3.4.7 PDMS casting with NanoClear

Since PDMS-casting plays a big role in rapid prototyping, and 3D-printed molds for casting PDMS are highly valuable, the newly characterized resin "NanoClear" was also evaluated for being used as PDMS-mold. First the green part (not yet post-processed) needed to be washed thoroughly with isopropanol and dried with compressed air. After the part has been cleaned, it was placed in a fresh batch of isopropanol over night. Then the part was cured for 4 hours in a UV chamber with a light intensity of  $\sim 10 \text{ mW/cm}^2$ .

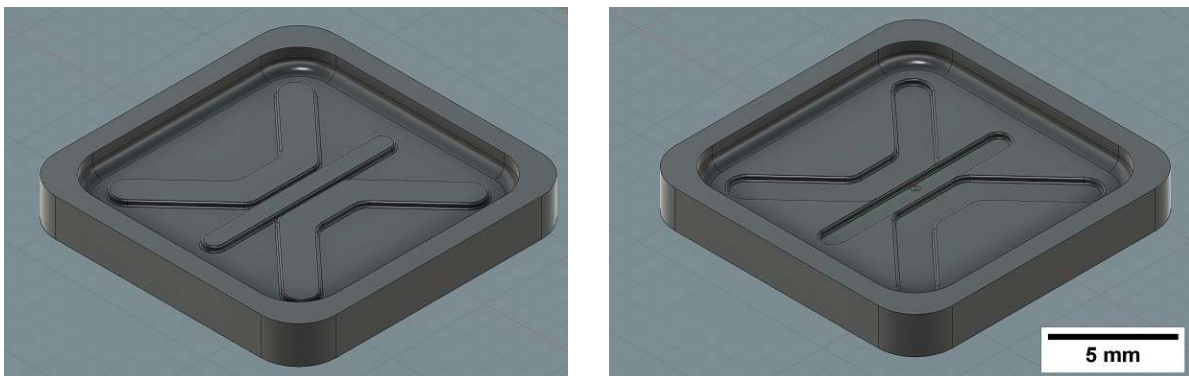


Figure 27: Left: PDMS mold lofted. Right: PDMS mold sunken.

### 3.5 Reagent Storage and Release

#### 3.5.1 3D printed holder

A 3D printed holder for the Eppendorf tube (fluid collection) and the 3D printed chip was designed and printed to lock both objects in place (see Figure 28).

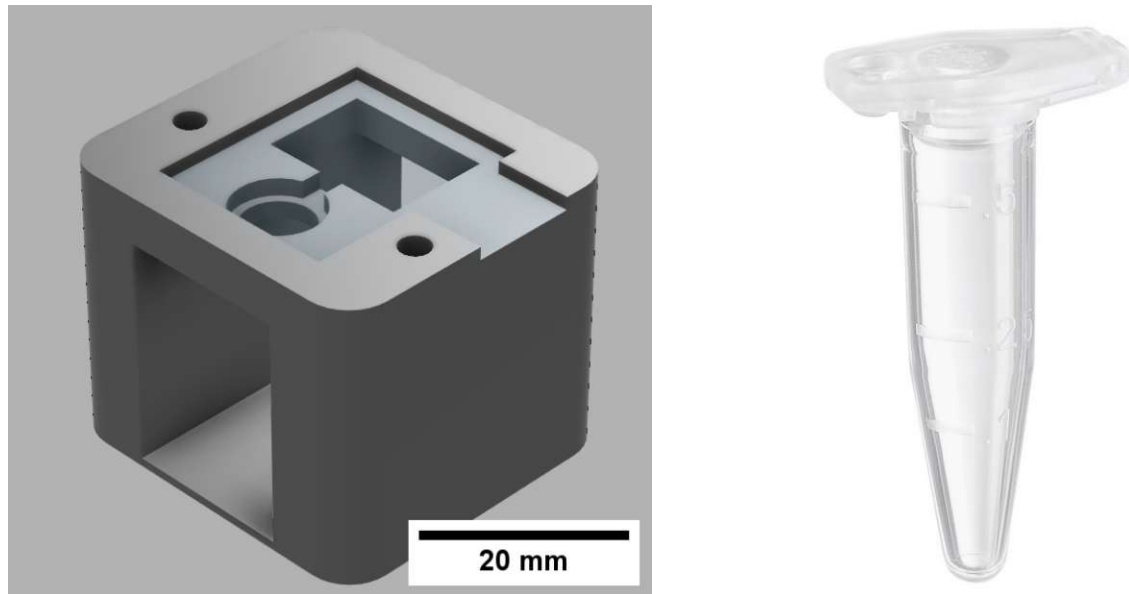


Figure 28: Left: 3D printed holder. Right: 0.5mL Eppendorf tube. [77]

#### 3.5.2 3D printed microfluidic devices

Figures 29 and 30 show the created devices for AuNP release, blister storage and the combination of both mechanisms.

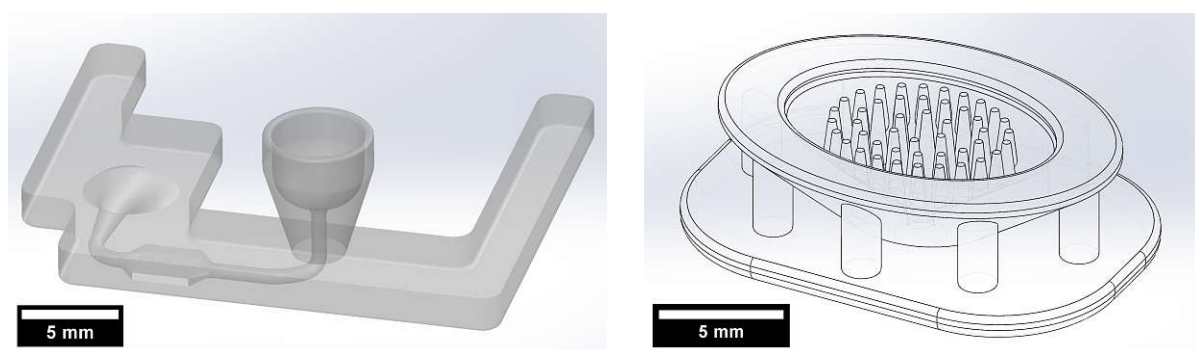


Figure 29: Left: Device for AuNP-pad. Right: Device for blister mechanism.

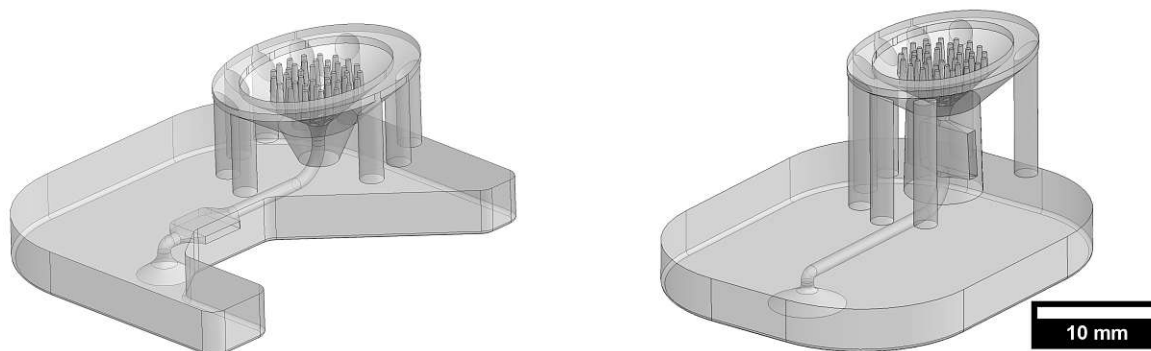


Figure 30: Combined device for AuNP and blister storage, CAD render. Left: variant I). Right: variant II).

### 3.5.3 AuNP - conjugate pad

A conjugate pad containing gold-nanoparticles was prepared by Dr.in Silvia Schobesberger. Materials include Steptavidin Gold Conjugate (40nm, ab186864, ABCAM), conjugate pads (ST17, Cytiva) and conjugate buffer solution (PBS + 0.05% Tween 20 + 10% sucrose). The procedure to manufacture said pads is the following [60]: 1) centrifugation of 2 Eppendorf tubes with 65  $\mu\text{L}$  AuNP-Streptavidin (1400RCF, 15 min), 2) carefully remove supernatant, 3) resuspend with 104  $\mu\text{L}$  conjugate buffer respectively, 4) combine the two aliquots, 5) prepare different dilutions (OD6: 120  $\mu\text{L}$ , OD3: 60  $\mu\text{L}$  OD6 + 60  $\mu\text{L}$  conjugate buffer, OD1.5: 30  $\mu\text{L}$  OD3 + 90  $\mu\text{L}$  conjugate buffer), 5) pipette 3.5  $\mu\text{L}$  onto each pad, and 6) dry in oven (37°C for 1.5h).

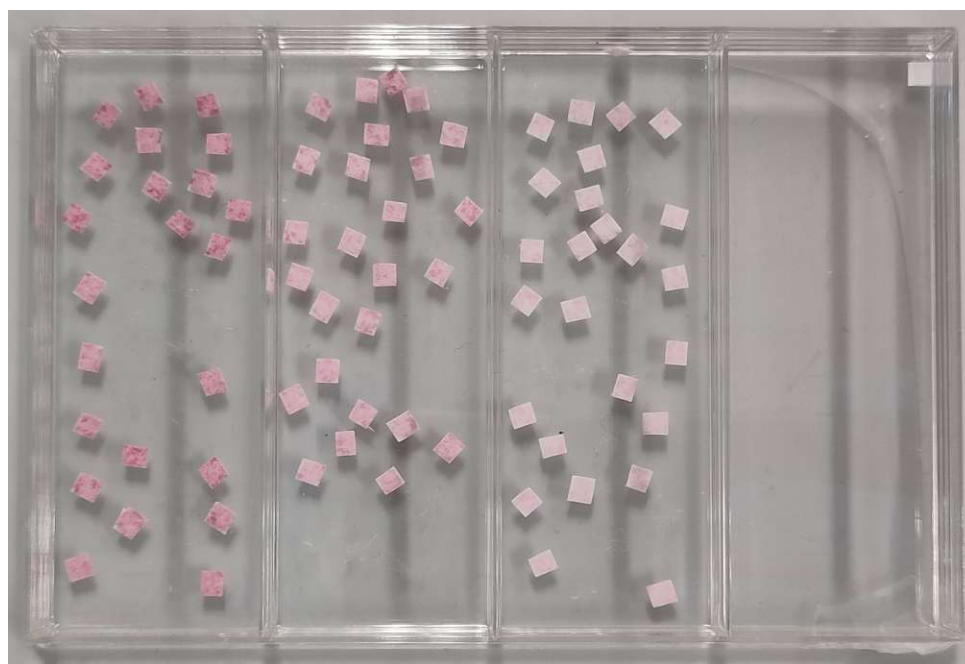


Figure 31: AuNP conjugate pads. From left to right: OD6, OD3, OD1.5.

### 3.5.4 Empty blister packs

Empty blister packs were taken from GeloMyrtol and vitamin D capsule packaging.



Figure 32: Empty blister packs. Left: GeloMyrtol. [78] Right: Vitamin D3. [79]

### 3.5.5 Blister preparation and device assembly

Play-doh was used to hold the blister in place. First a before cut piece of double sided adhesive was placed on the rim of the blister. Then the blister was filled with 200 $\mu$ L of PBS/Tween buffer solution. After that, the blister was sealed with tin foil and excess tin foil was wrapped around the blister. Then double sided adhesive was placed onto the rim of the chip. And as a last step, the blister was placed on top of the chip, held in place by the double sided adhesive. The preparation for creating the device can be seen in Figure 33.

The tape was cut into the desired shape with a cutter plotter (Manufacturer: Roland, Model: CAMM-1 GS24, Figure 34). The double sided adhesive had a thickness of 140 $\mu$ m and was a pressure sensitive adhesive (Manufacturer: Adhesives Research, Model: ARcare 90106NB).

As a last step, the AuNP pad was put into the designated slit and sealed with thick transparent tape.

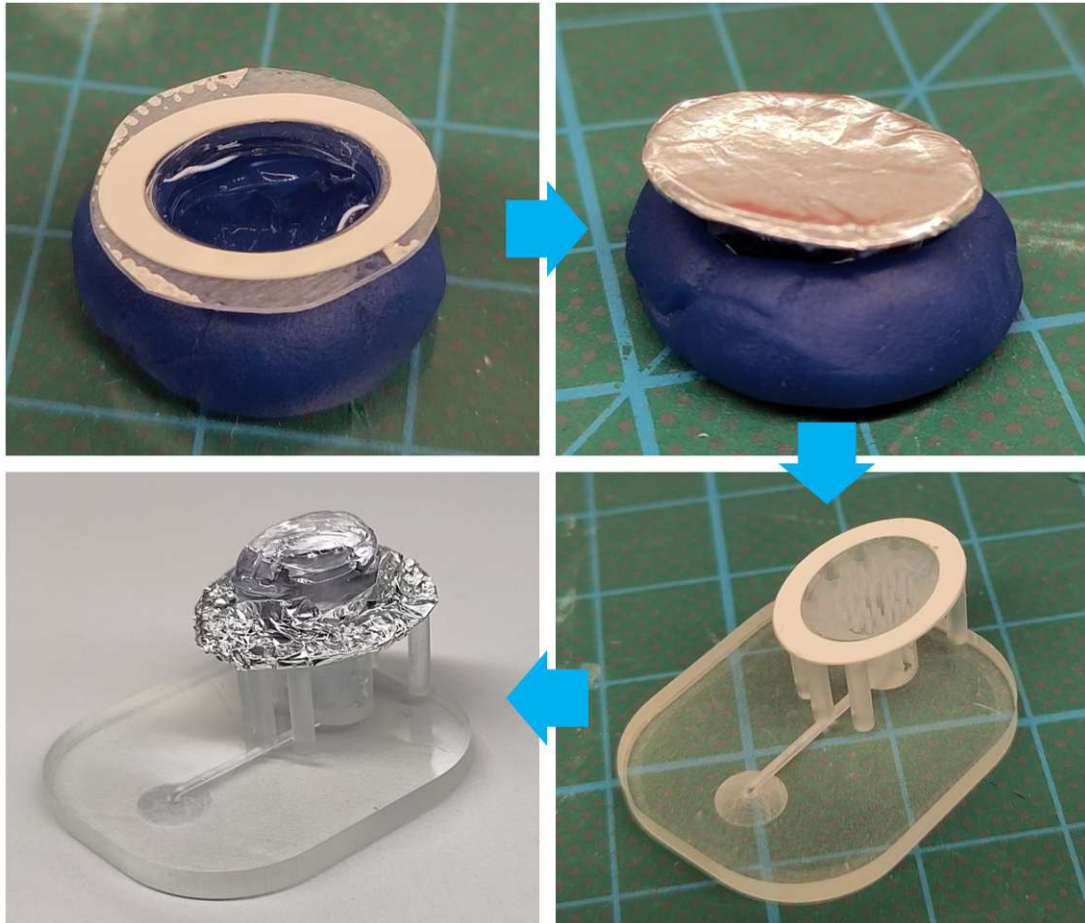


Figure 33: Preparation for combined device (AuNP + blister).



Figure 34: Roland GS24 cutter plotter. [80]

## 3.6 Software and Equipment

### 3.6.1 Software

All mentioned CAD models were created with "SolidWorks 2023" [81] or "Autodesk Fusion360" [82]. After designing, the parts were sliced and uploaded to the printers. "Asiga Composer" [83] software was used for slicing DLP prints, "Prusa slicer" [84] software was used for slicing FDM prints.

After the objects from the various assessments mentioned above have been printed and post-processed, the features needed to be analyzed and evaluated. First, the features were imaged with one of the below quoted microscopes. Then, the images were analyzed further either in imageJ [85] or MATLAB [86], either by measuring the features manually or with an algorithm. After that, the data was analyzed further, values were calculated and the results plotted and visualized in diagrams either in Excel [87], MATLAB [86] or Graphpad Prism. Generated MATLAB scripts can be found in the appendix (section 5.3). To create image arrays and visual timelines of experiment iterations, "DrawBoard PDF" [88] and "MS PowerPoint" [89] were used.

### 3.6.2 Microscopes

The inverted microscope **Olympus IX83** [90] and a **Scanning Electron Microscope** were used for channel inspection.

The inverted microscope **Olympus IX71** [91] was used for all other assessments.

The stereo microscope **Leica S8 APO** [92] was used for imaging objects where less zoom was required to get a broader perspective on the object.

### 3.6.3 AI tools

ChatGPT (GPT-3.5, GPT-4, GPT-4o) by openAI and Microsoft Copilot were used for reformulating text, programming and as a scientific writing aid. Petal (petal.org) was used for analysis of scientific papers. Elicit (elicit.com) was used to search for scientific papers.

### 3.7 Helper Objects and other 3D printed objects

**Containment Cylinder** A simple cylinder for containing the low-viscosity NanoClear resin. It was sealed by FEP-film and play-doh.

**Centering Device** To ensure that the container with resin is placed exactly in the middle of the empty vat, where the spot of UV-light will be illuminated, a centering device was printed. It was designed in a way that it was 1) directly in the center without having to eyeball the position and 2) with small cavities around the center to be able to move the resin container to 5 different spots to facilitate the "material test" creation process.

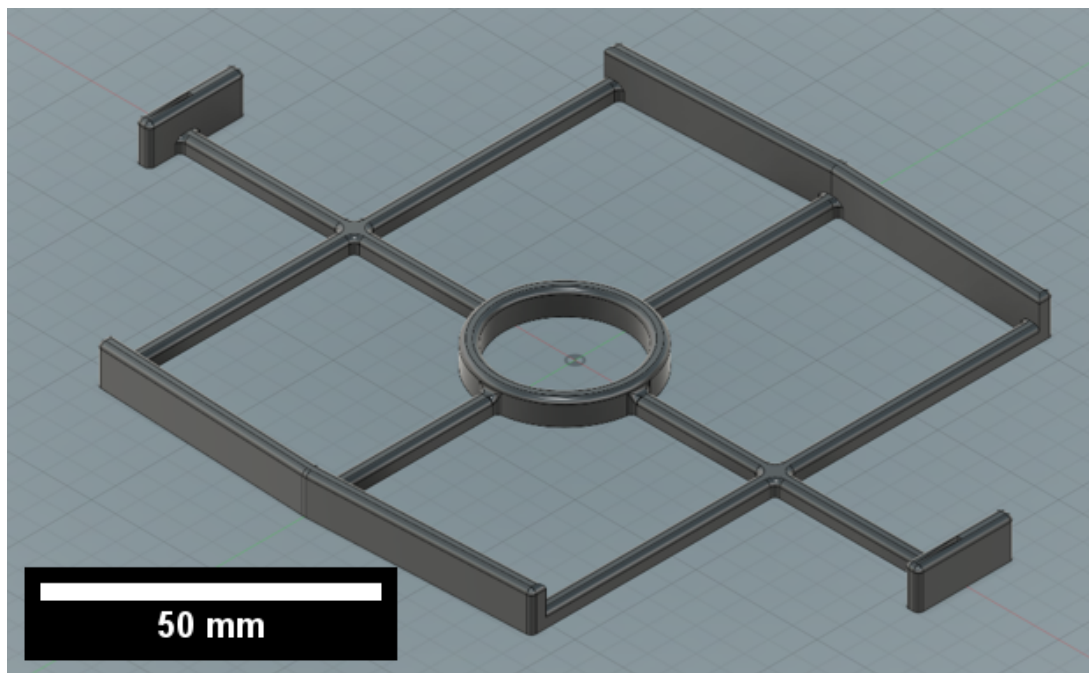


Figure 35: Centering device for "material-test".

**Build Tray Lid** Since the resin "NanoClear" is so low-viscose, when handling the tray or slightly tilting it, the danger of liquid resin spilling over the edges of the tray and further contaminate the inside of the printer is given. Therefore a two-component lid was printed, with flexible TPU-filament as sealant and PLA-filament as cover. That way, the lid can be placed firmly on top of the build tray containing liquid resin and prevent spillage.

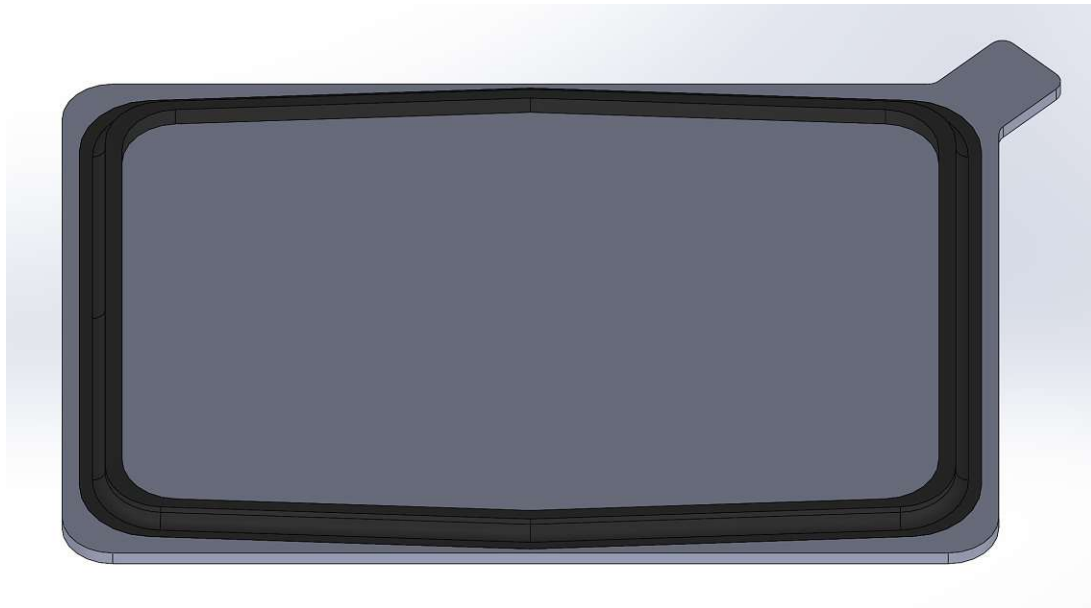


Figure 36: Anti-spillage lid for build tray containing NanoClear resin.

**Capillary device for lacrimal fluid collection** For fluid collection, an either directly 3D-printed or 3D-printed mold was created. That way, the abilities of the printed were tested. Both, pillars and channels, were successfully printed with a diameter of  $300\mu\text{m}$ .

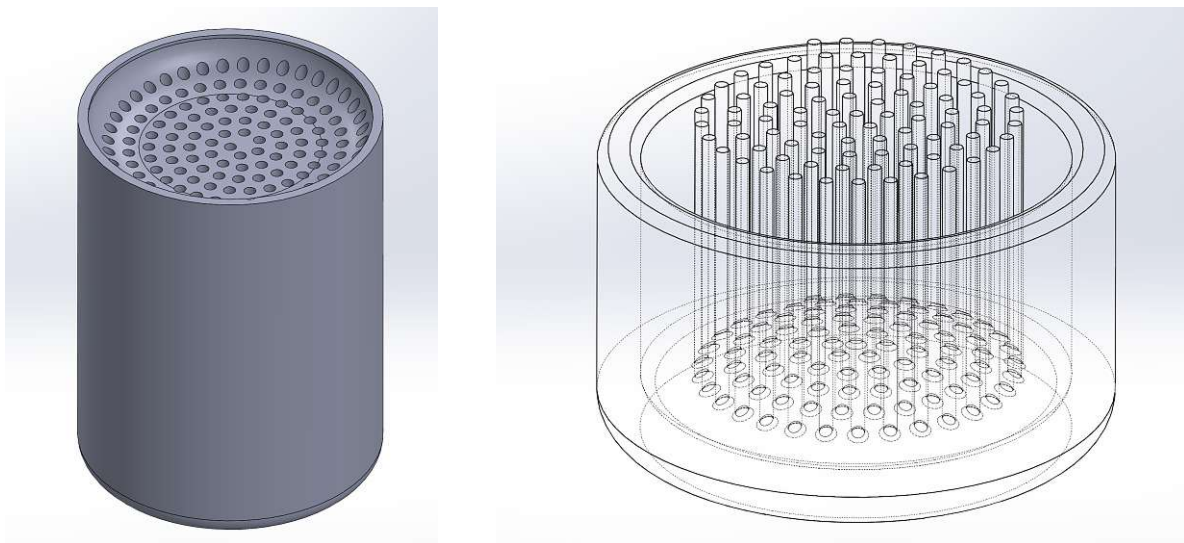


Figure 37: Left: Capillaries "negative". Right: capillaries "positive".

## 4 Results and Discussion

### 4.1 Characterization of NanoClear Resin

Transparency in microfluidics enables the integration of optical readouts but also to monitor cells under the microscope, especially important in the field of organ-on-a-chip. Additionally, low-viscose resins facilitate the removal of uncured resin from microfluidic channels. Therefore, NanoClear resin with relatively low viscosity (83 mPa·s) was set up (see section 3.3) for printing. For comparison, "PlasClear" resin by Asiga is also transparent, but has a higher viscosity (342 mPa·s [74]) compared to NanoClear.

#### 4.1.1 Z-calibration curve

To utilize the NanoClear for the DLP printer, the curing energy and the thickness of the cured spot needed to be experimentally determined to feed to printer with information about the dynamics of the material (detailed description in chapter 3.3). The results for a set light intensity of  $7.05 \frac{\text{mW}}{\text{cm}^2}$  can be seen in Figure 38. Since the curing energy is the light intensity multiplied with the curing time, the time is displayed on the x-axis. A second z-calibration was done with a light intensity of  $3 \frac{\text{mW}}{\text{cm}^2}$ , the data and plot can be found in the appendix (section 5.3).

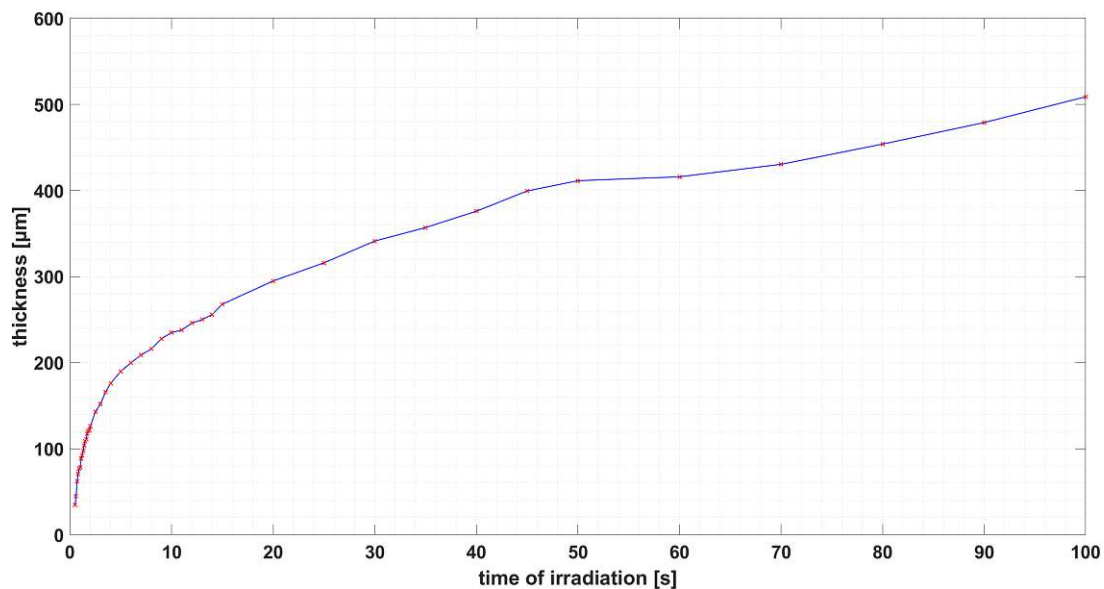


Figure 38: Z-Calibration curve for  $7.05 \text{ mW}/\text{cm}^2$ .

#### 4.1.2 Offset value

According to the supporting document for the creation of a new material file by Asiga, a good starting point for choosing the offset value lies between 0.06mm and 0.12mm. Therefore, different offset values were tested, and then the quality of the printed parts

assessed. The offset value (in [mm]) ensures that the different layers bond firmly to one another by slightly extending its exposure to UV light beyond the duration specified by the z-curing table. The actual layer size is still determined by the gap of the build platform and the vat membrane. As an example, when trying to print with an offset of 0.00mm, the layers did not bond to each other, resulting in breaking of the part. Also the poor bonding can be seen in Figure 39 on the left, with cavities remaining inside the formed layer. Overcuring can be seen in Figure 39 on the right, with parts of the layer solidifying as a bulky segment. The finally chosen curing parameters were a light intensity of  $7.05 \frac{\text{mW}}{\text{cm}^2}$  and an offset value of **0.070 mm**, the layers can be seen in Figure 40.

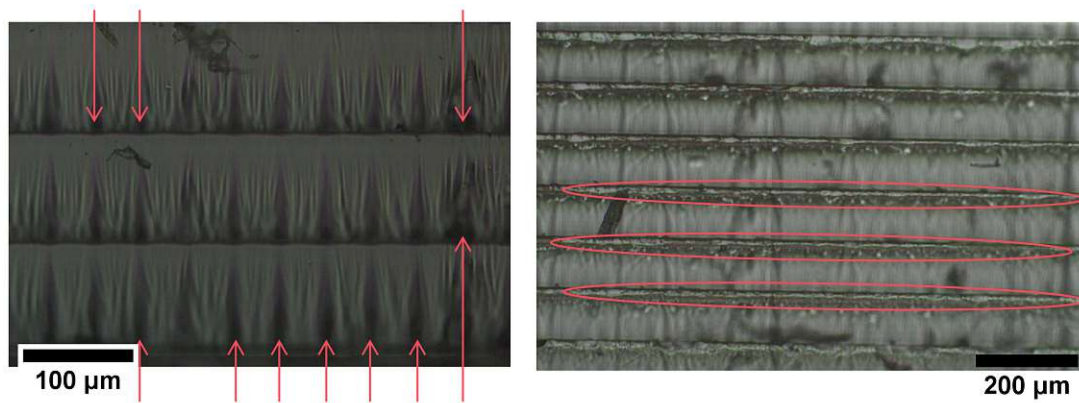


Figure 39: Left: Undercuring of the resin, indicated by the cavities (pointed at with red arrows). Right: Overcuring of the resin, indicated by bulky segments between the layers, marked with red ellipses.

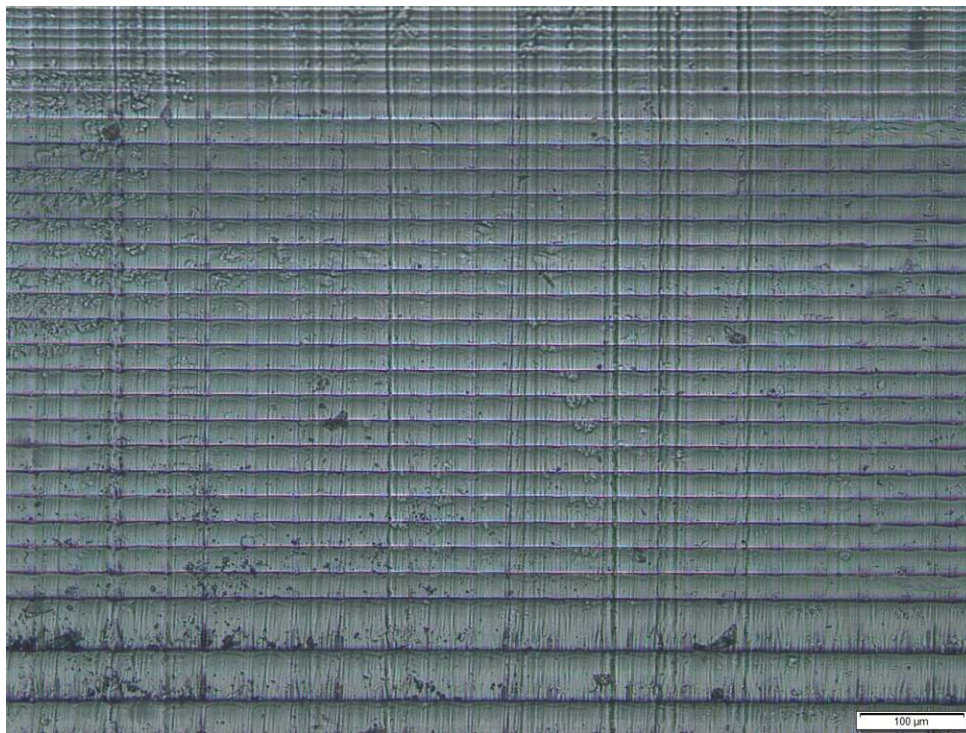


Figure 40: Side-view of layers with the chosen print parameters.

### 4.1.3 XY curing parameters

The curing parameters "XY shrinkage" and "XY growth" were determined to ensure the dimensional accuracy of the printed parts in the XY plane. They were inserted into the .ini file and the printers' software will automatically apply those parameters when printing. Based on the Excel sheet provided by Asiga (see section 3.3.6 and Figure 84) the values for 'XY shrinkage' and 'XY-growth' parameters were evaluated, and in Table 9 the results for printed stairs, before and after application of said parameters, can be found.

XY shrinkage: =58% → yields: Scale = [1.009847946, 1.009847946, 1.000]

XY growth (LH = Layer Height):

- LH 10 $\mu$ m: 0.00962mm
- LH 25 $\mu$ m: 0.008548mm
- LH 50 $\mu$ m: 0.00646mm
- LH 100 $\mu$ m: 0.017625mm

Table 9: XY-stairs evaluation. Before and after application of XY correction factor.

Stairs Layer height:	Actual step dimensions in [mm]					
	25 $\mu$ m		50 $\mu$ m		100 $\mu$ m	
Nominal, [mm]	Before	After	Before	After	Before	After
5	4.99	4.99	4.98	4.99	5.00	4.94
10	9.96	10	9.94	9.99	9.96	9.94
15	14.94	15	14.92	14.99	14.94	14.95
20	19.89	20.03	19.87	20.01	19.88	19.92
25	24.88	25.06	24.85	25.03	24.86	24.94
30	29.85	30.09	29.81	30.06	29.83	29.96

### 4.1.4 Testing of determined print settings

**FunToDo Calibration Object:** As mentioned in section 3.3.8, the calibration object with numerous features relevant for 3D printing was printed with success (see Figure 41), all the structures could be printed, even the walls angled at 15°.

**CCG shaped fluid router:** The fluid router was printed with NanoClear, with a layer height of 50 $\mu$ m. The channels had a diameter of 0.8mm, and the intertwining channels were visualized by placing pipette tips into the in- and outlets and filling them with food-colored water (see Figure 42).

The successful printing of both structures demonstrates that the preparation of the Nanoclear was successful and features like channels, overhangs and intricate details can be printed.

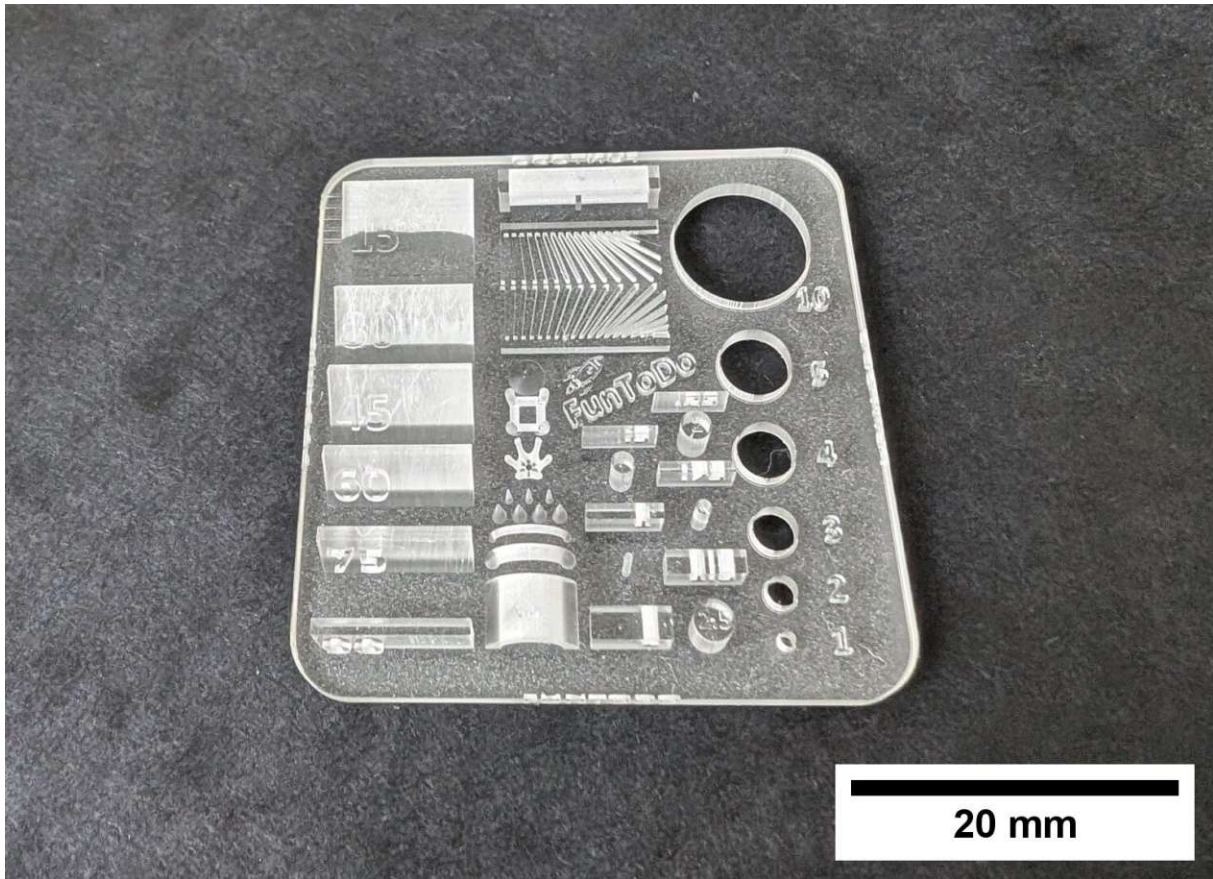


Figure 41: FunToDo Calibration Object. Printed with a layer height of 50 $\mu$ m.

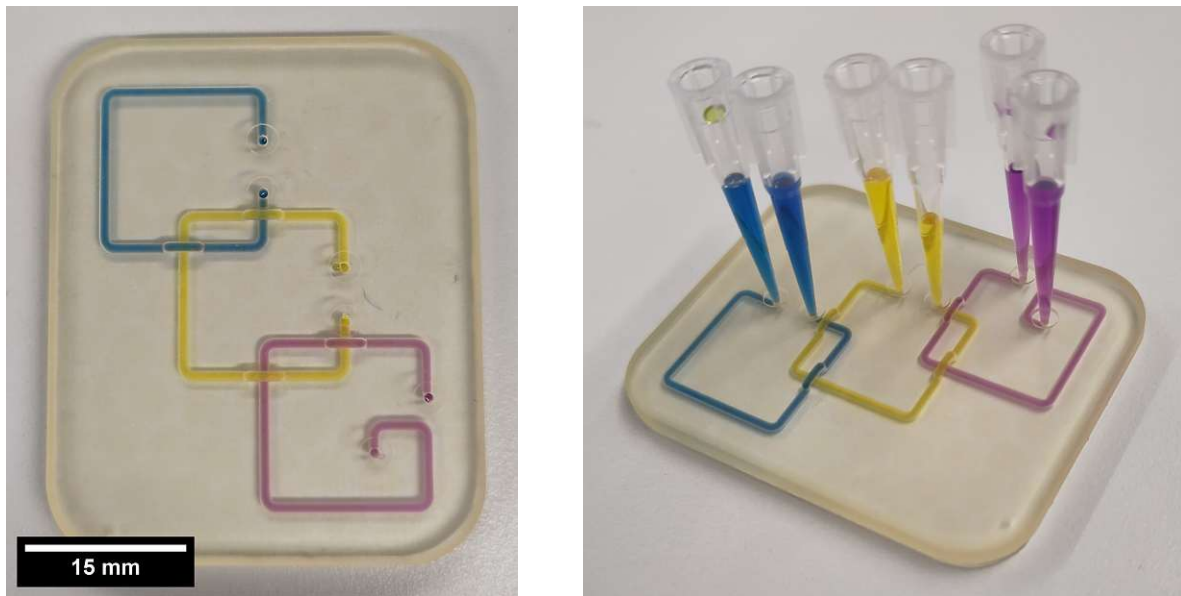


Figure 42: CCG shaped fluid router. Left: Filled channels. Right: Filling of the channels with pipette tips.

## 4.2 Classification of ASIGA 3D-Printer

### 4.2.1 Geometry Assessment

To assess the ability to print dimensionally accurate objects, an array of circles, squares and triangles were printed, varying in size. The features were printed as positive (lofted) and negative (sunken), and additionally with different layer heights.

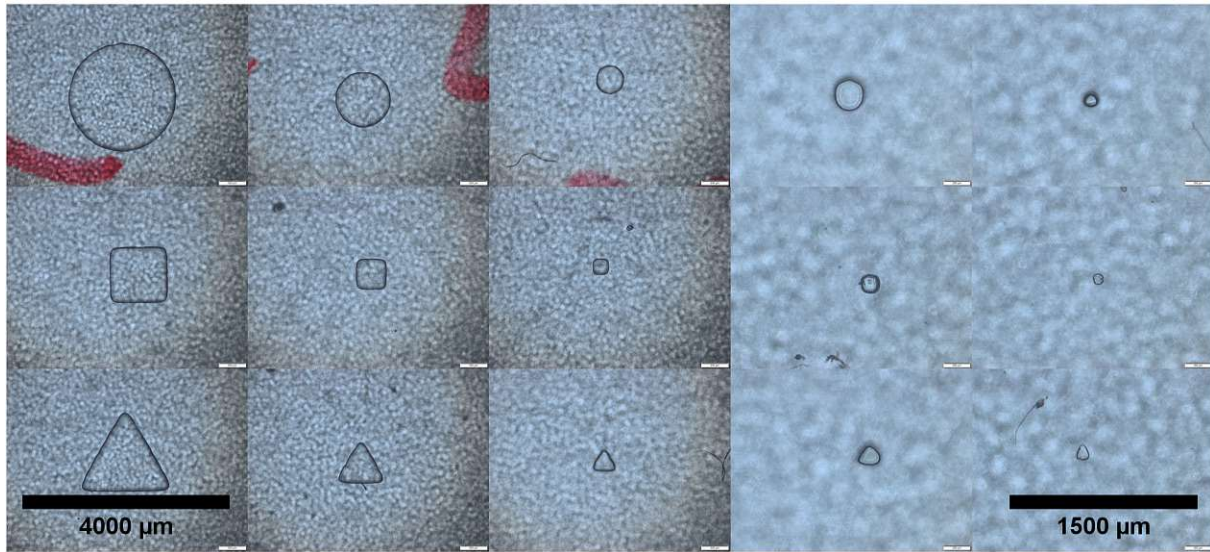


Figure 43: Lofted features, 25µm layer height. Material: PlasClear. The left scalebar accounts for image columns 1, 2 and 3. The right scalebar accounts for image columns 4 and 5.

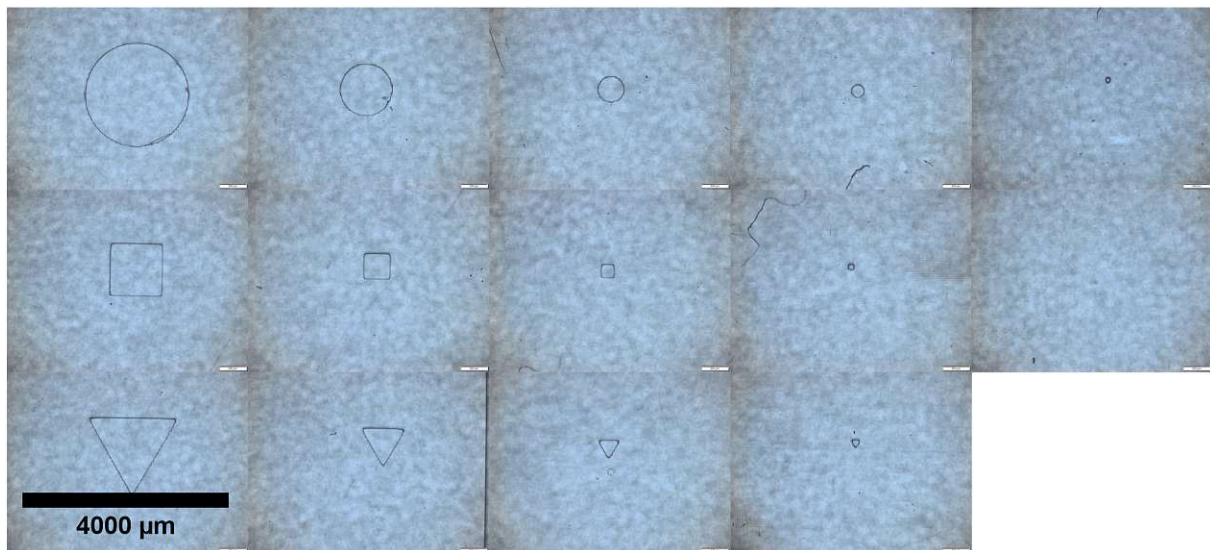


Figure 44: Sunken features, 25µm layer height. Material: NanoClear.

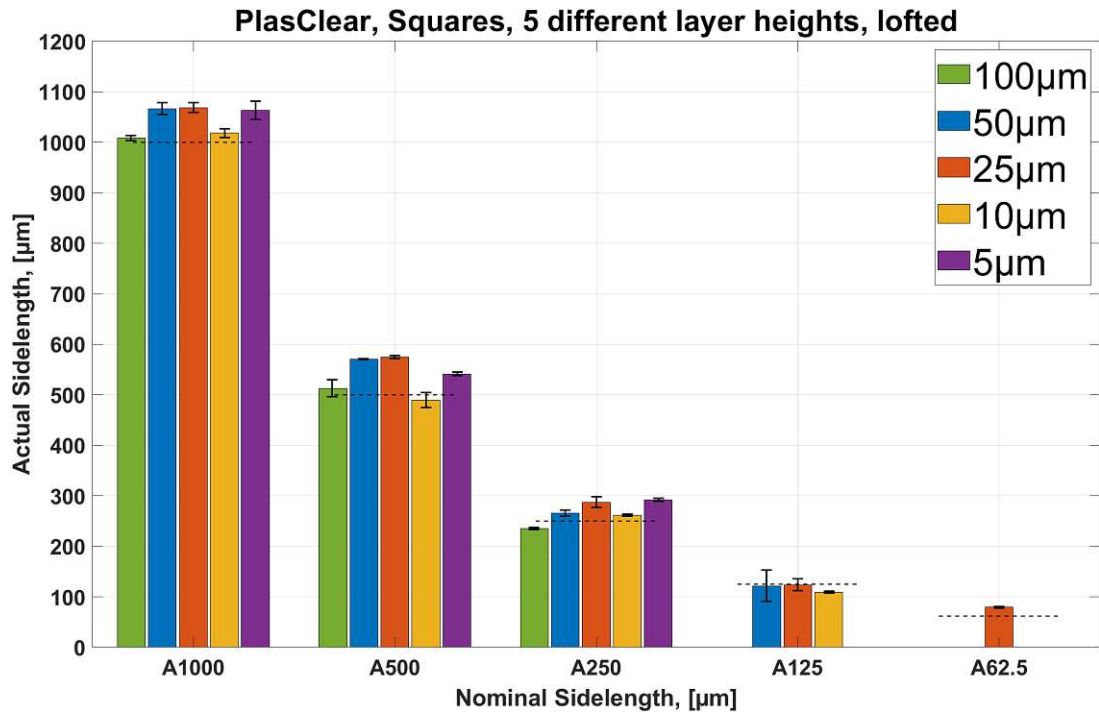


Figure 45: Actual over nominal sidelength of squared, lofted features. Printed with PlasClear, observed via brightfield microscopy (measurements form individual features, n=3), dotted line represents the nominal sidelength.

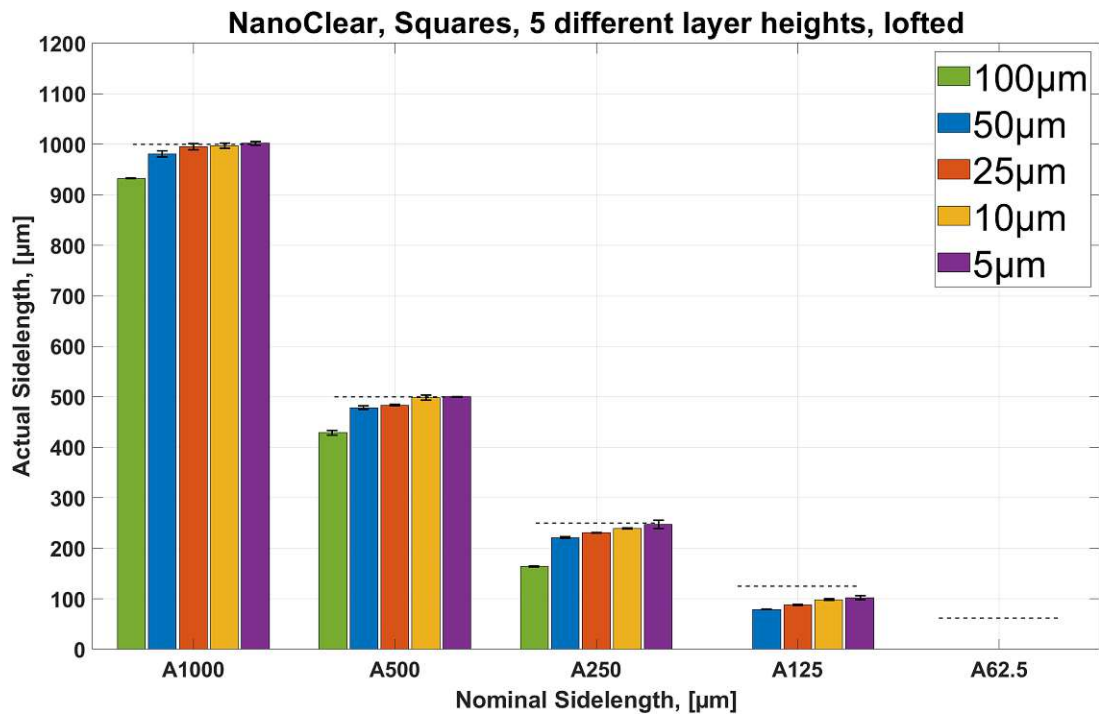


Figure 46: Actual over nominal sidelength of squared, lofted features. Printed with NanoClear, observed via brightfield microscopy (measurements form individual features, n=3), dotted line represents the nominal sidelength.

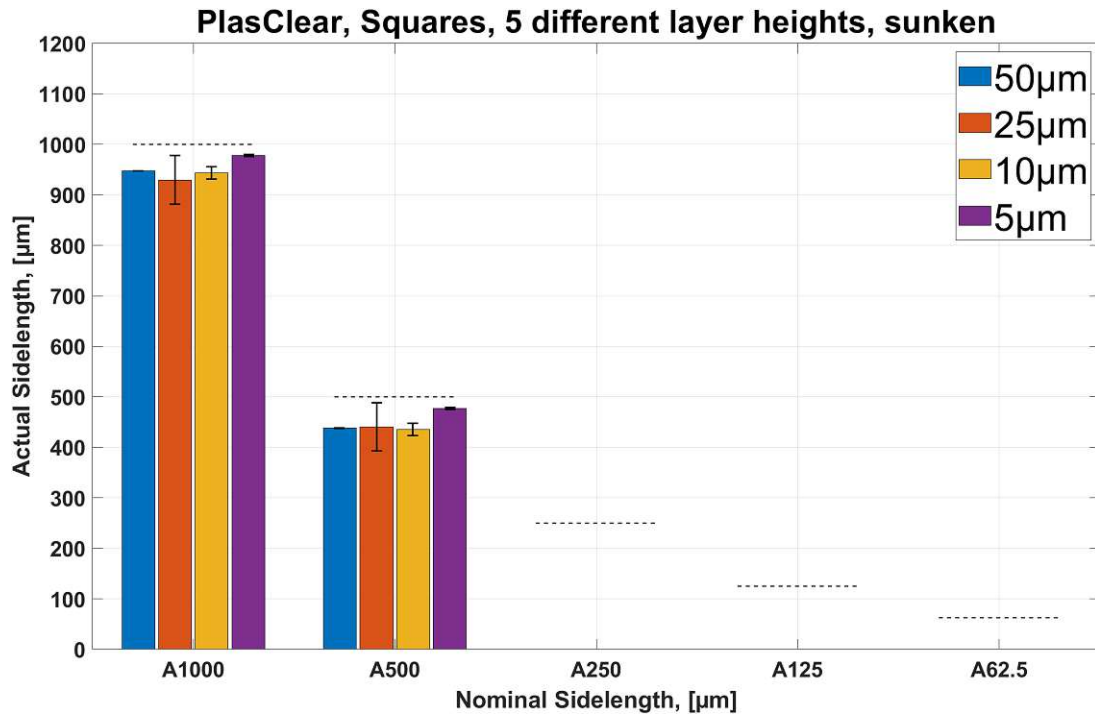


Figure 47: Actual over nominal sidelength of squared, sunken features. Printed with PlasClear, observed via brightfield microscopy (measurements form individual features,  $n=3$ ), dotted line represents the nominal sidelength.

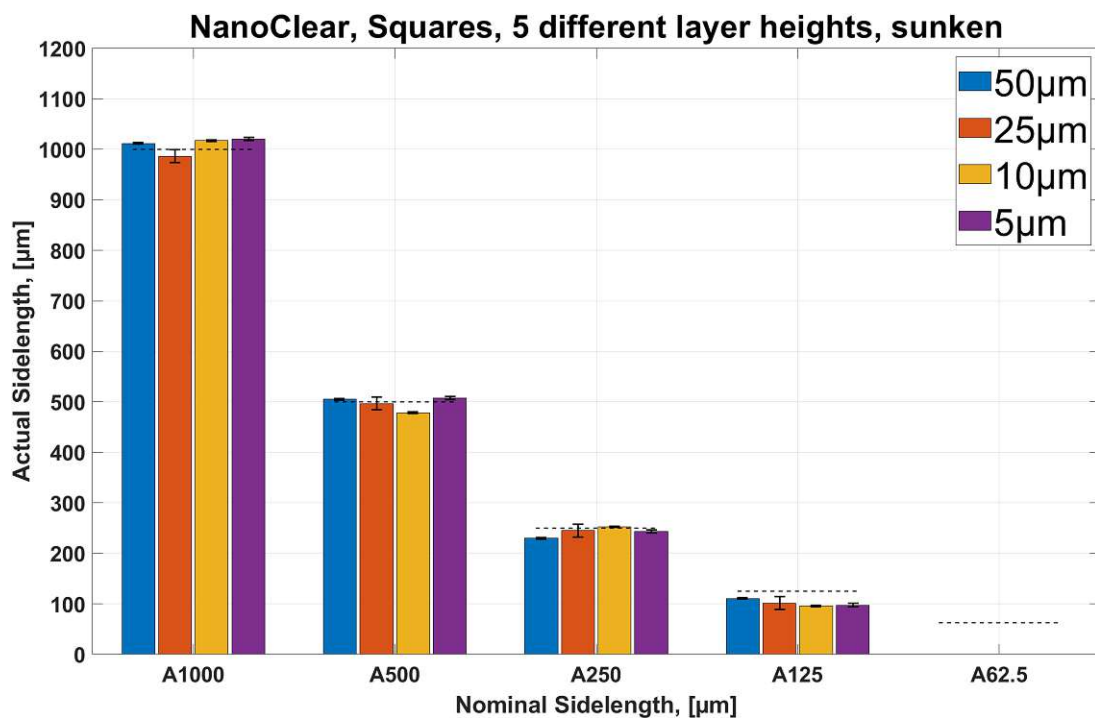


Figure 48: Actual over nominal sidelength of squared, sunken features. Printed with NanoClear, observed via brightfield microscopy (measurements form individual features,  $n=3$ ), dotted line represents the nominal sidelength.

The "squares assessment" is visualized in Figures 45, 46, 47 and 48. On the x-Axis, the nominal length of the squares side is represented, 'A' indicating the sidelength, followed by the numerical value of the length in  $[\mu\text{m}]$ . The measurement data for all geometries (circles, squares and triangles) can be found in the appendix in Table 15 and 16. The features were printed positive (lofted) and negative (sunken). With NanoClear, smaller sunken features could be created compared to PlasClear. The smallest visible sunken features with NanoClear had a sidelength of  $125\mu\text{m}$ , whereas PlasClear could only produce sunken features with a sidelength of  $500\mu\text{m}$ . This effect is most likely due to the difference in viscosity.

#### 4.2.2 Height Assessment

**Total print height evaluation:** After receiving strongly deviating object heights for different prints, further examination was required. To investigate this issue, an array of  $10\text{mm} \times 10\text{mm} \times 1\text{mm}$  cuboids was distributed across the build platform. After analyzing their thickness, it turned out that the total object height was dependent on the placement of the printed part on the build plate. After consultation with the vendor, a corrective measure was found. Figure 49 shows cuboids before (left) and after (right) proper z-axis calibration, demonstrating that the effect could be mitigated, but not eliminated completely.

Table 10: Z-axis calibration effect on cuboid thickness.

Z-axis calibration	Thickness measured [mm]	
	before calibration	after calibration
LB	1.07	1.01
LF	1.07	1.01
M	1.07	1.02
RB	1.00	1.00
RF	1.00	1.00

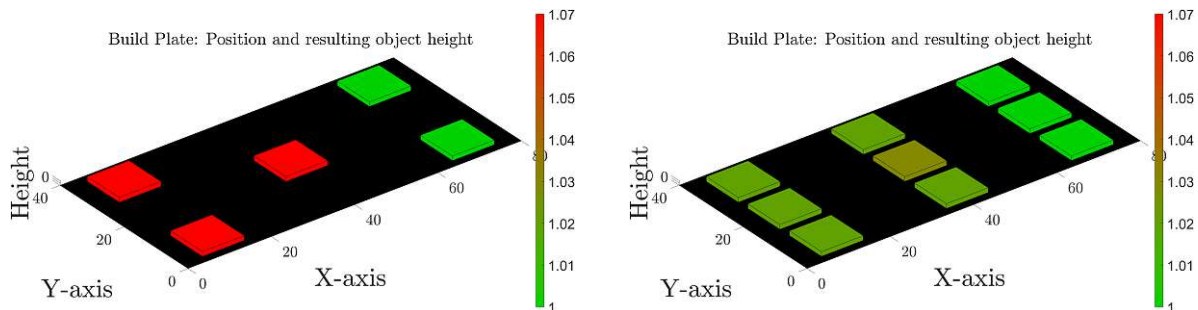


Figure 49: Build plate skewness effect. Left: before calibration. Right: after calibration.

**Local height evaluation:** To analyze the height of smaller features of an object, two different methods were established. First, for PlasClear, a rod with features (half-circles)

distributed across it was printed and later analyzed under the microscope. Those values need to be interpreted carefully, since there might be inaccuracies due to the placement of the rod and problems with focussing the small features inside the microscope. Nevertheless, the results can be found in Table 11, showing that the actual height lies within a range of 10-20 microns from the actual value. As mentioned above, the result might not be 100% accurate since there is the possibility of the analyzed object being tilted while inspected with the microscope. To increase the accuracy of the measurement, the layers were analyzed from the side for NanoClear. Further, to eliminate measurement errors, the distance between multiple layers was measured and then divided by the number of layers inbetween. The mean of multiple measurements and their standard deviation can be found in Table 12, showing that the accuracy in z-direction lies within a maximum deviation of 3  $\mu\text{m}$  from the nominal value.

Table 11: PlasClear, evaluated feature height.

Actual measured object height for different layer heights	
Layer Height	Nominal Height: 200 $\mu\text{m}$
100 $\mu\text{m}$	214.00 $\pm$ 11.69 $\mu\text{m}$
10 $\mu\text{m}$	215.01 $\pm$ 6.27 $\mu\text{m}$
5 $\mu\text{m}$	209.97 $\pm$ 6.31 $\mu\text{m}$

Table 12: Accuracy in z-direction for NanoClear.

Nominal Height	Actual Height
10 $\mu\text{m}$	9.555 $\pm$ 0.248 $\mu\text{m}$
25 $\mu\text{m}$	24.960 $\pm$ 0.904 $\mu\text{m}$
50 $\mu\text{m}$	48.453 $\pm$ 0.404 $\mu\text{m}$
100 $\mu\text{m}$	97.384 $\pm$ 0.471 $\mu\text{m}$

### 4.2.3 Partial Walls Assessment

Partial walls are an essential feature in microfluidics and lab-on-a-chip applications, since they enable the loading of a hydrogel without leaking into a parallel channel (e.g. one containing medium). Therefore, the printers ability to produce them was assessed. The partial walls were printed with a height of 100  $\mu\text{m}$  and 200  $\mu\text{m}$ , and had a thickness range of 50-200  $\mu\text{m}$ , which corresponds to an aspect ratio of maximum 4:1 and minimum 1:2. The walls were printed with four different layer heights, 5  $\mu\text{m}$ , 10  $\mu\text{m}$ , 25  $\mu\text{m}$  and 50  $\mu\text{m}$ . NanoClear performed better overall compared to PlasClear, especially for the sunken walls. The smallest lofted walls printed with NanoClear were 80  $\mu\text{m}$  in thickness, and they could be produced with all four tested layer heights. For PlasClear, the smallest walls had a thickness of 120  $\mu\text{m}$  and could also be produced with all four tested layer heights. The results are visualized below, in Figures 50 and 51.

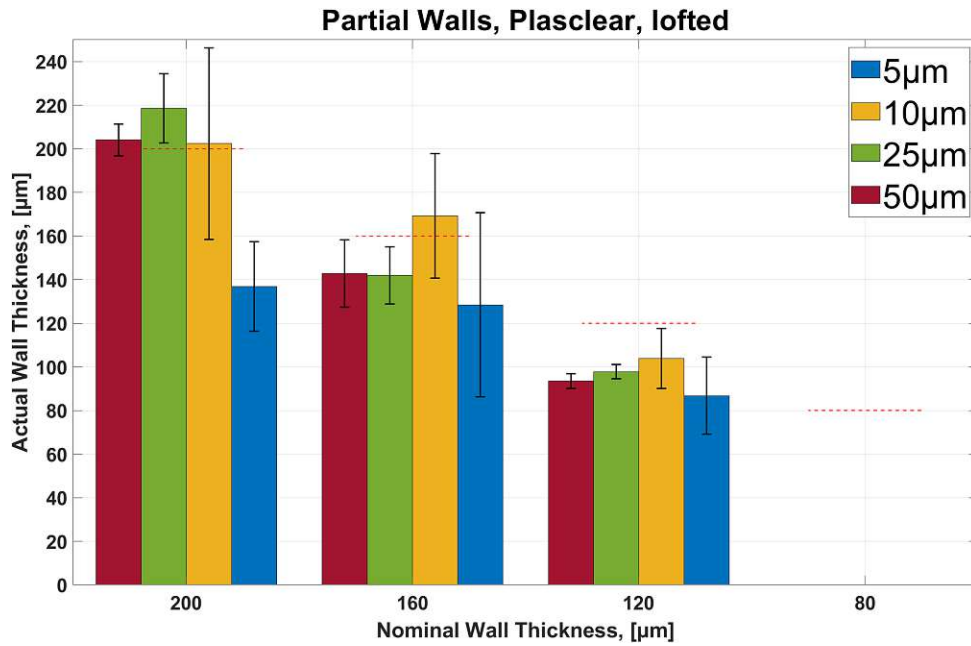


Figure 50: Actual over nominal thickness of lofted walls. Printed with PlasClear, observed via brightfield microscopy (measurements form individual walls, n=4), dotted line represents the nominal sidelength.

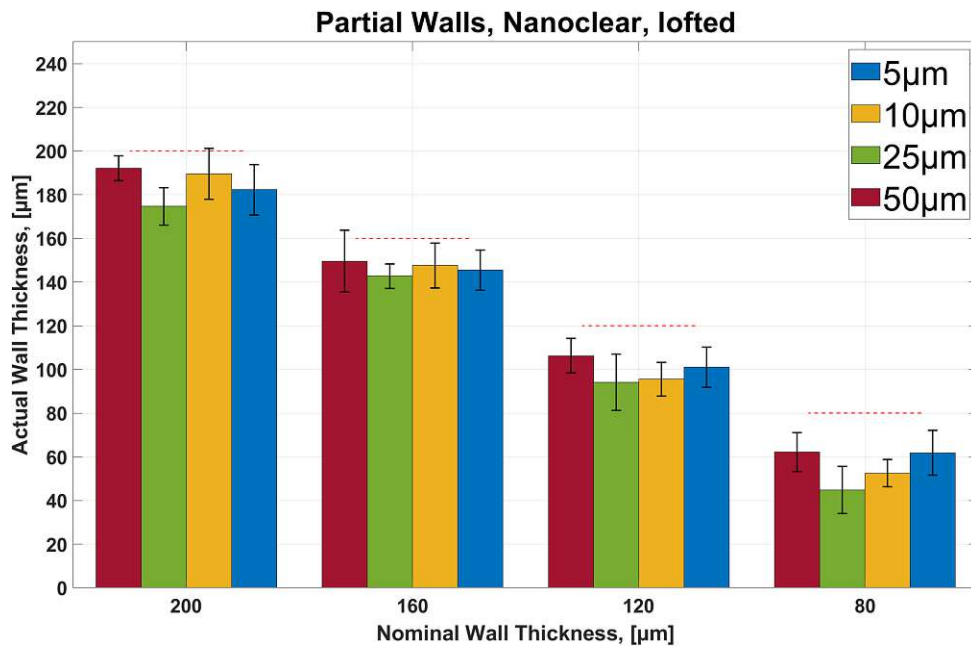


Figure 51: Actual over nominal thickness of lofted walls. Printed with NanoClear, observed via brightfield microscopy (measurements form individual walls, n=4), dotted line represents the nominal sidelength.

The smallest sunken 'walls' printed were 80  $\mu\text{m}$  in thickness for NanoClear, with layer heights 50  $\mu\text{m}$  and 10  $\mu\text{m}$  delivering the smallest walls. For PlasClear, the smallest sunken walls could be created with a layer height of 10  $\mu\text{m}$ , and the value was a minimum wall thickness of 120  $\mu\text{m}$ . The results are visualized in Figures 52 and 53.

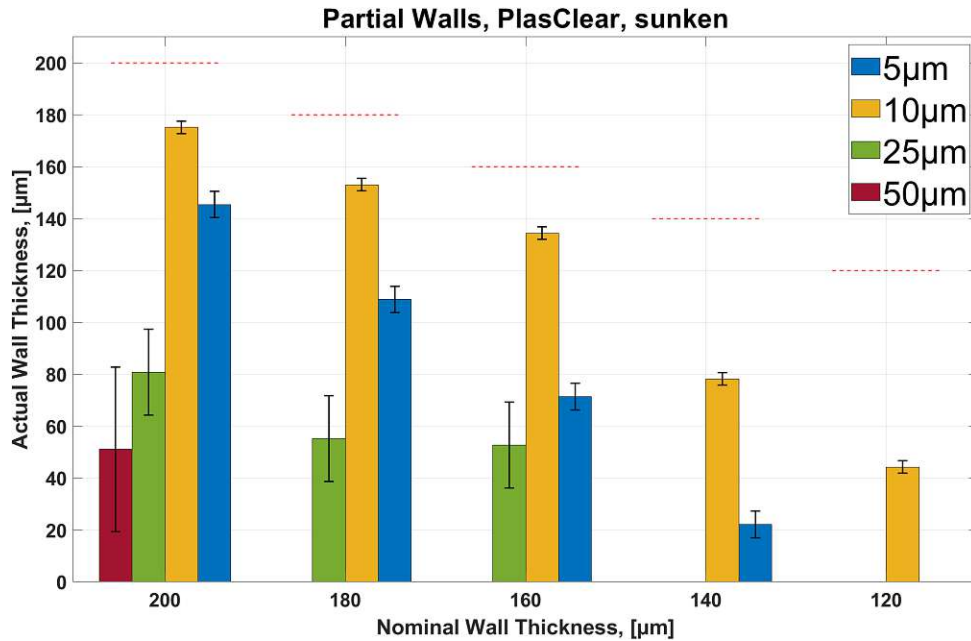


Figure 52: Actual over nominal thickness of sunken "walls". Printed with PlasClear, observed via brightfield microscopy (measurements form individual walls,  $n=4$ ), dotted line represents the nominal sidelength.

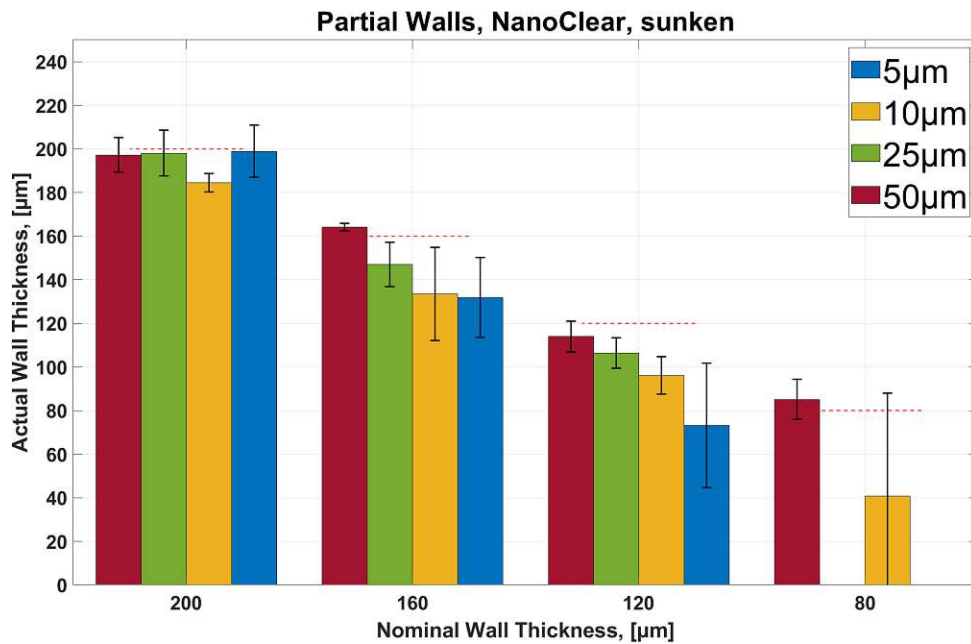


Figure 53: Actual over nominal thickness of sunken "walls". Printed with NanoClear, observed via brightfield microscopy (measurements form individual walls,  $n=4$ ), dotted line represents the nominal sidelength.

#### 4.2.4 Pillars Assessment

Another important feature in microfluidics are pillars, since as an example, pillars enable gel loading without leaking into parallel channels - similar to the partial walls. Five pillars, with 43  $\mu\text{m}$  increments from 43  $\mu\text{m}$  to 215  $\mu\text{m}$  were printed, visualized in Figure 54. Those values were chosen due to the single pixel size of 43  $\mu\text{m}$  for the DLP printer.

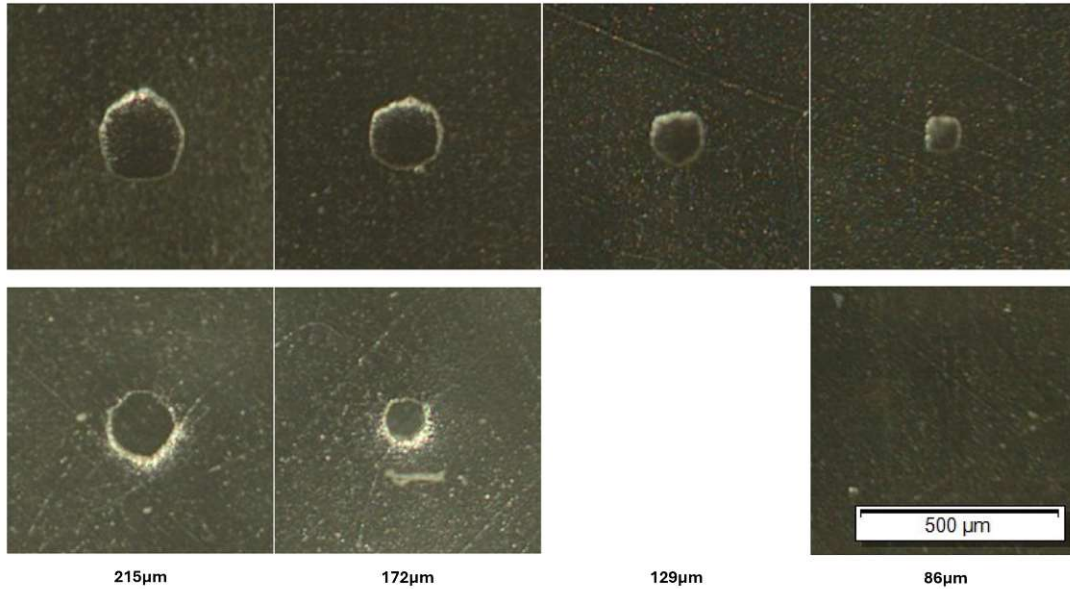


Figure 54: Pillars, printed with NanoClear. Top: lofted. Bottom: sunken. Size: from left to right: 215  $\mu\text{m}$ , 172  $\mu\text{m}$ , 129  $\mu\text{m}$ , 86  $\mu\text{m}$  and 43  $\mu\text{m}$ .

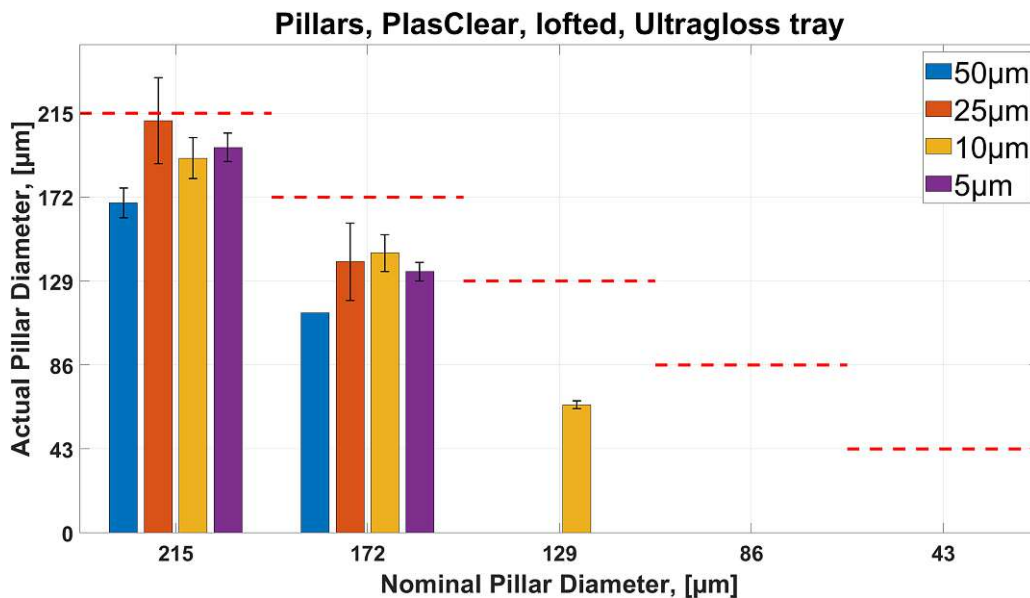


Figure 55: PlasClear, actual vs. nominal pillar diameter, lofted. Observed via brightfield microscopy (measurements from individual pillars,  $n=5$ ), dotted line: nominal diameter.

**Lofted Pillars:** NanoClear performed better compared to PlasClear, the smallest pillar produced with NanoClear was 86  $\mu\text{m}$  in diameter for both, the universal tray and the LowForce tray (see Figures 56 and 57). The smallest pillar produced with PlasClear was 129  $\mu\text{m}$  in diameter, and could only be performed with a layer height of 10  $\mu\text{m}$  (see Figure 55). The empty columns (86 $\mu\text{m}$  and 43 $\mu\text{m}$  for PlasClear, 43  $\mu\text{m}$  for NanoClear) signify that the pillars could not be created by the printer.

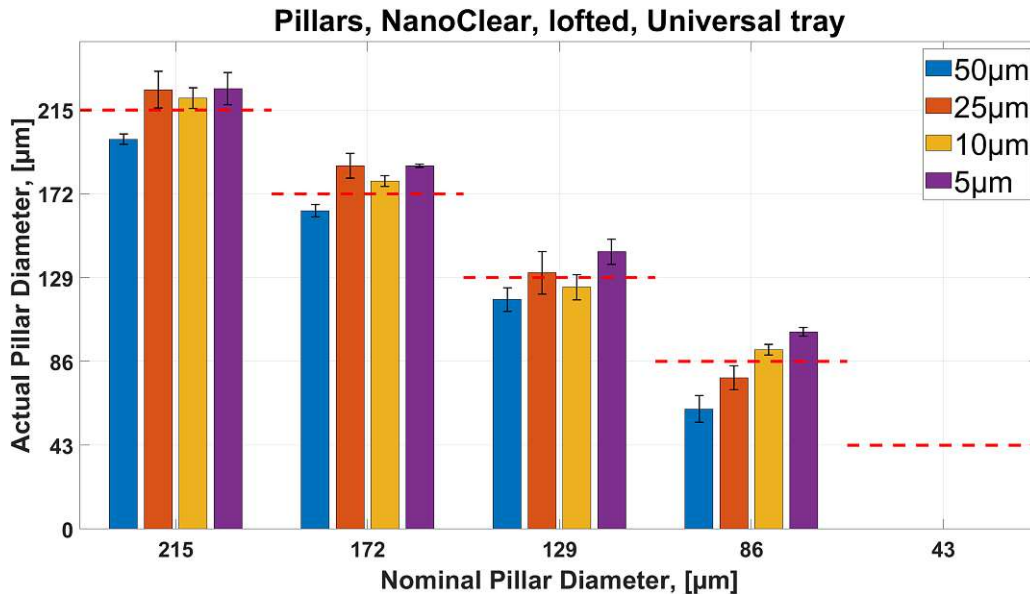


Figure 56: NanoClear, actual vs. nominal pillar diameter, lofted, Universal tray. Observed via brightfield microscopy (measurements form individual pillars,  $n=5$ ), dotted line: nominal diameter.

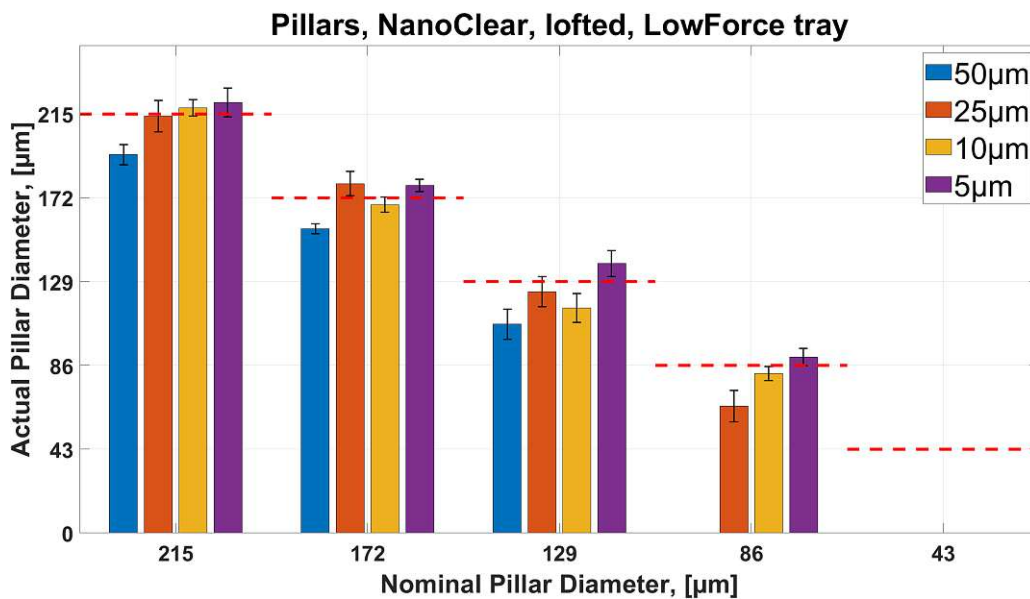


Figure 57: NanoClear, actual vs. nominal pillar diameter, lofted, LowForce tray. Observed via brightfield microscopy (measurements form individual pillars,  $n=5$ ), dotted line: nominal diameter.

**Sunken Pillars:** For PlasClear, the sunken features were too small to be visible, the holes remained closed although the contour could be seen vaguely. This is again most likely due to the viscosity of the resin. However, sunken pillars could be printed when using the NanoClear resin, as shown in Figures 58 and 59. Compared to the lofted features, the sunken pillars had their limit at a nominal diameter of 172 $\mu\text{m}$ , and the actual diameter was around 90 $\mu\text{m}$  smaller than nominal. The empty columns (129  $\mu\text{m}$ , 86  $\mu\text{m}$  and 43  $\mu\text{m}$ ) signify that the pillars could not be created by the printer.

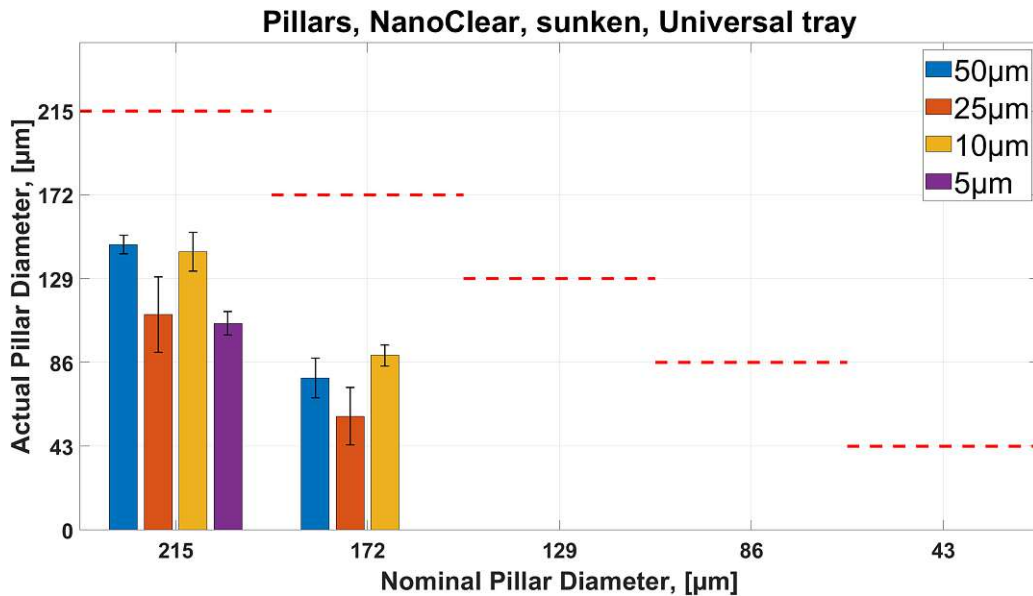


Figure 58: NanoClear, actual vs. nominal pillar diameter, sunken, Universal tray. Observed via brightfield microscopy (measurements form individual pillars, n=5), dotted line: nominal diameter.

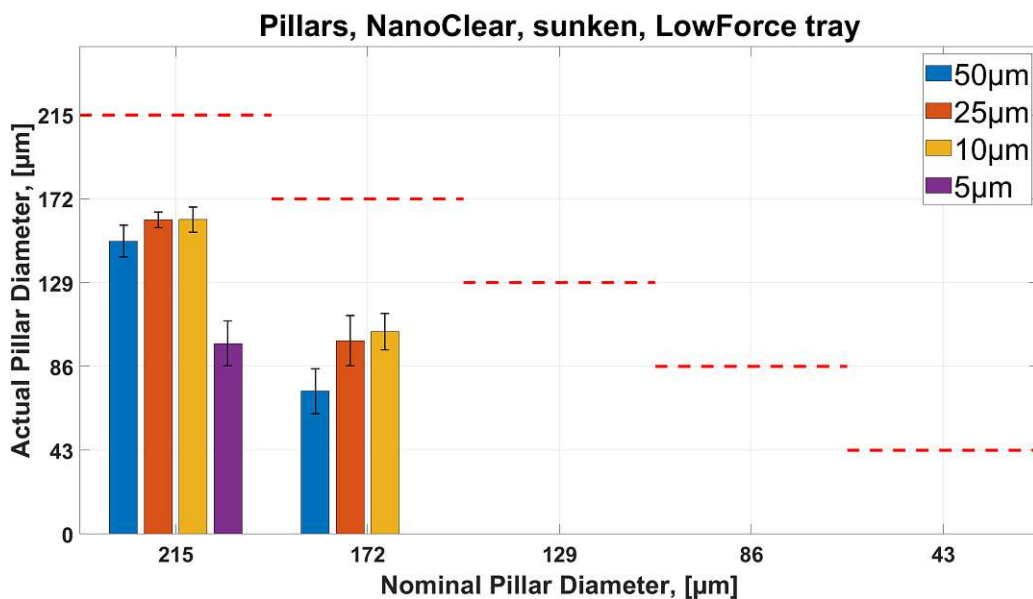


Figure 59: NanoClear, actual vs. nominal pillar diameter, sunken, LowForce tray. Observed via brightfield microscopy (measurements form individual pillars, n=5), dotted line: nominal diameter.

### 4.2.5 Channels Assessment

As mentioned in chapter 1.2, printing microfluidic chips at once is highly valuable in microfluidics because it eliminates the need for additional manufacturing steps. To achieve this, low-viscosity resins are beneficial because they allow for easier removal of residual resin material from the channels after printing. The mechanism of trapping resin in a microfluidic channel during a print is illustrated in Figure 60. The resins ("PlasClear" by Asiga, "BioMed Clear" by FormLabs) imposed difficulties when trying to remove them from microfluidic channels during post-processing, due to its relatively high viscosity. Factors that impact resin removal from channels are, among others, flow-resistance, channel length and surface roughness. With a low-viscosity resin, the cleaning would become easier, and more complex microfluidic chips could be printed.

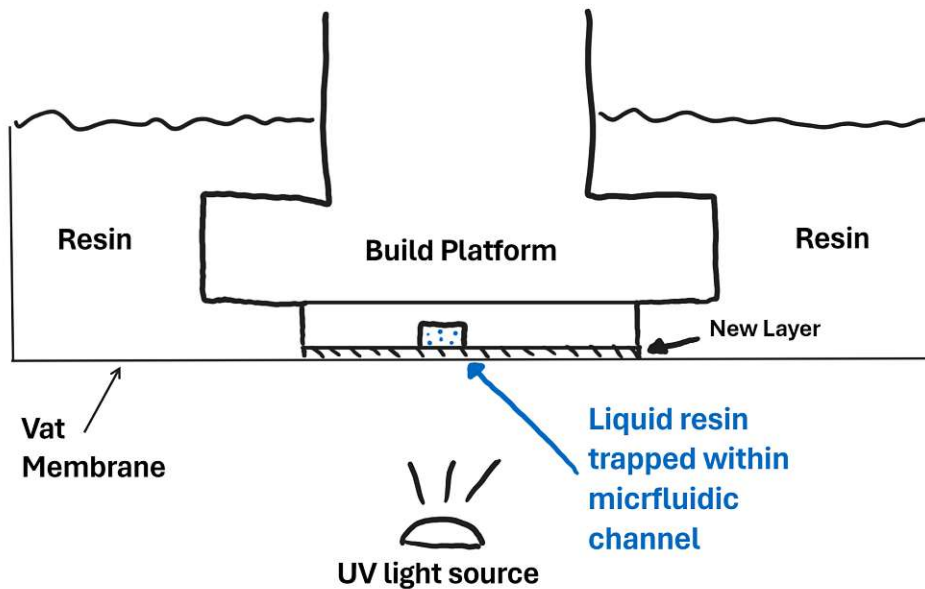


Figure 60: Schematic of trapped resin in a microfluidic channel.

After evaluating channels, that were laid out flat on the build platform, under the microscope, a pillary structure was emerging at the channels' "lid". This structure stems from stray UV-light penetrating into the channel, and since the channel is filled with resin (see Figure 60), some parts of the trapped resin get cured by the light. This is a strong limitation in resin 3D-printing, however, it could be mitigated by Zhiming et al. [50] A cross section of the channel can be seen in Figure 62. Here, the single pillars represent the single pixels of the DLP printer. These pillars influence the overall geometry and furthermore a higher surface roughness is imposed at the site of the the channel-lid.

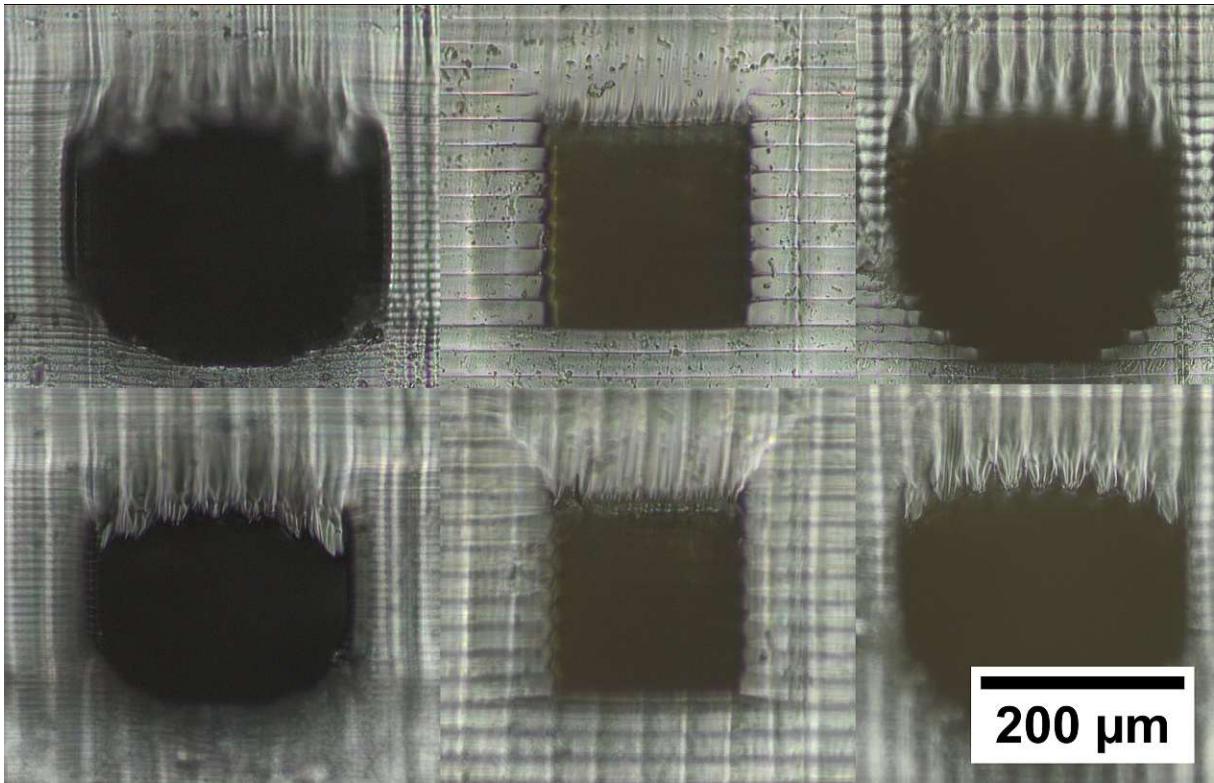


Figure 61: Emerging structure at channel "lid". Image acquired with optical microscope Olympus IX83.

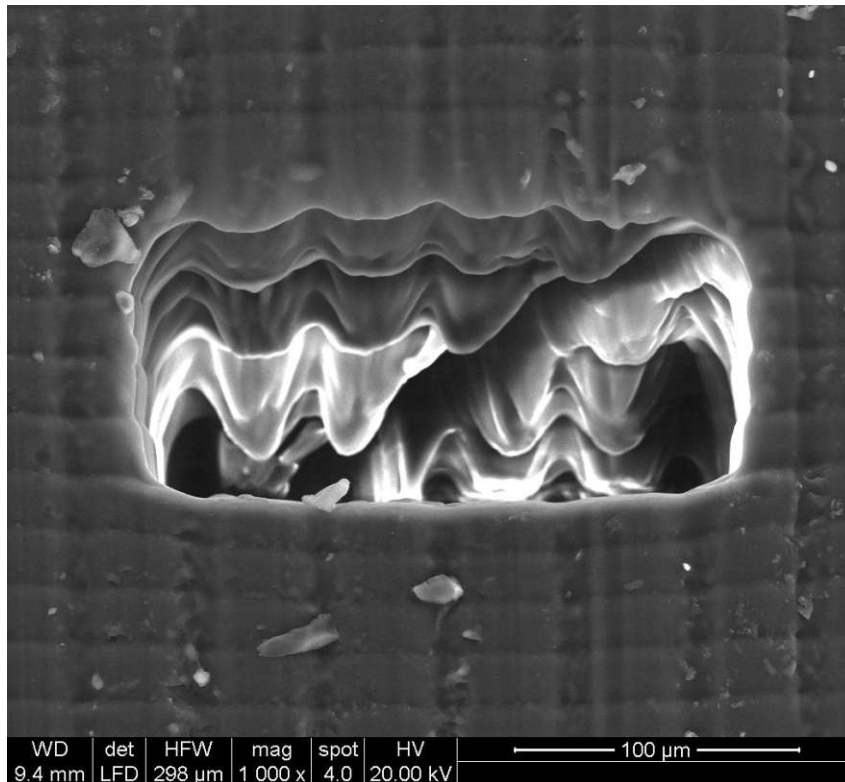


Figure 62: Scanning Electron Microscope image of a rectangular channel.

Another important finding of printing channels is illustrated in Figure 63. The border of the printed part is less affected by stray light compared to the inside. When looking at a print with channels from the top (see Figure 64), this dynamic can also be observed. As a result, the channel appears to be unclogged at the borders, but is blocked on the inner part, since the pillary structure extends thus far into the channel.

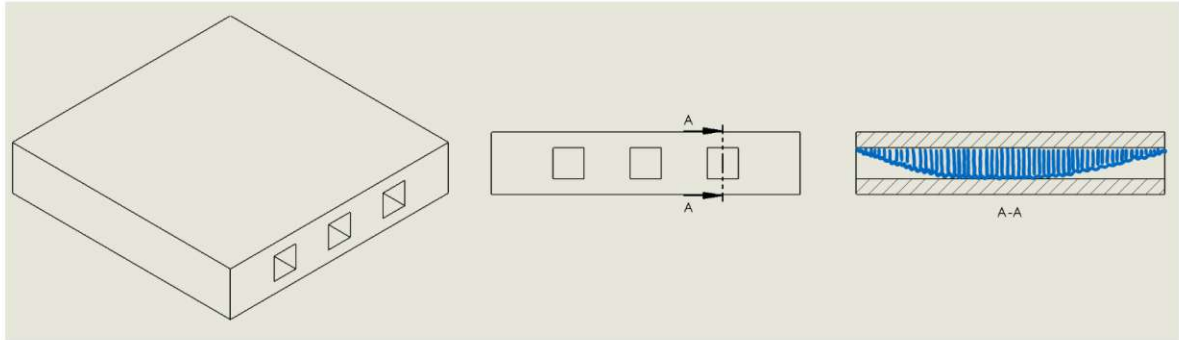


Figure 63: Curing dynamics: Difference between the border and the inside of channels. A-A indicates a sectional view of the inside of a channel. The emerging structure is visualized in blue. On the inside of the channel, the pillary structure reaches the bottom of the channel, subsequently blocking it, whereas on the sides, the channel remains free.

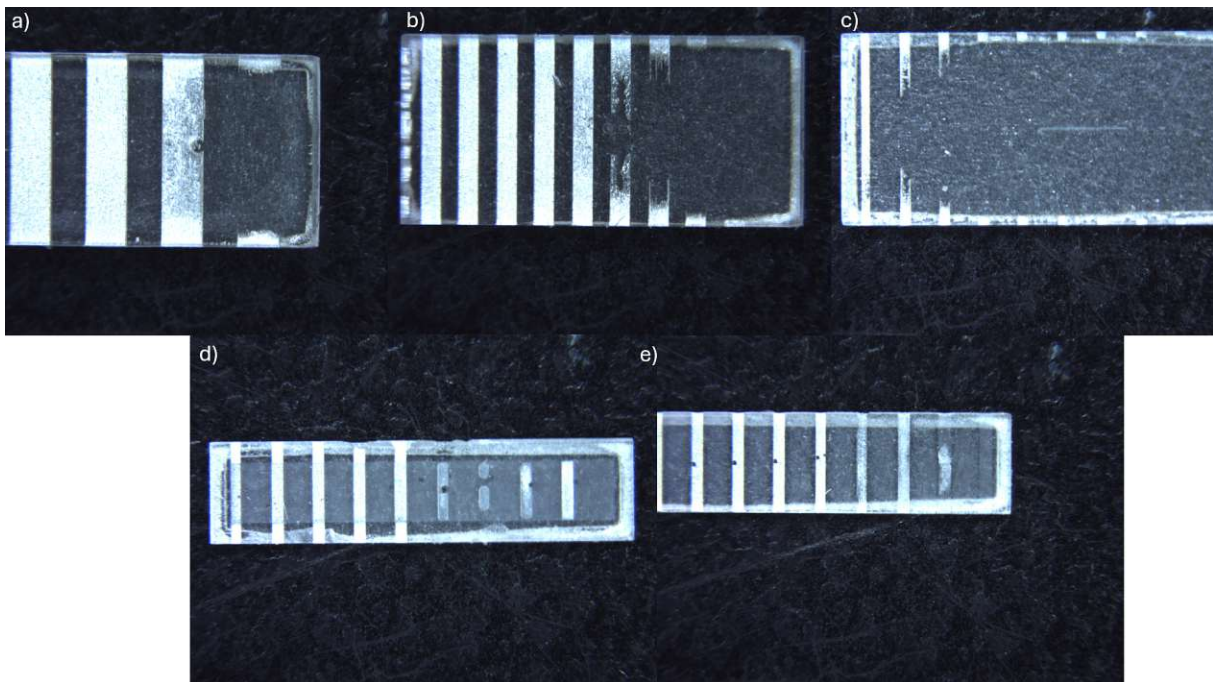


Figure 64: Topview. a) 100µm layer height, nominal value of narrowest non-clogged channel: 300µm. b) 50µm layer height, nominal value of narrowest non-clogged channel: 350µm. c) 25µm layer height, nominal value of narrowest non-clogged channel: 250µm, d) layer height 25µm, adaptation with reduced fill-exposure, nominal value of narrowest non-clogged channel: 150µm, e) layer height 25µm, adaptation with build manipulation, nominal value of narrowest non-clogged channel: 125µm.

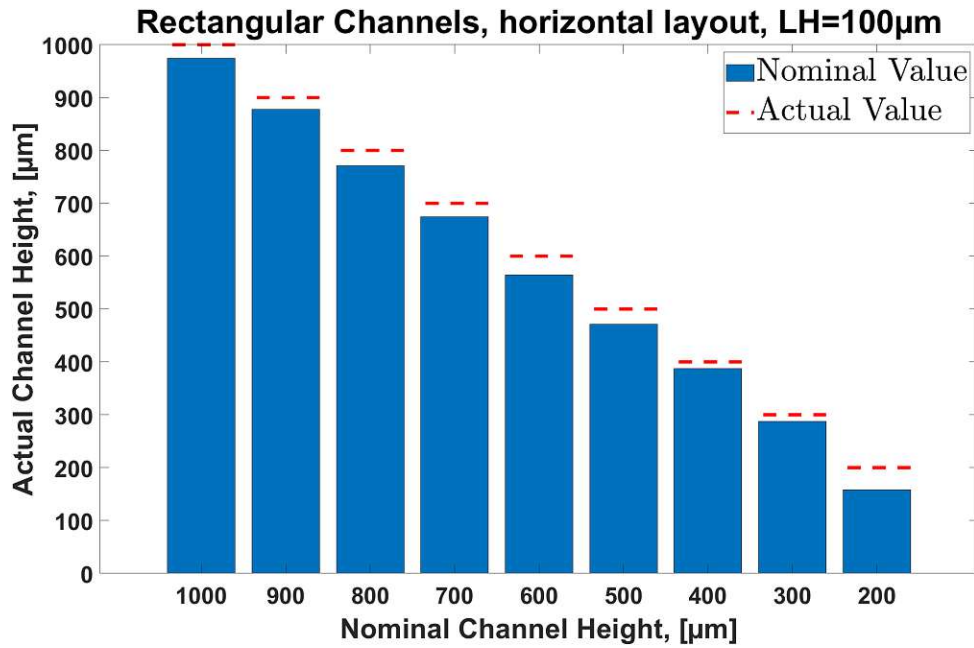


Figure 65: Evaluated channel heights. Material: NanoClear. Rectangular channels. Print layout: horizontal. 100µm layer height.

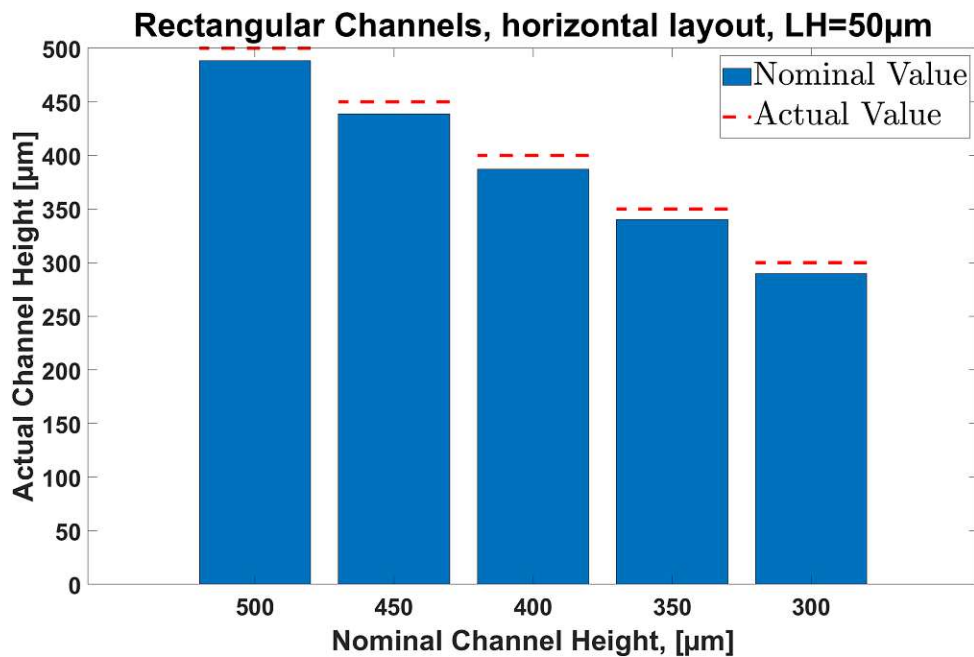


Figure 66: Evaluated channel heights. Material: NanoClear. Rectangular channels. Print layout: horizontal. 50µm layer height.

Figures 65, 66 and 67 show the evaluation of rectangular channels printed with different layer heights with NanoClear resin. The biggest channel dimension was for each layer height a tenfold of the layer height, whereas the smallest channel was dimensioned with the same value as the layer height. For example, when printing channels with 100 µm layer height, the biggest channel was  $100 \mu\text{m} * 10 = 1000 \mu\text{m}$ , and the smallest was 100 µm.

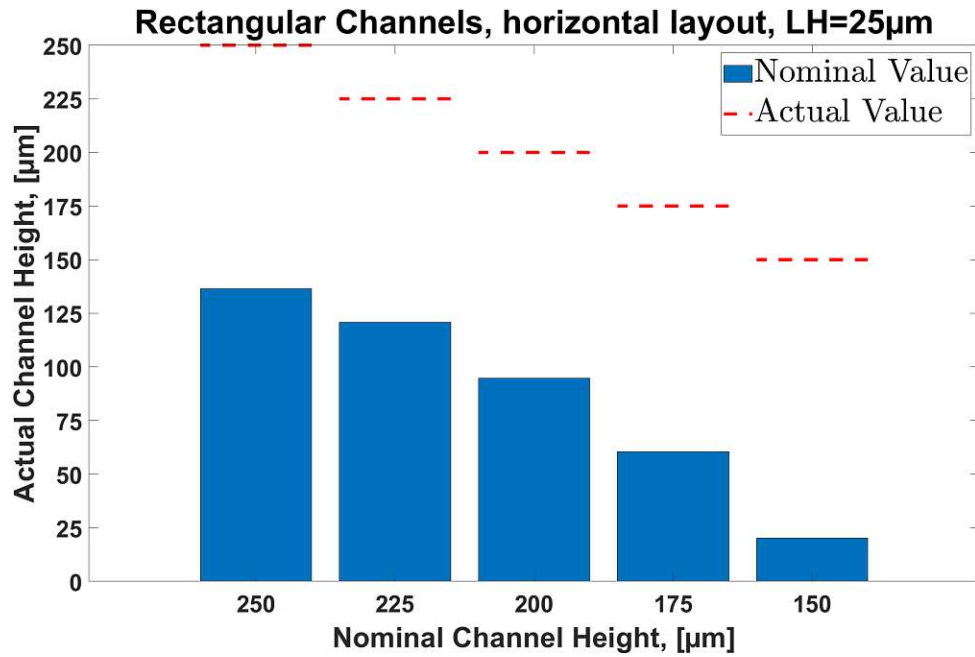


Figure 67: Evaluated channel heights. Material: NanoClear. Rectangular channels. Print layout: horizontal. 25µm layer height.

Table 13: Deviation from nominal channel height for different channels

Nominal vs. Actual channel height, Material: NanoClear								
LH 100µm			LH 50µm			LH 25µm		
Nom.	Act.	Diff.	Nom.	Act.	Diff.	Nom.	Act.	Diff.
1000	974.194	25.806	500	488.312	11.688	250	136.364	113.636
900	877.419	22.581	450	438.961	11.039	225	120.779	104.221
800	770.968	29.032	400	387.013	12.987	200	94.805	105.195
700	674.194	25.806	350	340.26	9.74	175	60.39	114.61
600	564.516	35.484	300	289.61	10.39	150	20.13	129.87
500	470.968	29.032						
400	387.097	12.903						
300	287.097	12.903						
200	158.065	41.935						
<b>Mean Diff.: 26.17µm</b>			<b>Mean Diff.: 11.17µm</b>			<b>Mean Diff.: 113.51µm</b>		

Table 13 shows the actual values of the in Figure 65, 66 and 67 plotted graphs, with additional absolute deviation from the nominal value. For a layer height of 10 µm, all channels were blocked. For a layer height of 25µm, the deviation was relatively large, resulting in channels that were about 50% smaller than the nominal value.

It has to be pointed out that the validity is to be questioned, since the sample size was only one for each channel.

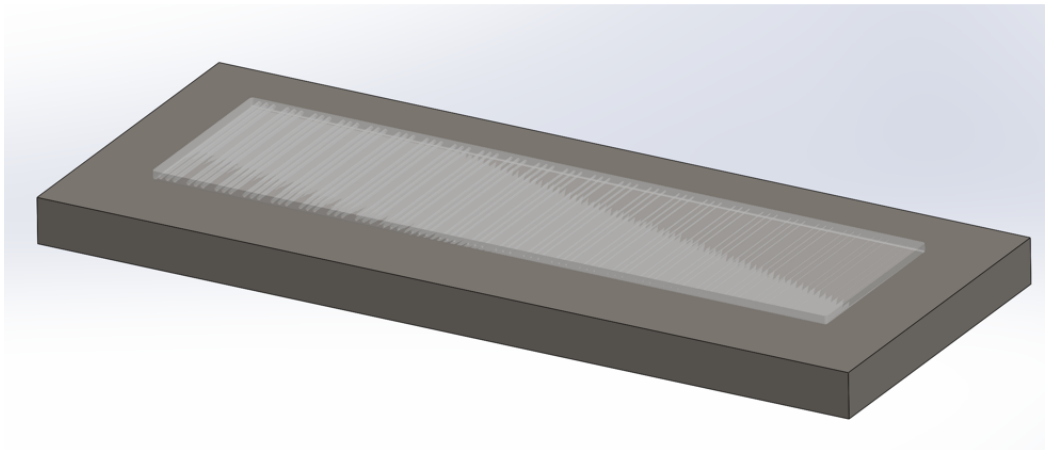
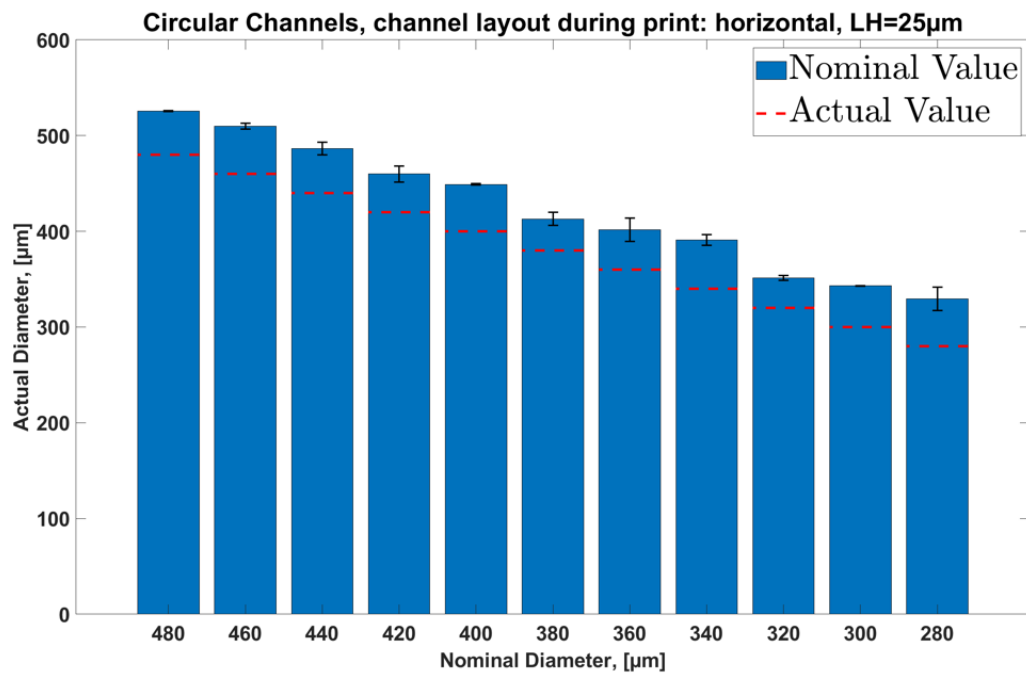


Figure 68: Circular channels, printed horizontally ("flat").

After trying several ways to develop a workflow for printing microfluidic channels without too rough surface at the roof layer, those pillary structures still emerge, regardless of what preventive method was tested. The pillary structure (roughness due to stray light) emerged for both, PlasClear and Nanoclear.

Changing the light intensity or layer thickness does not change the overall energy put into the layer, due to the calibration curve for the material that the printer uses, therefore still a very rough surface emerges.

The only thing left to try was a reduction of exposure time. This resulted in failed prints, most likely due to the weak adhesion between the layers.

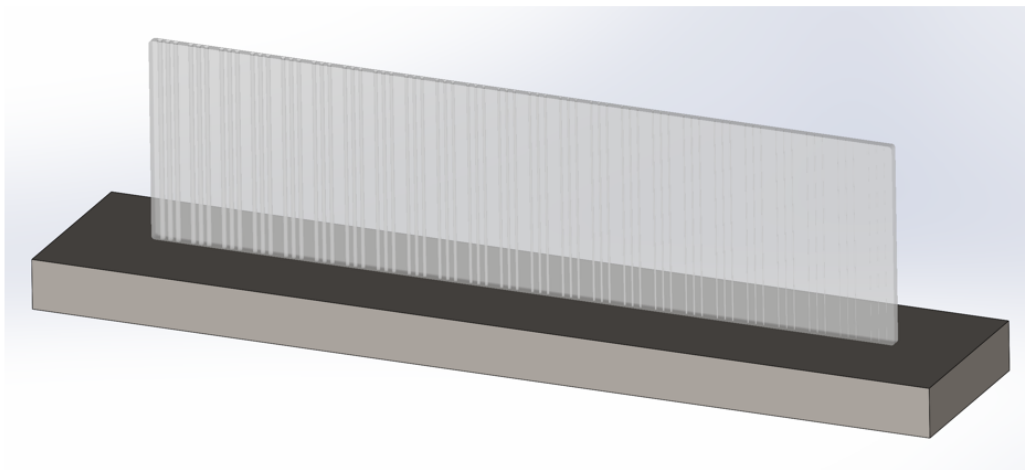
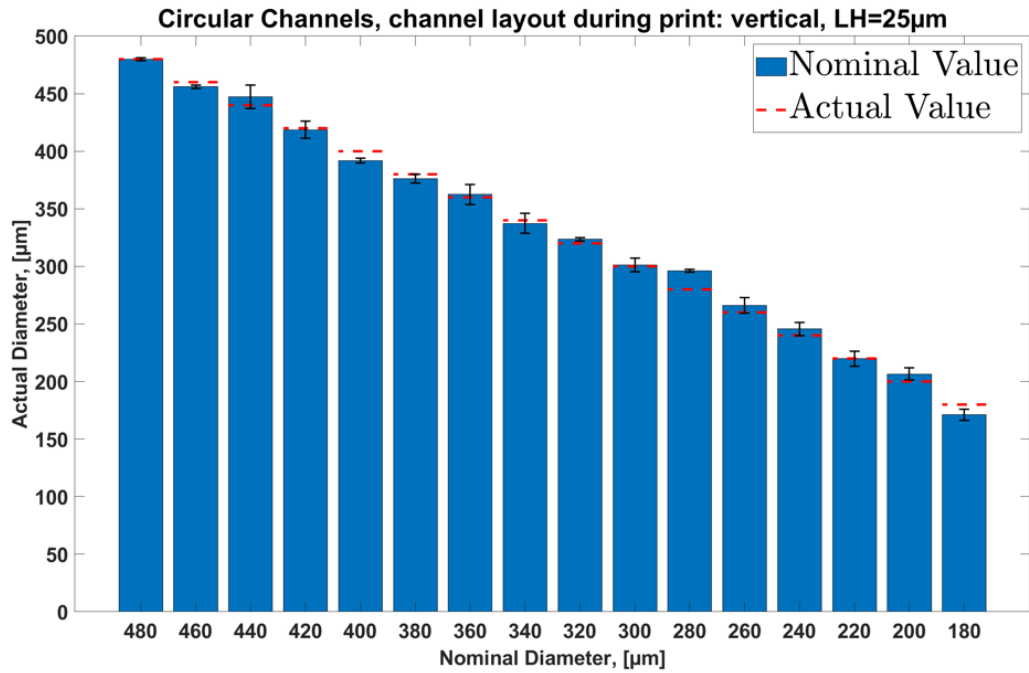


Figure 69: Circular channels, printed vertically ("upright").

**Printing channels vertically:** One way to prevent the above mentioned phenomenon is to print the microfluidic device upright, with the channel being oriented alongside the z-direction, although it has to be pointed out that there are limitations: i) print times for microfluidic chips may increase drastically, ii) the alignment only works for uni-directional channels, and iii) inlet and outlet might be affected by the same phenomenon as before, depending on the orientation on the chip.

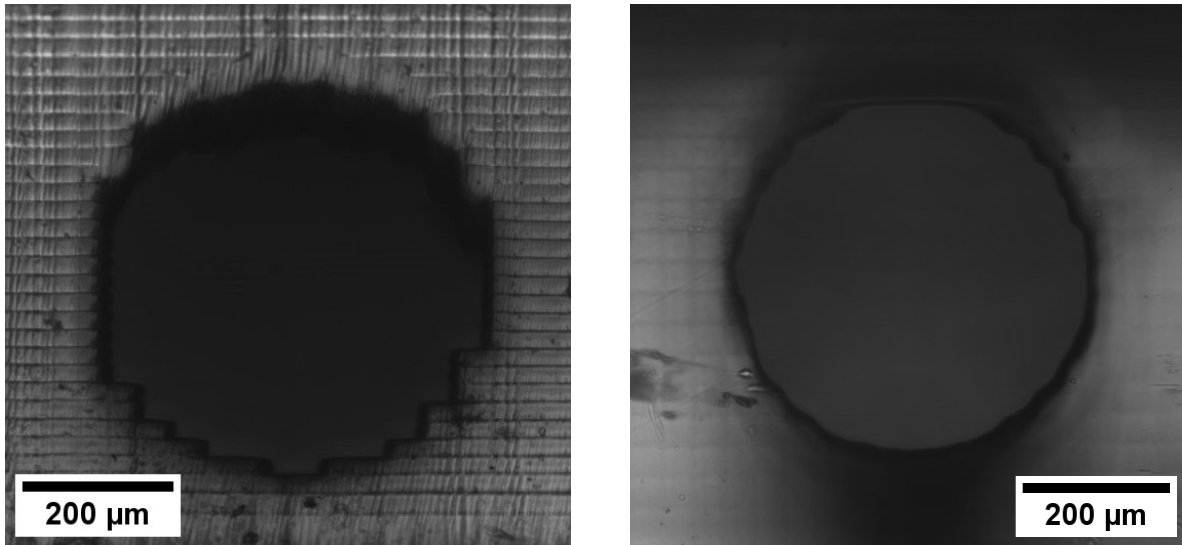


Figure 70: Effect of different printing orientations. Left: Channels printed flat. Right: Channels printed upright. Channel diameter (both):  $480\mu\text{m}$ .

Printing channels horizontally ("flat") resulted in a minimal actual channel diameter of around  $330\mu\text{m}$  (see results in Figure 68), a close-up of the channel can be seen in Figure 70 on the left.

Printing channels vertically ("upright") resulted in a minimal actual channel diameter of around  $171\mu\text{m}$  (see results in Figure 69), a close-up of the channel can be seen in Figure 70 on the right.

In summary, printing channels vertically, in alignment with the printers z-axis, results in a smoother, rounder channel as well as smaller producible channels, compared to printing channels horizontally.

#### 4.2.6 PDMS casting with NanoClear

PDMS casting can be done by 3D printing a mold, acting as a master for PDMS microfluidic chips. Since PlasClear was previously used for molding, and the new resin NanoClear was now available for printing, the ability of NanoClear to act as a PDMS mold was assessed. The molds were printed with  $25\mu\text{m}$  and  $50\mu\text{m}$  layer height. A positive and a negative mold was tested, resulting in a PDMS channel and a PDMS wall, respectively.

The nominal spacing for both, the channel and wall feature, was  $150\mu\text{m}$ . Table 14 shows the results of the actual dimensions. Printing the molds with a layer height of  $25\mu\text{m}$  resulted in a very thick PDMS wall for the horizontal alignment, and no results for the vertical alignment, whereas the PDMS channels delivered results that were closer to the nominal value of  $150\mu\text{m}$ . For the  $25\mu\text{m}$  layer height molds, there was still a lot of liquid PDMS remaining after removing the mold, and the poor results might stem from the PDMS not hardening properly due to certain factors.

For a layer height of  $50\mu\text{m}$ , the results of PDMS walls and channels lie in closer vicinity to the nominal value of  $150\mu\text{m}$ , the removal of the mold was easier and less liquid resin remained in the mold.

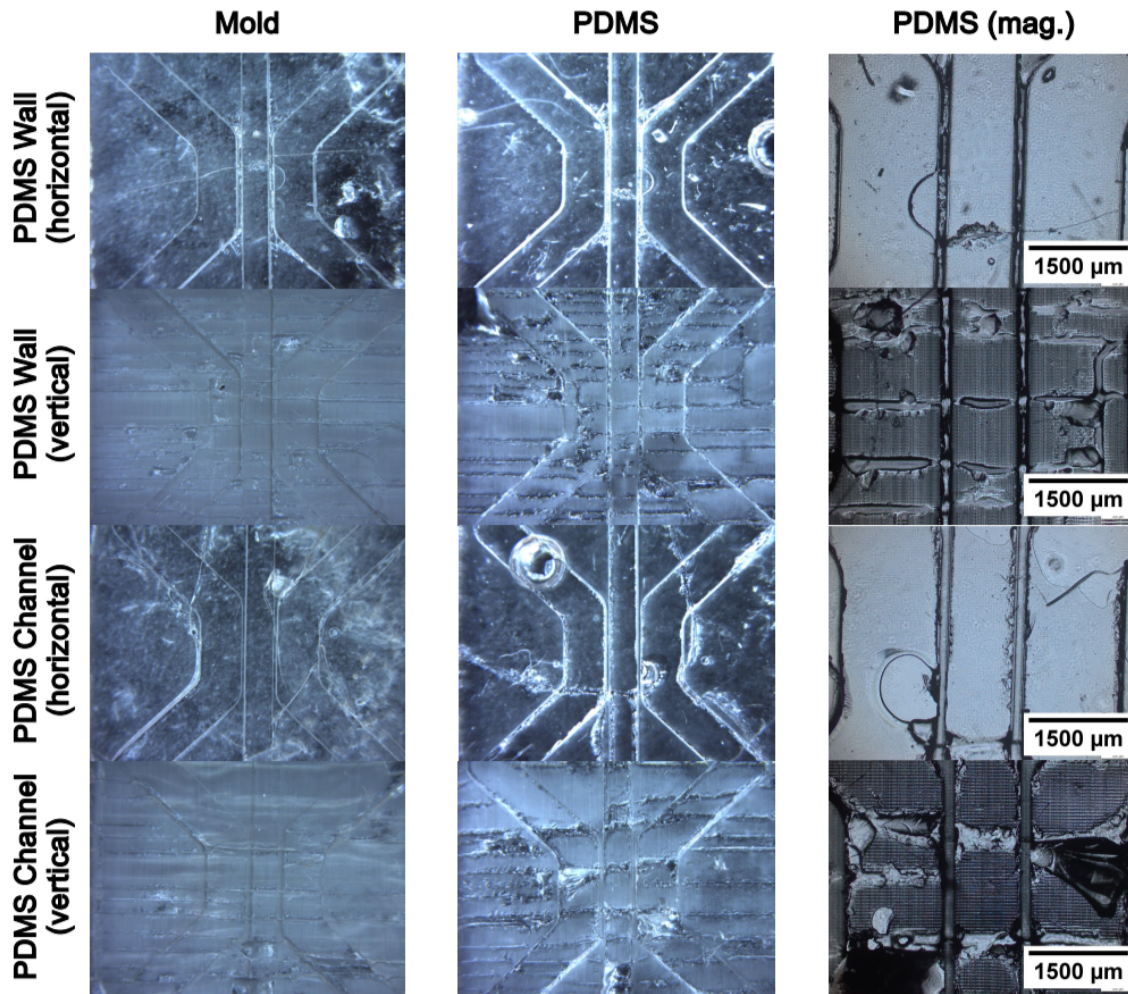


Figure 71: PDMS mold (left) and PDMS chip (middle) inspected under a microscope. Right: magnified (mag.) PDMS features (wall/channel).

Table 14: PDMS-Channel and -Wall actual measured dimensions. Nominal wall/channel width:  $150\mu\text{m}$ .

Nominal: <b><math>150\mu\text{m}</math></b>	$25\mu\text{m}$		$50\mu\text{m}$	
	Horizontal	Vertical	Horizontal	Vertical
PDMS Wall	$261.99\mu\text{m}$	NaN	$147.99\pm 21.64\mu\text{m}$	$166.68\pm 9.64\mu\text{m}$
PDMS Channel	$151.38\pm 2.43\mu\text{m}$	$176.9\pm \mu\text{m}$	$136.1\pm 4.8$	$142.88\pm 4.78$

### 4.3 Reagent-Storage and -Release

A functional microfluidic device with integrated storage and release mechanisms was fabricated by 3D-printing combined with rapid prototyping methods. For the storage, i) gold nanoparticles (AuNP) stored on a conjugate pad were used. ii) A blister storage mechanism was used for the liquid storage of buffer solution. For the release mechanism, i) a tin foil membrane was perforated by 3D printed spikes. Thereby, the tin foil acted as the seal for the blister, and at the same time served as part of the release mechanism. And ii) the AuNPs were flushed with the buffer solution and subsequently released from the conjugate pad into the liquid.

#### 4.3.1 AuNP-pad: on-chip storage and release

Figure 72 shows the design iteration timeline for developing a storage and release mechanism on a microfluidic chip. First a device for simply pipetting the buffer solution through the microfluidic channel was created. A small cavity (3.1mm x 3.1mm x 0.5mm) was created to hold the AuNP-pad. The cavity was sealed with thick transparent tape. After a few iterations, the AuNPs were release successfully, and a multiplexer was created (see paragraph below). Additionally to the pipetting device, a reservoir was placed at the inlet, to ensure fluid flow by solely the differential pressure due to the height difference. Problems arose especially at the end of the device, due to capillary forces preventing the liquid from flowing into the Eppendorf tube. Those problems were eliminated by creating a bigger outlet, reducing the capillary forces at the end of the device.

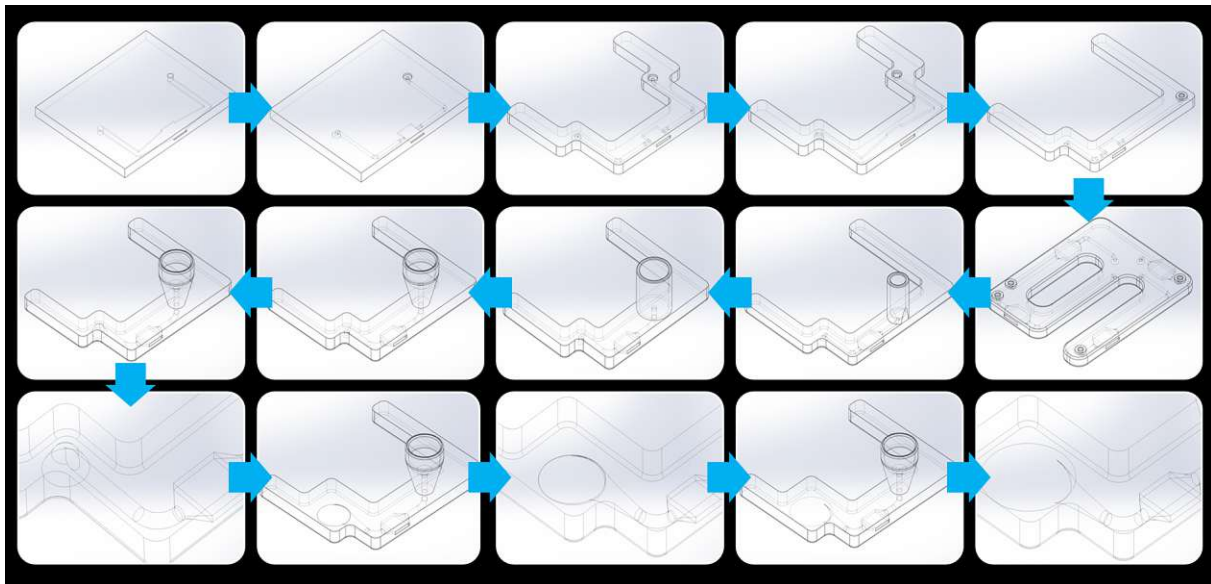


Figure 72: Timeline of design iterations for Gold-Nanoparticle release.

## Multiplexer

To ease the process, a multiplexing device was created (see Figure 73). Four pads were loaded into the device, and flushed with PBS/Tween. Three different optical densities were created beforehand (see section 3.5.3), and after flushing the chip and collecting the liquid within an Eppendorf tube, the absorbance at 530nm was evaluated using a plate reader.

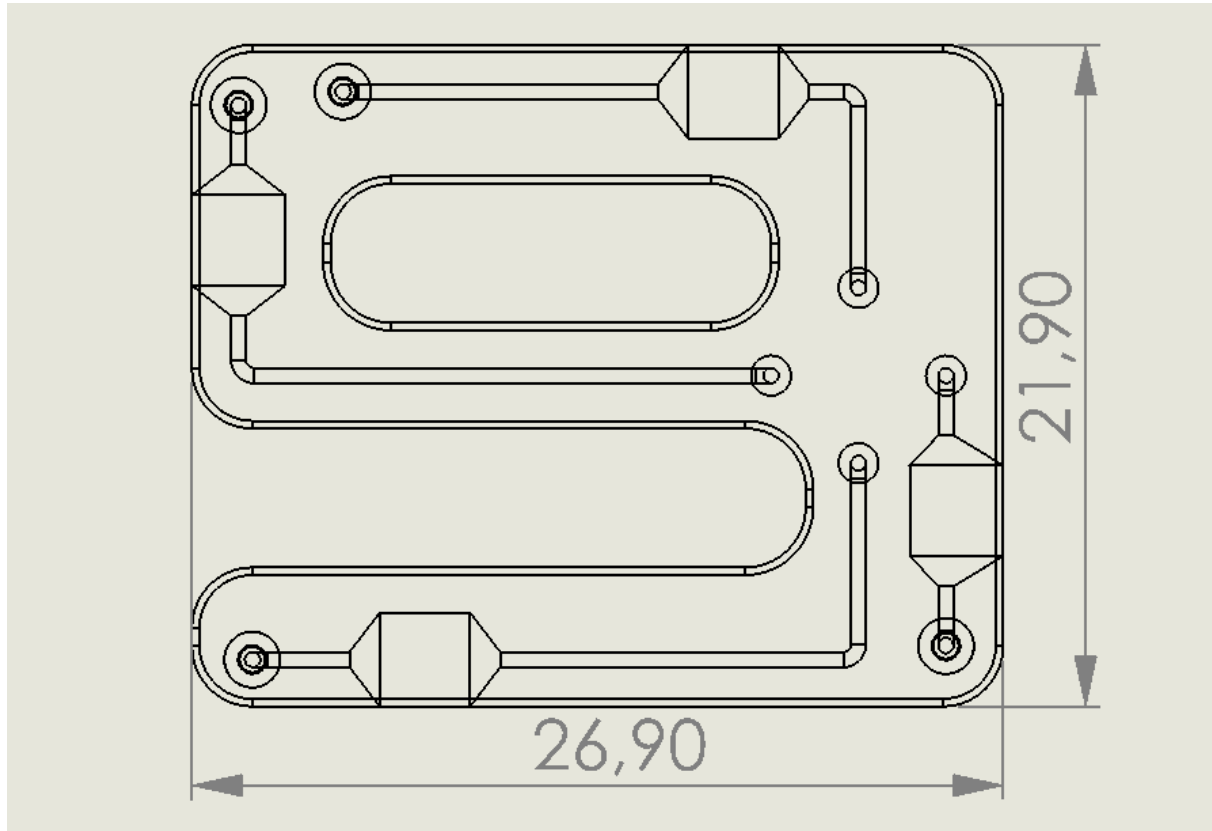


Figure 73: Multiplexing device for AuNP release evaluation. The outer dimensions are 26.9 mm x 21.9 mm.

### AuNP-pad coupled with hydrostatic reservoir

Previously the differential pressure was created by pipetting. For the next design iteration, a hydrostatic reservoir was placed at the inlet, which creates the differential pressure necessary to flush the AuNP-pad with PBS/Tween. Initially, the outlet was too small and the liquid never dropped into the Eppendorf tube, as shown in Figure 76. Figure 77 on the other hand shows a successful experiment, since the liquid (60 $\mu$ L) was added into the chip, and due to the hydrostatic pressure, it was pushed through the channel, releasing the AuNPs. Figure 77, in the bottom right corner, shows a bright red hanging drop containing the AuNP sitting at the outlet.

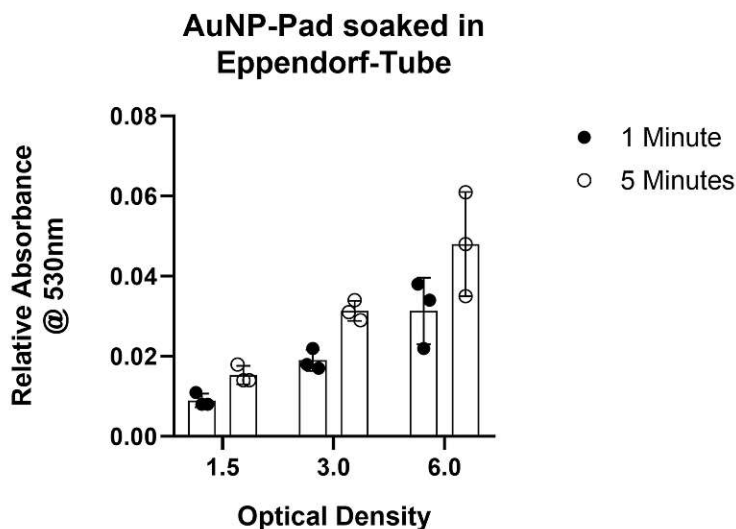


Figure 74: AuNP-pads soaked in Eppendorf-tube for 1 and 5 minutes.

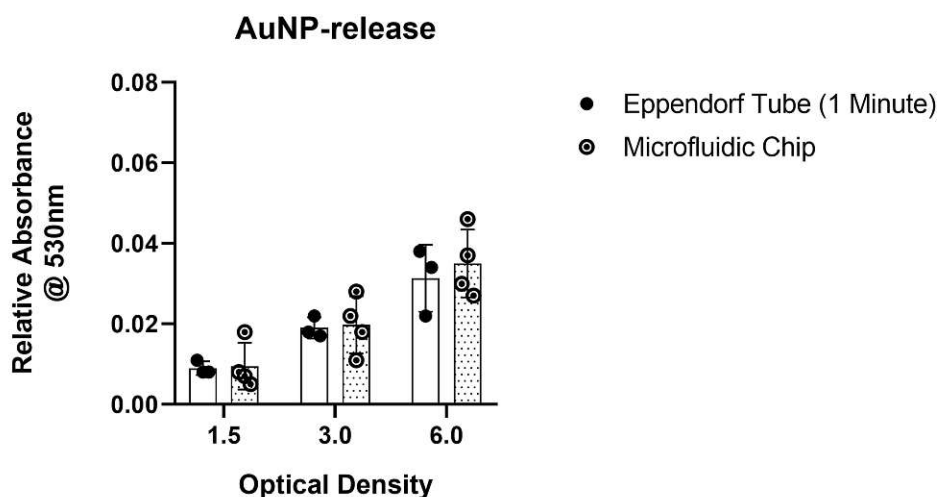


Figure 75: AuNP-pads: soaked for 1 minute versus flushed within microfluidic chip.

Figure 74 and 75 show relative absorbance values at 530nm wavelength for different methods tried for the AuNP release. Figure 74 shows a direct comparison of AuNP-pads submerged in PBS/Tween for 1 and 5 minutes, respectively. Soaking the pad for 5 minutes resulted in higher absorbance values for all three optical densities. Figure 75 shows a direct comparison of AuNP-pads submerged in PBS/Tween for 1 minute and AuNP-pads flushed with PBS/Tween in a microfluidic chip. The absorbance values lie within close vicinity to each other, which means that i) the mechanism of AuNP release actually transports the particles through the carrier medium into the eppendorf tube, and ii) delivers the same effect as submerging the pad for 1 minute in buffer solution.

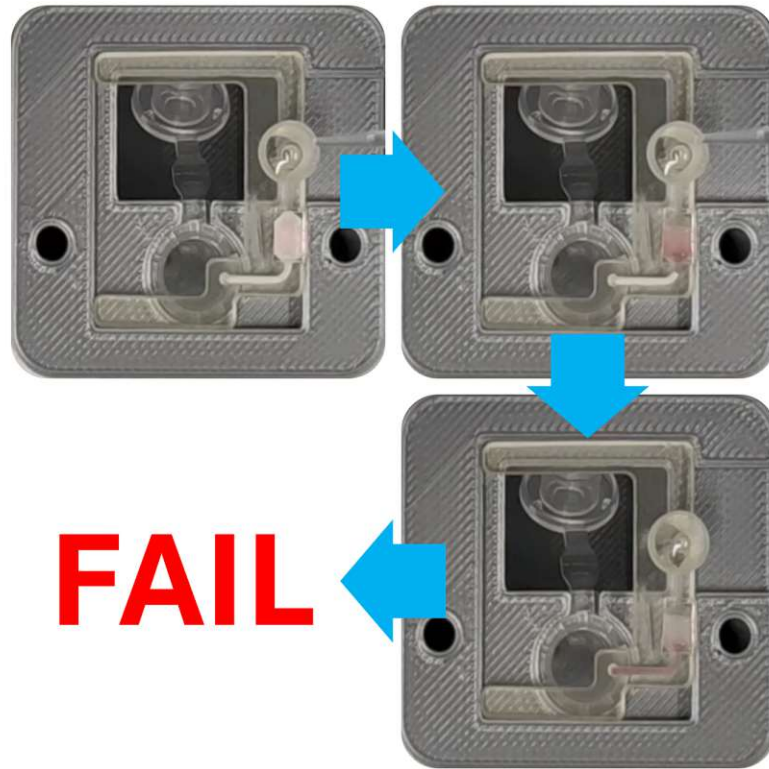


Figure 76: Initial design with loaded AuNP-pad and hydrostatic reservoir, leading to AuNPs being trapped inside the channel.

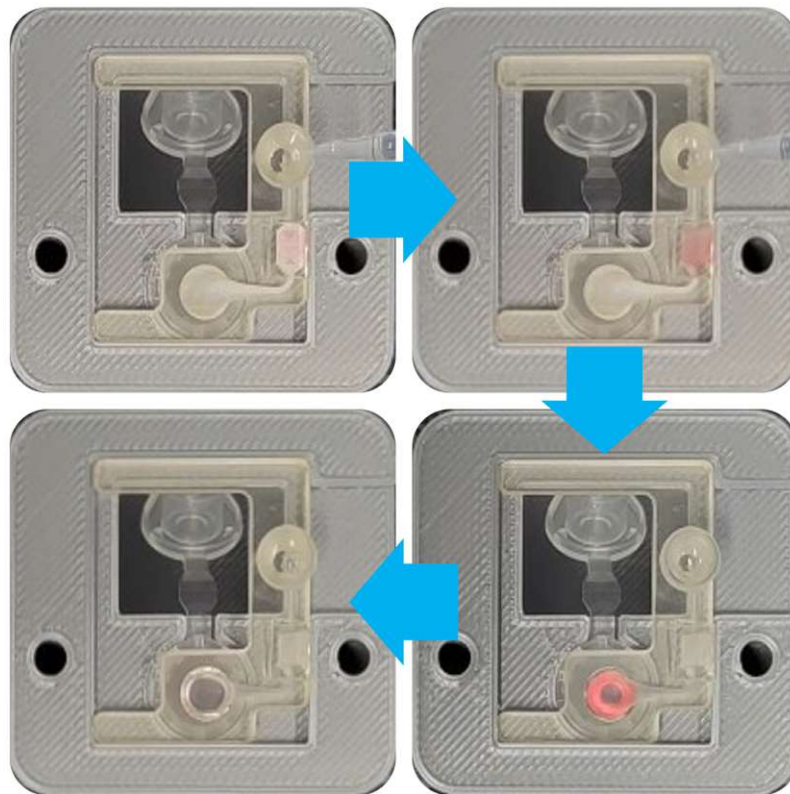


Figure 77: Successful experiment with loaded AuNP-pad and hydrostatic reservoir.

### 4.3.2 Blister-Mechanism

The blister mechanism was adapted from Smith et al. [64]. The spikes were 3D printed directly into the device onto which the sealed blister was attached. The device was designed in a way that the fluid within the blister would flow through a hole at the bottom into the channel. The spikes were adapted, since for prior designs, the spikes were too thin, resulting in a blockage of fluid flow. The final design resulted in capped spikes, which perforated the tin foil so that i) the foil was pierced and ii) the resulting holes ensured fluid flow. A microscopic image of the 3D printed spikes can be seen in Figure 79.

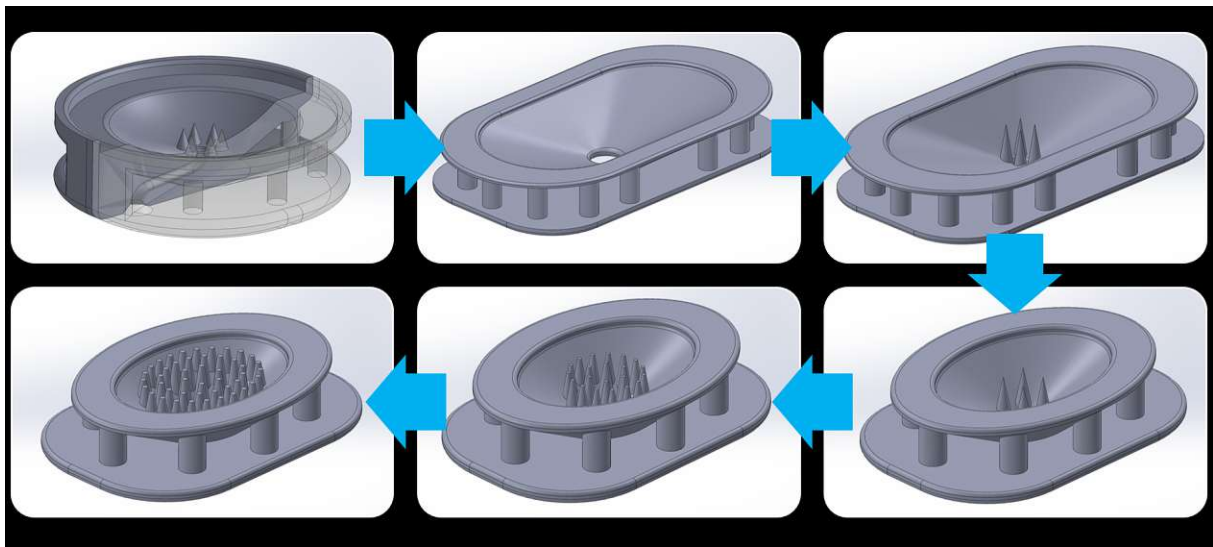


Figure 78: Timeline of design iterations for blister mechanism.

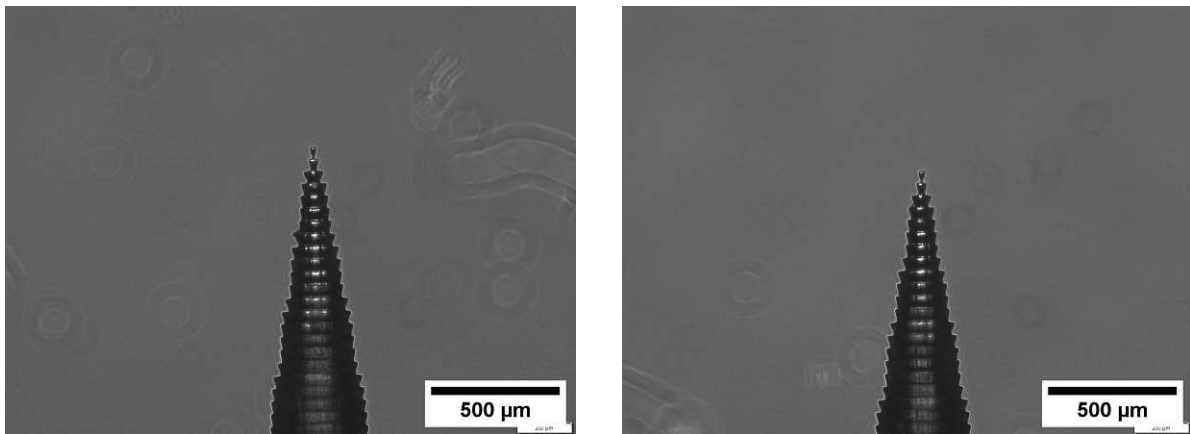


Figure 79: 3D-printed spikes, inspected under a microscope.

To test the created device, the blister was filled with food-colored water, and pressure was applied by pressing a finger into the blister. The resulting pressure deflected the tin foil membrane, pushing the tin foil towards the spikes, and subsequently the spikes perforated the foil. The holes created by the spikes can be seen in Figure 81.

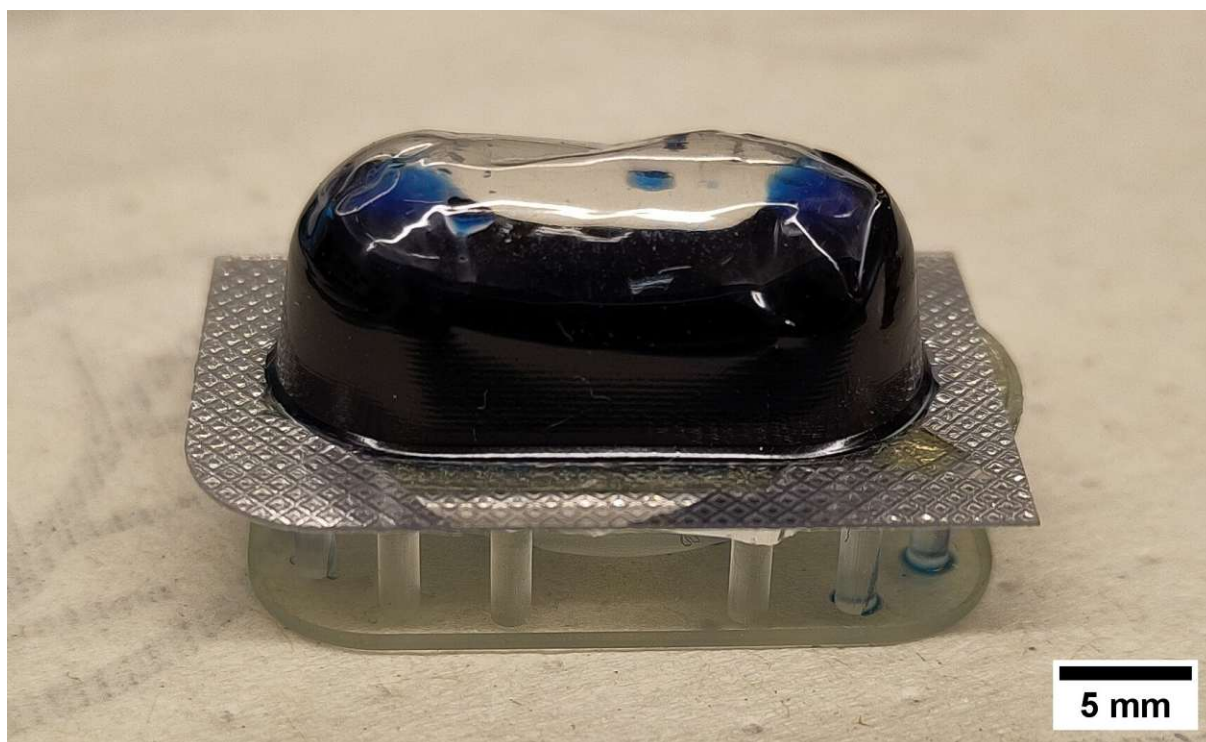


Figure 80: Blister, filled with food-colored water.

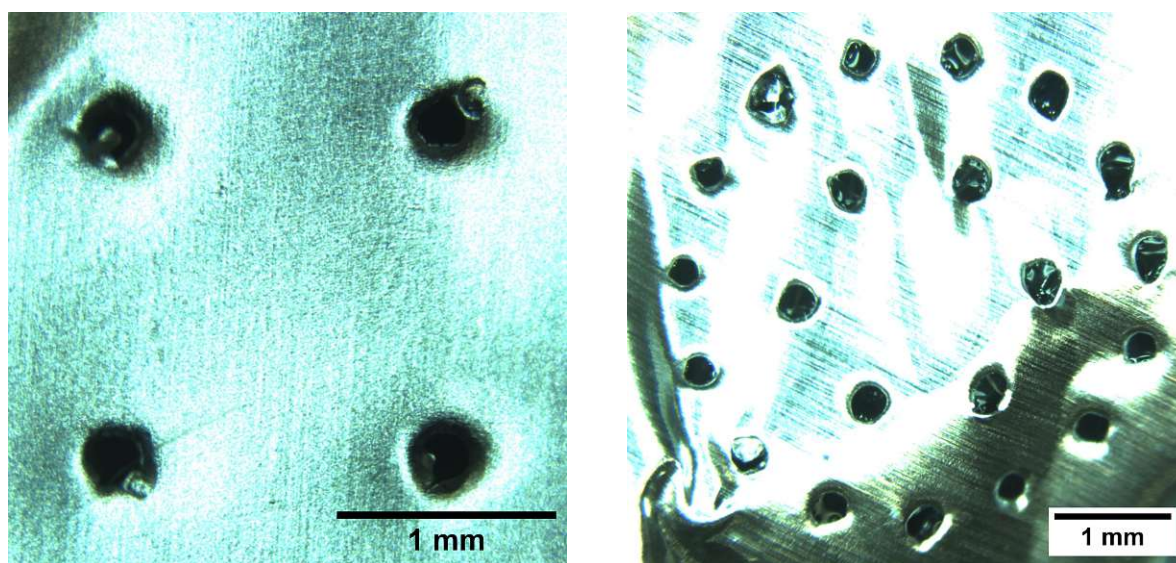


Figure 81: Tin foil, close-up image of punctures from 3D printed spikes. Left: 4 spikes. Right: Array of spikes for higher flow rate.

#### 4.3.3 Combination: AuNP and Blister

To combine the above mentioned methods for reagent storage and release, the devices were simply combined into a single device. The gold nanoparticles were stored in the bottom part, whereas the blister was sitting at the top. The pressure necessary to induce fluid flow was achieved by a finger-push into the blister.



Figure 82: Combination of AuNP and blister device. Left: Variant I). Right: Variant II).

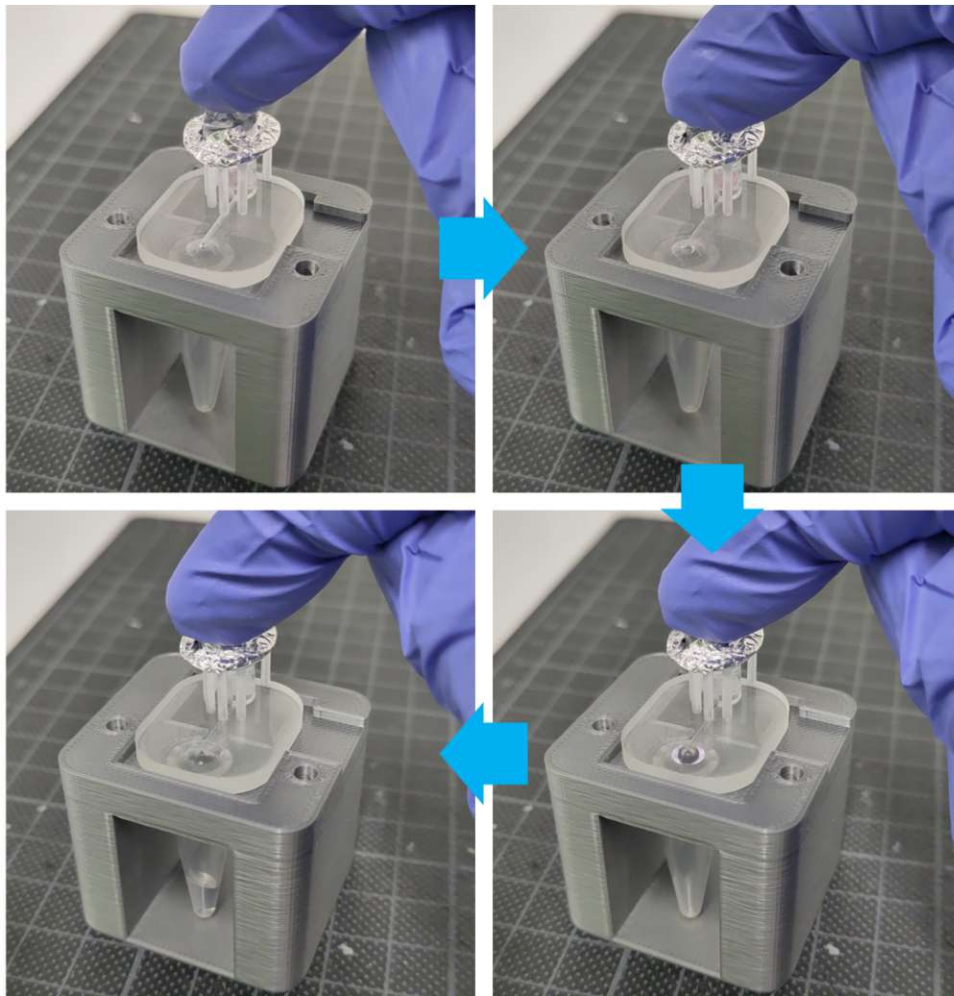


Figure 83: Experiment with combined device (AuNP + blister).

To release the liquid (see Figure 83), pressure was applied with a finger, which deflected the tin foil membrane/seal, the 3D printed spikes perforated the foil and the liquid was released into the chip. The AuNP was sitting in a cavity inside the chip, sealed by adhesive tape, and the buffer solution released the AuNPs out of the conjugate pad and into the chip. The fluid was then collected by an Eppendorf tube, to be able to analyze the fluid.

## 5 Conclusion

This thesis tackled three main questions: i) 'Material characterization: preparation of a third-party resin for printability', ii) 'What are the capabilities and limitations of a DLP 3D printer' and iii) the 'Development of a functional reagent storage & release device'. These questions were answered in detail in Section 4. i) Material characterization of NanoClear resin was completed, and it was successfully prepared for printing. While challenges related to resin viscosity—such as blocked channels and difficulties in removing high-viscosity resin from 3D-printed channels—were not completely eliminated, printability of the channels was improved. ii) The limitations of the printer were analyzed in detail, and the results can be used for microfluidic features, such as pillars, partial walls or channels. Therefore testing and trying of said features will be eliminated or at least facilitated for readers of this thesis. iii) The PoC microfluidic device demonstrated the application of rapid prototyping techniques to create a reagent storage and release device, which can be used fully or partly in other projects, requiring the controlled release of nanoparticles.

### 5.1 Principal Findings

This study demonstrated the successful material file creation for NanoClear resin, documenting the process of characterizing and preparing a resin for the Asiga Max X43 DLP printer, enabling the reader to follow the workflow and prepare other third-party resins. By investigating the capabilities of the 3D printer in terms of microfluidic chip fabrication, limitations as well as the opportunities could be identified. As an example, the printers ability to print single objects with different layer heights enables the significant reduction of printing time depending on the design. Bulk-segments of an object that do not require fine details can be printed with a greater layer height and therefore save time. For features and fine details, the layer height can be reduced to ensure higher accuracy and printability, which will result in longer printing times. Additionally, when printing microfluidic channels, this work demonstrated that the orientation of the channels during the print is detrimental for dimensional accuracy and printability in general. The findings were employed to successfully print a microfluidic device that can store and release gold-nanoparticles on demand. The successful on-demand release can be implemented into other projects, where integrated reagents release is needed.

### 5.2 Outlook for future research

Other third-party resins can be characterized in the future, since this printer allows for the use of any resin. Presumably there will be a variety of new resins on the market in the future, which might be interesting for the field of microfluidic and lab-on-a-chip applications.

Based on the novel method for dosing- and zoning-controlled vat photopolymerization [50], there might be a way to perform this method with the Asiga DLP printer. Finding a workaround would ensure i) printing channels in the correct dimensions, ii) creation of significantly smaller channels, and iii) smoother channels. Thereby, the utilization of 3D printers in microfluidic chip fabrication can further increase.

### 5.3 Final thoughts

Through the successful characterization of NanoClear resin and the exploration of the Asiga Max X43 DLP printer's capabilities, this research has laid the foundation for future innovations in the field. The journey of developing a functional reagent storage and release device showed the possibility to 3D print a prototype for a PoC device. This work underscores the significance of adapting existing technologies to meet specific needs of research fields, such as lab-on-a-chip and point-of-care applications. As the field of microfluidics continues to evolve, it is my hope that the insights gained from this research will inspire further exploration and refinement.

## References

- [1] S. Daley, *How does 3d printing work?* Jul. 2022. [Online]. Available: <https://builtin.com/3d-printing>.
- [2] A. Davis, *Layer-by-layer: The evolution of 3-d printing*, Nov. 2014. [Online]. Available: <https://spectrum.ieee.org/layerbylayer-the-evolution-of-3d-printing>.
- [3] Sculpteo, *Layer of construction by 3d printing objects*. [Online]. Available: <https://www.sculpteo.com/en/glossary/layer-definition/>.
- [4] C. A. Manufacturing, *What is additive manufacturing?* [Online]. Available: <https://www.croftam.co.uk/what-is-additive-manufacturing/>.
- [5] M. Attaran, “The rise of 3-d printing: The advantages of additive manufacturing over traditional manufacturing,” *Business Horizons*, vol. 60, pp. 677–688, 5 Sep. 2017, ISSN: 00076813. DOI: 10.1016/j.bushor.2017.05.011.
- [6] T. Xometry, *3d printing vs. traditional manufacturing: Differences and comparison*, Aug. 2022. [Online]. Available: <https://www.xometry.com/resources/3d-printing/3d-printing-vs-traditional-manufacturing/>.
- [7] Khatabook, *Understanding conventional manufacturing processes: Methods and limitations*. [Online]. Available: <https://khatabook.com/blog/conventional-manufacturing-process/>.
- [8] Z. Padasak, *Top 10 advantages and disadvantages of additive manufacturing*, Oct. 2022. [Online]. Available: <https://www.alphaprecisionpm.com/blog/top-10-advantages-and-disadvantages-of-using-additive-manufacturing>.
- [9] M. Chan, *12 advantages of additive manufacturing and 5 disadvantages*, May 2021. [Online]. Available: <https://www.unleashedsoftware.com/blog/12-benefits-of-additive-manufacturing-and-5-disadvantages>.
- [10] 3DSourced, *How much does a 3d printer cost? (price and maintenance)*, Feb. 2024. [Online]. Available: <https://www.3dsourced.com/3d-printers/how-much-does-a-3d-printer-cost-price/>.
- [11] 3DSourced, *The complete history of 3d printing: From 1980 to 2023*, Feb. 2024. [Online]. Available: <https://www.3dsourced.com/guides/history-of-3d-printing/>.
- [12] A. Alammar, J. C. Kois, M. Revilla-León, and W. Att, *Additive manufacturing technologies: Current status and future perspectives*, Mar. 2022. DOI: 10.1111/jopr.13477.

- [13] M. Regehly, Y. Garmshausen, M. Reuter, *et al.*, “Xolography for linear volumetric 3d printing,” *Nature*, vol. 588, pp. 620–624, 7839 Dec. 2020, ISSN: 14764687. DOI: 10.1038/s41586-020-3029-7.
- [14] C. W. Hull, *United states patent 4.575.330*, Mar. 1986. [Online]. Available: <https://patentimages.storage.googleapis.com/5c/a0/27/e49642dab99cf6/US4575330.pdf>.
- [15] J. M. Norman, *Chuck hull invents stereolithography or 3d printing and produces the first commercial 3d printer*. [Online]. Available: <https://www.historyofinformation.com/detail.php?id=3864>.
- [16] T. R. Mhmood and N. K. Al-Karkhi, “A review of the stereo lithography 3d printing process and the effect of parameters on quality,” *Al-Khwarizmi Engineering Journal*, vol. 19, pp. 82–94, 2 Jun. 2023, ISSN: 1818-1171. DOI: 10.22153/kej.2023.04.003.
- [17] T. Mechninja, *Sla printing it’s working and technology*, Aug. 2021. [Online]. Available: <https://themechninja.com/08/sla-printing-its-working-and-technology-explained/>.
- [18] J. Lie, *Post processing for sls parts*. [Online]. Available: <https://www.runsom.com/technology/post-processing-for-sls-parts/>.
- [19] R. Curley, “3d printing,” *Encyclopaedia Britannica*, Oct. 2011. [Online]. Available: <https://www.britannica.com/technology/3D-printing>.
- [20] 3Dprinting.com, *What is 3d printing?* [Online]. Available: <https://3dprinting.com/what-is-3d-printing/>.
- [21] AMFG, *An introduction to electron beam melting*, May 2018. [Online]. Available: <https://amfg.ai/2018/05/16/electron-beam-melting-introduction/>.
- [22] D. Directory, *What is electron beam melting?* Apr. 2021. [Online]. Available: <https://www.3d.directory/community/what-is-electron-beam-melting>.
- [23] I. Kauppila, *Selective laser melting (slm 3d printing) – the ultimate guide*, Feb. 2023. [Online]. Available: <https://all3dp.com/1/selective-laser-melting-guide/>.
- [24] R. Engineering, *The genius of 3d printed rockets*, Aug. 2023. [Online]. Available: <https://www.youtube.com/watch?v=kz165f1g8-E&t=962s>.
- [25] C. Q. Choi, *3d-printing hollow structures with ”xolography”*, Dec. 2020. [Online]. Available: <https://spectrum.ieee.org/xolography-printing>.
- [26] C. Darkes-Burkey and R. F. Shepherd, “High-resolution 3d printing in seconds,” *Nature*, vol. 588, pp. 594 –595, 2020. DOI: 10.1038/d41586-020-03543-3. [Online]. Available: <https://www.nature.com/articles/d41586-020-03543-3>.

- [27] A. Kaffle, E. Luis, R. Silwal, H. M. Pan, P. L. Shrestha, and A. K. Bastola, *3d/4d printing of polymers: Fused deposition modelling (fdm), selective laser sintering (sls), and stereolithography (sla)*, Sep. 2021. DOI: 10.3390/polym13183101.
- [28] H. H. Parikh, R. Jadav, and P. Joshi, “3-d printing: A review of manufacturing methods, materials, scope and challenges, and applications,” Springer Science and Business Media Deutschland GmbH, 2023, pp. 243–256, ISBN: 9789811942075. DOI: 10.1007/978-981-19-4208-2\_18.
- [29] Admin, *Everything to know about the fdm 3d printing*, Feb. 2021. [Online]. Available: <https://www.php elephant.com/2021/02/17/everything-to-know-about-the-fdm-3d-printing/>.
- [30] M. Jiménez, L. Romero, I. A. Domínguez, M. D. M. Espinosa, and M. Domínguez, “Additive manufacturing technologies: An overview about 3d printing methods and future prospects,” *Complexity*, vol. 2019, 2019, ISSN: 10990526. DOI: 10.1155/2019/9656938.
- [31] T. Xometry, *All about digital light process (dlp) 3d printing*, Aug. 2022. [Online]. Available: <https://www.xometry.com/resources/3d-printing/digital-light-process-dlp/>.
- [32] C. Lalwani, *Lcd vs. dlp vs. sla: Which 3d printer is best for you*, Dec. 2020. [Online]. Available: <https://phrozen3d.com/blogs/guides/sla-vs-dlp-vs-lcd-which-resin-3d-printer-is-the-best-for-you>.
- [33] M. Parenti, *Dlp vs lcd 3d printer: The main differences*, Jul. 2023. [Online]. Available: <https://all3dp.com/2/lcd-vs-dlp-3d-printing-technologies-compared/>.
- [34] All3DP, *What is an stl file? – the stl format simply explained*, May 2023. [Online]. Available: <https://all3dp.com/1/stl-file-format-3d-printing/>.
- [35] T. Instruments, *Dlp ® technology and products*. [Online]. Available: <https://www.ti.com/lit/ml/dlpb010e/dlpb010e.pdf?ts=1704790868502>.
- [36] L. Ge, L. Dong, D. Wang, Q. Ge, and G. Gu, “A digital light processing 3d printer for fast and high-precision fabrication of soft pneumatic actuators,” *Sensors and Actuators A-physical*, vol. 273, pp. 285–292, 2018. [Online]. Available: <https://www.sciencedirect.com/science/article/pii/S0924424717320502>.
- [37] P. S. Heath, “3d printing; hardware and software for the consumer market,” *International Journal of Students Research in Technology and Management*, 2015. [Online]. Available: <https://core.ac.uk/download/pdf/268006786.pdf>.

- [38] I. D. Tsvetkova and P. Z. Zahariev, “A study on 3d printing technologies and their applications,” *Electrotechnica and Electronica (E+E)*, 2016. [Online]. Available: <https://epluse.ceec.bg/wp-content/uploads/2018/04/20160910-07.pdf>.
- [39] M Jeong, K Radomski, D Lopez, J. T. Liu, and J. D. Lee, “Materials and applications of 3d printing technology in dentistry: An overview,” *Dentistry Journal*, 2023. [Online]. Available: <https://www.mdpi.com/2304-6767/12/1/1/pdf>.
- [40] H. B. Nguyen, T Vo, and T. K. Nguyen, “A research of design controller of 3d printer dlp technology,” *Applied Mechanics and Materials*, 2020. [Online]. Available: <https://www.scientific.net/AMM.902.71>.
- [41] M. N. M. Azlin, R. A. Ilyas, M. Y. M. Zuhri, and S. M. Sapuan, “3d printing and shaping polymers, composites, and nanocomposites: A review,” *Polymers*, 2022. [Online]. Available: <https://www.mdpi.com/2073-4360/14/1/180/pdf>.
- [42] M Pagac, J Hajnys, Q. P. Ma, L Jancar, J Jansa, and P Stefek, “A review of vat photopolymerization technology: Materials, applications, challenges, and future trends of 3d printing,” *Polymers*, 2021. [Online]. Available: <https://www.mdpi.com/2073-4360/13/4/598/pdf>.
- [43] P Rodriguez and W Sun, “The influence of the digital light processing (dlp) 3d printing parameters on the precision of microfeatures,” *Micromachines*, 2020. [Online]. Available: <https://www.mdpi.com/2072-666X/11/12/1125>.
- [44] L. Schittecatte, V. Geertsen, D. Bonamy, T. Nguyen, and P. Guenoun, “From resin formulation and process parameters to the final mechanical properties of 3d printed acrylate materials,” *MRS Communications*, vol. 13, pp. 357–377, 3 Jun. 2023, ISSN: 21596867. DOI: 10.1557/s43579-023-00352-3.
- [45] R. Su, F. Wang, and M. C. McAlpine, *3d printed microfluidics: Advances in strategies, integration, and applications*, Feb. 2023. DOI: 10.1039/d2lc01177h.
- [46] G. Team, *Evaluating the accuracy of a 3d printed part against the cad model*, Aug. 2018. [Online]. Available: <https://gomeasure3d.com/blog/evaluating-the-accuracy-of-a-3d-printed-part-against-the-cad-model/>.
- [47] M. P., *The different types of resins available for 3d printing*, Jan. 2023. [Online]. Available: [https://www.3dnatives.com/en/different-types-of-resins-3d-printing-281220225/#!\\$](https://www.3dnatives.com/en/different-types-of-resins-3d-printing-281220225/#!$).
- [48] E. Fleck, C. Keck, K. Ryszka, E. DeNatale, and J. Potkay, “Low-viscosity polydimethylsiloxane resin for facile 3d printing of elastomeric microfluidics,” *Micromachines*, vol. 14, 4 Apr. 2023, ISSN: 2072666X. DOI: 10.3390/mi14040773.

- [49] R. Su, F. Wang, and M. C. McAlpine, *3d printed microfluidics: Advances in strategies, integration, and applications*, Feb. 2023. DOI: 10.1039/d21c01177h.
- [50] Z. Luo, H. Zhang, R. Chen, *et al.*, “Digital light processing 3d printing for microfluidic chips with enhanced resolution via dosing- and zoning-controlled vat photopolymerization,” *Microsystems and Nanoengineering*, vol. 9, 1 Dec. 2023, ISSN: 20557434. DOI: 10.1038/s41378-023-00542-y.
- [51] H. Shafique, V. Karamzadeh, G. Kim, *et al.*, “High-resolution low-cost lcd 3d printing for microfluidics and organ-on-a-chip devices,” *Lab on a Chip*, vol. 24, pp. 2774–2790, 10 Apr. 2024, ISSN: 14730189. DOI: 10.1039/d31c01125a.
- [52] ELEGOO, *Elegoo compare products*. [Online]. Available: <https://www.elegoo.com/pages/compare-products>.
- [53] R. Junker, H. Schlebusch, and P. B. Luppá, *Patientennahe labordiagnostik in klinik und praxis*, Aug. 2010. DOI: 10.3238/arztebl.2010.0561.
- [54] K. Daimi, A. Alsadoon, S. Seabra, and D. Reis, *Current and future trends in health and medical informatics*.
- [55] J. R. Mejía-Salazar, K. R. Cruz, E. M. M. Vásques, and O. N. de Oliveira, “Microfluidic point-of-care devices: New trends and future prospects for ehealth diagnostics,” *Sensors (Switzerland)*, vol. 20, 7 Apr. 2020, ISSN: 14248220. DOI: 10.3390/s20071951.
- [56] A Ojha, *Master 3d printing of microfluidic chips with different modules for point-of-care testing applications*.
- [57] D. Siegle, *The role of point-of-care technology in healthcare*, Oct. 2023. [Online]. Available: <https://getvim.com/blog/the-role-of-point-of-care-technology-in-healthcare/>.
- [58] K. Plevniak and M. He, *3d printed microfluidic device for point-of-care anemia diagnosis*, 2014.
- [59] A. Shaikhmag, *Mit researchers innovate 3d printed self-heating microfluidic devices for affordable disease detection*, Jan. 2024. [Online]. Available: <https://3dprintingindustry.com/news/mit-researchers-innovate-3d-printed-self-heating-microfluidic-devices-for-affordable-disease-detection-227713/>.
- [60] M. Rasekh, S. Harrison, S. Schobesberger, P. Ertl, and W. Balachandran, *A review of reagent storage and delivery on integrated microfluidic chips for point-of-care diagnostics*.

- [61] D. Czurratis, Y. Beyl, S. Zinober, R. Zengerle, and F. Lärmer, “Long-term on-chip storage and release of liquid reagents for diagnostic lab-on-a-chip applications,” *World Academy of Science, Engineering and Technology, International Journal of Mathematical, Computational, Physical, Electrical and Computer Engineering*, vol. 7, pp. 1266–1269, 2013. [Online]. Available: <https://api.semanticscholar.org/CorpusID:34570745>.
- [62] J. Deng and X. Jiang, “Advances in reagents storage and release in self-contained point-of-care devices,” *Advanced Materials Technologies*, vol. 4, 6 Jun. 2019, ISSN: 2365709X. DOI: 10.1002/admt.201800625.
- [63] H. Ordutowski, F. D. Dosso, W. D. Wispelaere, *et al.*, “Next generation point-of-care test for therapeutic drug monitoring of adalimumab in patients diagnosed with autoimmune diseases,” *Biosensors and Bioelectronics*, vol. 208, Jul. 2022, ISSN: 18734235. DOI: 10.1016/j.bios.2022.114189.
- [64] S. Smith, R. Sewart, H. Becker, P. Roux, and K. Land, “Blister pouches for effective reagent storage on microfluidic chips for blood cell counting,” *Microfluidics and Nanofluidics*, vol. 20, 12 Dec. 2016, ISSN: 16134990. DOI: 10.1007/s10404-016-1830-2.
- [65] A. P. Iakovlev, A. S. Erofeev, and P. V. Gorelkin, *Novel pumping methods for microfluidic devices: A comprehensive review*, Nov. 2022. DOI: 10.3390/bios12110956.
- [66] M. Bauer, M. Ataei, M. Caicedo, K. Jackson, M. Madou, and L. Bousse, “Burst valves for commercial microfluidics: A critical analysis,” *Microfluidics and Nanofluidics*, vol. 23, 7 Jul. 2019, ISSN: 16134990. DOI: 10.1007/s10404-019-2252-8.
- [67] ElveFlow, *Pdms quake valves and co.* [Online]. Available: <https://www.elveflow.com/microfluidic-reviews/general-microfluidics/pdms-quake-valves-and-co-a-review/>.
- [68] S. M. Yang, S. Lv, W. Zhang, and Y. Cui, *Microfluidic point-of-care (poc) devices in early diagnosis: A review of opportunities and challenges*, Feb. 2022. DOI: 10.3390/s22041620.
- [69] H. Ordutowski, C. Parra-Cabrera, C. Achille, *et al.*, “A multistep immunoassay on a 3d-printed capillarity-driven microfluidic device for point-of-care diagnostics,” *Applied Materials Today*, vol. 32, Jun. 2023, ISSN: 23529407. DOI: 10.1016/j.apmt.2023.101788.
- [70] K. Dalvand, A. Ghiasvand, S. Keshan-Balavandy, F. Li, and M. Breadmore, “A simple 3d printed microfluidic device for point-of-care analysis of urinary uric acid,” *Australian Journal of Chemistry*, vol. 76, pp. 74–80, 2 Feb. 2023, ISSN: 0004-9425. DOI: 10.1071/ch22180.

- [71] J. Prusa, *Introducing the original prusa enclosure: Modular box with advanced features for your mk3s+!* May 2022. [Online]. Available: [https://blog.prusa3d.com/original-prusa-enclosure\\_67656/](https://blog.prusa3d.com/original-prusa-enclosure_67656/).
- [72] Asiga, *Precise. defined. the max x.* [Online]. Available: <https://www.asiga.com/max-x/>.
- [73] FunToDo, *Nano clear.* [Online]. Available: <https://funtodo.eu/shop/nano-clear/nano-clear/>.
- [74] M. ASIGA, *Plasclear technical datasheet.* [Online]. Available: <https://pdf.medicaexpo.com/pdf/asiga/plasclear/102400-141336.html>.
- [75] FunToDo, *How to post-process lcd, dlp and sla 3d printed objects.* [Online]. Available: <https://funtodo.net/how-to-post-process-lcd-dlp-and-sla-3d-printed-objects/>.
- [76] FormLabs, *From cure.* [Online]. Available: <https://formlabs.com/de/shop/post-processing/form-cure/>.
- [77] Eppendorf, *Eppendorf safe-lock tubes.* [Online]. Available: <https://www.eppendorf.com/de-de/Produkte/Spitzen-Reaktionsgef%C3%A4%C3%9Fe-und-Platten/Reaktionsgef%C3%A4%C3%9Fe/Eppendorf-Safe-Lock-Tubes-p-0030121023>.
- [78] adlershop.ch, *Gelomyrtol.* [Online]. Available: <https://www.adlershop.ch/pph/84907/0/1600x1600.jpg>.
- [79] BIPA, *Bi life vitamin d3.* [Online]. Available: <https://www.bipa.at/p/bi-life-vitamin-d3/B3-425090>.
- [80] GJS, *Roland camm-1 servo gs-24 vinyl cutter.* [Online]. Available: [https://gjs.co/images/products/wm\\_3732042-roland-camm-1-servo-gs-24-desktop-sign-maker-vinyl-cutter.jpg](https://gjs.co/images/products/wm_3732042-roland-camm-1-servo-gs-24-desktop-sign-maker-vinyl-cutter.jpg).
- [81] D. Systemes, *Solidworks 3d cad.* [Online]. Available: <https://www.solidworks.com/product/solidworks-3d-cad>.
- [82] Autodesk, *Autodesk fusion360.* [Online]. Available: <https://www.autodesk.com/products/fusion-360/overview>.
- [83] Asiga, *Asiga slicer software.* [Online]. Available: <https://www.asiga.com/software-composer/>.
- [84] P. Research, *Prusaslicer.* [Online]. Available: [https://www.prusa3d.com/de/page/prusaslicer\\_424/](https://www.prusa3d.com/de/page/prusaslicer_424/).
- [85] ImageJ, *Imagej, image processing and analysis in java.* [Online]. Available: <https://imagej.net/ij/>.

- [86] MathWorks, *Matlab r2022b*. [Online]. Available: [https://de.mathworks.com/products/new\\_products/release2022b.html](https://de.mathworks.com/products/new_products/release2022b.html).
- [87] Microsoft, *Microsoft excel*. [Online]. Available: <https://www.microsoft.com/de-de/microsoft-365/excel>.
- [88] Drawboard, *Drawboard pdf*. [Online]. Available: <https://www.drawboard.com/pdf/pdf>.
- [89] Microsoft, *Microsoft powerpoint*. [Online]. Available: <https://www.microsoft.com/de-de/microsoft-365/powerpoint>.
- [90] Olympus, *Inversmikroskop ix83*. [Online]. Available: <https://www.olympus-lifescience.com/de/microscopes/inverted/ix83/>.
- [91] Olympus, *Research inverted system microscope ix2 series brochure*. [Online]. Available: <https://www.olympus-lifescience.com/data/olympusmicro/brochures/pdfs/ix71.pdf?rev=EABE>.
- [92] Leica, *S8 apo unique greenough stereo microscope with apochromatic optics*. [Online]. Available: <https://www.leica-microsystems.com/products/light-microscopes/stereo-microscopes/p/leica-s8-apo/>.

## Appendix

### MATLAB-script: plot and generation of z-curing table

```

clc;
clearvars;
%insert set light intensity value here
%under: MAINTENANCE --> LED --> Radiometer
LI = 3;
m = readtable("Material_Test_3mW.xlsx");
intensity = LI*ones(height(m),1);
time = m.time;
% Sample datasets
M1 = m.M1;
M2 = m.M2;
M3 = m.M3;
mean_values = NaN(size(M1));
% Loop through each element and calculate the mean
for i = 1:length(M1)
    values = [M1(i), M2(i), M3(i)];
    non_nan_values = values(~isnan(values));
    if ~isempty(non_nan_values)
        mean_values(i) = mean(non_nan_values);
    end
end
measurements_mm = mean_values/1000;
energy = time .* intensity;
%interpolate: define the interpolation-points
xq = [0.010, 0.025, 0.05, 0.1];
interpolated_value = interp1(measurements_mm, energy, xq, '
    pchip');
time_check = interpolated_value/LI
%% generate textfile
%plot
figure(1)
plot(time, mean_values, 'b-', 'LineWidth', 1, 'Marker', 'x',
    'MarkerEdgeColor', 'r', 'MarkerFaceColor', 'r')
ylabel("thickness [um]", 'Interpreter', 'none')
xlabel("time of irradiation [s]")
title("Thickness over Time")
grid minor
%%
content = [energy, measurements_mm, intensity];
filename = 'output.txt';
fileID = fopen(filename, 'w');
textfile = fprintf(fileID, 'Z = [%0.3f, %0.4f, %0.2f]\n',
    content');
fclose(fileID);

```

MATLAB-script: program for partial wall distance evaluation

```

clf;
clear;
clc;
folder = 'PW_NC_IN_SEL_FIN/cropped';
%folder = 'PW_NC_OUT_SEL_FIN';
%folder = 'PW_PC_OUT_SEL_FIN/cropped';
image_files = dir(fullfile(folder, '*.jpg'));
dist_left = [];
dist_right = [];
for p = 1:numel(image_files)
    img = imread(fullfile(folder, image_files(p).name));
    gray = rgb2gray(img);
    bw = imbinarize(gray, 'adaptive', 'ForegroundPolarity', '
        bright', 'Sensitivity', 0.7);
    [H,T,R] = hough(~bw, 'Theta', -90:1:89, 'RhoResolution', 1);
    P = houghpeaks(H,4, 'threshold', 0.8, 'NHoodSize', [53 61]);
    lines = houghlines(~bw,T,R,P, 'FillGap', 200, 'MinLength'
        ,200);
    x_vals = [];
    %take the x values and find the middle:
    for k =1:length(lines)
        x_vals = [x_vals; lines(k).point1(1)];
    end
    mean_x = mean(x_vals);
    x_leftside = [];
    x_rightside = [];
    for n = 1:length(x_vals)
        if x_vals(n) < mean_x
            x_leftside = [x_leftside; x_vals(n)];
        elseif x_vals(n) > mean_x
            x_rightside = [x_rightside; x_vals(n)];
        end
    end
    x_leftside = sort(x_leftside);
    x_rightside = sort(x_rightside);
    dist_x_left = x_leftside(end)-x_leftside(1);
    dist_x_right = x_rightside(end)-x_rightside(1);

    %for NCIN, PCIN, PCOUT
    pixelscale = 500/147;
    %for NC OUT
    %pixelscale = 200/144;

    dist_left = [dist_left; dist_x_left*pixelscale];
    dist_right = [dist_right; dist_x_right*pixelscale];
end

```

50µm along Y					
	#1	#2	#3	#4	Median
5	4.96	4.96	5	5	4.98
10	9.93	9.94	9.94	9.94	9.94
15	14.92	14.92	14.92	14.92	14.92
20	19.86	19.86	19.87	19.86	19.86
25	24.85	24.84	24.86	25.85	24.855
30	29.79	29.79	29.85	29.84	29.815

50µm along X					
	#1	#2	#3	#4	Median
5	5	4.97	4.96	4.99	4.98
10	9.95	9.95	9.94	9.94	9.945
15	14.94	14.9	14.92	14.92	14.92
20	19.87	19.89	19.86	19.89	19.88
25	24.86	24.84	24.85	24.85	24.85
30	29.8	29.84	29.8	29.81	29.805

100µm along Y					
	#1	#2	#3	#4	Median
5	5.01	5	5	5.02	5.005
10	9.96	9.97	9.97	9.95	9.965
15	14.93	14.93	14.94	14.93	14.93
20	19.87	19.88	19.89	19.87	19.875
25	24.86	24.86	24.87	24.86	24.86
30	29.86	29.81	29.81	29.84	29.825

100µm along X					
	#1	#2	#3	#4	Median
5	4.98	5.01	5.02	4.99	5
10	9.96	9.96	9.96	9.98	9.96
15	14.94	14.94	14.94	14.92	14.94
20	19.88	19.89	19.88	19.9	19.885
25	24.87	24.86	24.86	24.85	24.86
30	29.82	29.84	29.81	29.84	29.83

50µm Solid		Column	Nominal	Measured	Slope	Intercept
1	5	5	4.98	0.993314286	0.01283333	
2	10	10	9.9425			
3	15	15	14.92	Shrinkage	0.67%	
4	20	20	19.87	Growth	6.460 microns	
5	25	24.8525		XY Compensation	-0.006	
6	30	29.81		XY SCALE	1.00673071	
					1.01075764	
					1.01075764	

100µm Solid		Column	Nominal	Measured	Slope	Intercept
1	5	5	5.0025	0.992928571	0.035	
2	10	10	9.9625			
3	15	15	14.935	Shrinkage	0.71%	
4	20	19.88		Growth	17.625 microns	
5	25	24.86		XY Compensation	-0.018	
6	30	29.8275		XY SCALE	1.00712179	
					1.01115028	
					1.01115028	

Shrinkage:		Scale	
10µm	0.38%	"1st value"	"2nd value"
25µm	0.56%	Median	1.00618835
50µm	0.67%	Mean	1.00582465
100µm	0.71%		1.00984795
Median	0.62%		
Mean	0.58%		

Figure 84: Excel sheet for determination of XY-curing parameters

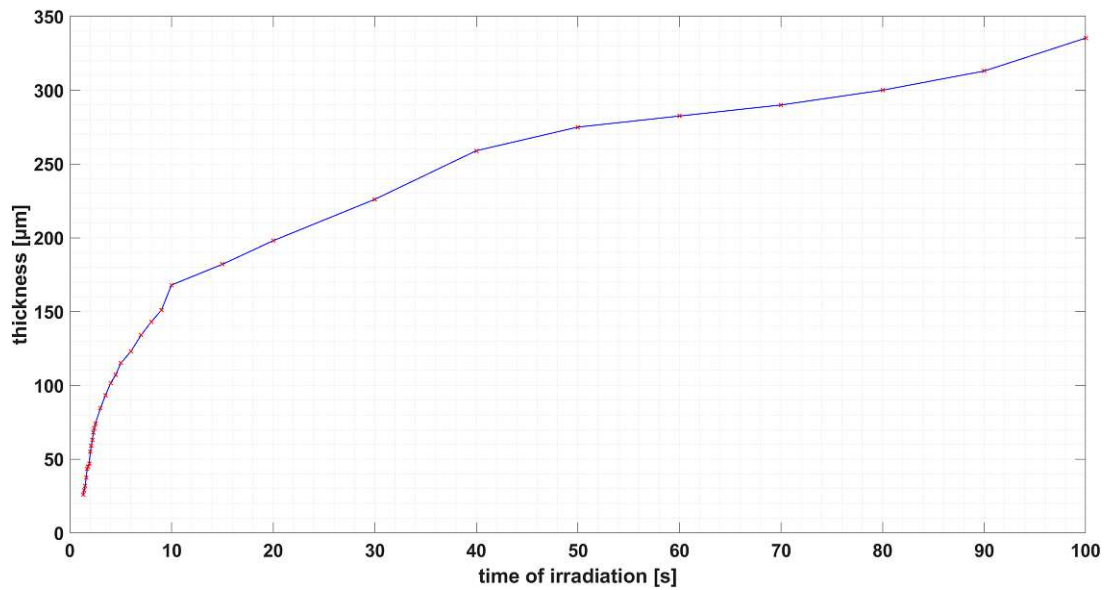


Figure 85: Z-Calibration curve for 3mW/cm<sup>2</sup>

Table 15: PlasClear "Geometry". Complete data table.

PlasClear		Actual measured values in [ $\mu\text{m}$ ]				
Nominal ( $\mu\text{m}$ )		Layer Height				
Obj.	Dim.	100 $\mu\text{m}$	50 $\mu\text{m}$	25 $\mu\text{m}$	10 $\mu\text{m}$	5 $\mu\text{m}$
$\bigcirc_{out}$	2000	2000.0 $\pm$ 7.8	2017.1 $\pm$ 14.4	2054.5 $\pm$ 9.5	2002.8 $\pm$ 6.1	2036.9 $\pm$ 1.0
	1000	1002.9 $\pm$ 7.7	1042.6 $\pm$ 6.8	1054.7 $\pm$ 5.0	1007.9 $\pm$ 6.4	1050.0 $\pm$ 5.2
	500	476.5 $\pm$ 5.4	499.6 $\pm$ 3.5	543.9 $\pm$ 3.2	508.9 $\pm$ 6.3	536.8 $\pm$ 3.8
	250	186.7 $\pm$ 0.0	221.3 $\pm$ 10.3	249.7 $\pm$ 12.2	225.7 $\pm$ 4.8	256.1 $\pm$ 0.9
	125	NaN $\pm$ NaN	NaN $\pm$ NaN	100.0 $\pm$ 1.0	63.2 $\pm$ 33.3	131.4 $\pm$ 26.0
$\bigcirc_{in}$	2000		1897.0 $\pm$ 15.6	1885.6 $\pm$ 3.5	1874.2 $\pm$ 19.8	1896.1 $\pm$ 10.3
	1000		887.5 $\pm$ 2.1	873.7 $\pm$ 6.4	817.3 $\pm$ 18.4	883.1 $\pm$ 16.0
	500		337.2 $\pm$ 6.4	331.7 $\pm$ 6.0	308.7 $\pm$ 23.6	414.3 $\pm$ 59.7
	250		NaN $\pm$ NaN	NaN $\pm$ NaN	NaN $\pm$ NaN	NaN $\pm$ NaN
	125		NaN $\pm$ NaN	NaN $\pm$ NaN	NaN $\pm$ NaN	NaN $\pm$ NaN
$\square_{out}$	1000	1008.5 $\pm$ 4.7	1066.8 $\pm$ 11.9	1068.7 $\pm$ 9.4	1018.4 $\pm$ 8.7	1063.6 $\pm$ 18.4
	500	513.0 $\pm$ 16.9	570.8 $\pm$ 1.0	574.6 $\pm$ 3.3	489.4 $\pm$ 14.7	541.6 $\pm$ 3.5
	250	235.4 $\pm$ 2.0	265.8 $\pm$ 6.0	287.4 $\pm$ 10.4	261.7 $\pm$ 2.0	292.0 $\pm$ 3.2
	125	NaN $\pm$ NaN	121.8 $\pm$ 31.0	123.7 $\pm$ 11.5	109.6 $\pm$ 1.9	NaN $\pm$ NaN
	62.5	NaN $\pm$ NaN	NaN $\pm$ NaN	79.5 $\pm$ 1.4	NaN $\pm$ NaN	NaN $\pm$ NaN
$\square_{in}$	1000		947.5 $\pm$ 0.3	929.6 $\pm$ 48.0	943.5 $\pm$ 12.5	977.7 $\pm$ 2.2
	500		438.2 $\pm$ 8.9	440.5 $\pm$ 4.3	435.3 $\pm$ 13.6	476.9 $\pm$ 3.8
	250		NaN $\pm$ NaN	NaN $\pm$ NaN	NaN $\pm$ NaN	NaN $\pm$ NaN
	125		NaN $\pm$ NaN	NaN $\pm$ NaN	NaN $\pm$ NaN	NaN $\pm$ NaN
	62.5		NaN $\pm$ NaN	NaN $\pm$ NaN	NaN $\pm$ NaN	NaN $\pm$ NaN
$\triangle_{out}$	1732	1758.6 $\pm$ 10.9	1794.8 $\pm$ 11.5	1850.6 $\pm$ 13.2	1787.4 $\pm$ 7.7	1825.9 $\pm$ 11.1
	866	894.4 $\pm$ 8.2	955.3 $\pm$ 13.9	974.0 $\pm$ 16.8	883.6 $\pm$ 10.2	924.7 $\pm$ 2.1
	433	435.0 $\pm$ 9.0	470.0 $\pm$ 13.4	482.6 $\pm$ 13.3	455.8 $\pm$ 9.0	507.5 $\pm$ 0.0
	216.5	NaN $\pm$ NaN	212.6 $\pm$ 2.0	202.5 $\pm$ 5.7	NaN $\pm$ NaN	NaN $\pm$ NaN
	108.25	NaN $\pm$ NaN	NaN $\pm$ NaN	106.7 $\pm$ 22.3	NaN $\pm$ NaN	NaN $\pm$ NaN
$\triangle_{in}$	1732		1542.5 $\pm$ 5.8	1546.4 $\pm$ 11.2	1468.9 $\pm$ 8.2	1561.2 $\pm$ 3.5
	866		638.7 $\pm$ 10.6	661.8 $\pm$ 12.9	570.8 $\pm$ 17.9	545.8 $\pm$ 94.4
	433		NaN $\pm$ NaN	NaN $\pm$ NaN	NaN $\pm$ NaN	NaN $\pm$ NaN
	216.5		NaN $\pm$ NaN	NaN $\pm$ NaN	NaN $\pm$ NaN	NaN $\pm$ NaN
	108.25		NaN $\pm$ NaN	NaN $\pm$ NaN	NaN $\pm$ NaN	NaN $\pm$ NaN

Table 16: NanoClear "Geometry". Complete data table.

NanoClear		Actual measured values in [ $\mu\text{m}$ ]				
Nominal ( $\mu\text{m}$ )		Layer Height				
Obj.	Dim.	100 $\mu\text{m}$	50 $\mu\text{m}$	25 $\mu\text{m}$	10 $\mu\text{m}$	5 $\mu\text{m}$
$\bigcirc_{out}$	2000	$1933.4 \pm 5.7$	$1972.1 \pm 9.2$	$1972.8 \pm 6.1$	$1985.8 \pm 6.0$	$1989.9 \pm 14.0$
	1000	$932.9 \pm 4.1$	$971.0 \pm 1.8$	$977.5 \pm 0.5$	$986.1 \pm 0.9$	$994.7 \pm 5.4$
	500	$427.3 \pm 5.2$	$464.0 \pm 10.0$	$474.3 \pm 5.7$	$479.9 \pm 5.2$	$490.6 \pm 9.5$
	250	NaN $\pm$ NaN	$209.0 \pm 2.0$	$221.2 \pm 2.3$	$225.9 \pm 1.2$	$231.7 \pm 1.8$
	125	NaN $\pm$ NaN	$66.0 \pm 1.8$	$76.5 \pm 4.7$	$90.1 \pm 1.0$	$96.3 \pm 1.7$
$\bigcirc_{in}$	2000		$2006.7 \pm 16.1$	$2015.1 \pm 2.4$	$2018.1 \pm 5.1$	$2009.8 \pm 9.6$
	1000		$998.5 \pm 9.0$	$1007.3 \pm 6.3$	$1001.2 \pm 5.7$	$997.4 \pm 1.9$
	500		$486.2 \pm 20.9$	$485.3 \pm 5.5$	$481.4 \pm 7.7$	$490.9 \pm 8.9$
	250		$246.3 \pm 7.8$	$236.5 \pm 11.9$	$229.7 \pm 0.7$	$224.8 \pm 6.7$
	125		NaN $\pm$ NaN	$71.6 \pm 5.9$	$57.6 \pm 9.8$	NaN $\pm$ NaN
$\square_{out}$	1000	$932.4 \pm 0.5$	$981.0 \pm 5.8$	$995.1 \pm 6.3$	$997.5 \pm 4.9$	$1002.2 \pm 3.4$
	500	$428.9 \pm 4.8$	$478.5 \pm 3.9$	$483.5 \pm 1.4$	$498.4 \pm 4.9$	$500.1 \pm 0.3$
	250	$163.8 \pm 1.1$	$221.1 \pm 1.5$	$230.9 \pm 0.6$	$239.4 \pm 1.2$	$247.4 \pm 8.1$
	125	NaN $\pm$ NaN	$79.0 \pm 0.6$	$88.1 \pm 1.0$	$98.5 \pm 1.9$	$102.2 \pm 3.9$
	62.5	NaN $\pm$ NaN	NaN $\pm$ NaN	NaN $\pm$ NaN	NaN $\pm$ NaN	NaN $\pm$ NaN
$\square_{in}$	1000		$1011.6 \pm 1.5$	$986.4 \pm 12.6$	$1017.3 \pm 1.3$	$1020.4 \pm 3.1$
	500		$505.4 \pm 2.5$	$496.8 \pm 2.3$	$478.4 \pm 5.8$	$508.0 \pm 0.5$
	250		$230.1 \pm 4.4$	$245.1 \pm 0.3$	$252.5 \pm 1.9$	$243.4 \pm 4.3$
	125		$110.4 \pm 5.4$	$101.6 \pm 5.9$	$95.6 \pm 6.3$	$97.5 \pm 16.6$
	62.5		NaN $\pm$ NaN	NaN $\pm$ NaN	NaN $\pm$ NaN	NaN $\pm$ NaN
$\triangle_{out}$	1732	$1623.0 \pm 31.1$	$1695.1 \pm 2.9$	$1721.7 \pm 6.9$	$1710.2 \pm 28.1$	$1733.8 \pm 2.8$
	866	$740.6 \pm 0.7$	$832.7 \pm 13.1$	$839.9 \pm 5.1$	$859.3 \pm 7.2$	$862.3 \pm 2.0$
	433	$296.0 \pm 8.5$	$385.0 \pm 2.8$	$398.3 \pm 3.5$	$417.5 \pm 5.2$	$421.1 \pm 2.6$
	216.5	NaN $\pm$ NaN	$140.1 \pm 1.5$	$161.8 \pm 1.8$	$178.8 \pm 2.8$	$182.0 \pm 3.3$
	108.25	NaN $\pm$ NaN	NaN $\pm$ NaN	NaN $\pm$ NaN	NaN $\pm$ NaN	$38.7 \pm 4.7$
$\triangle_{in}$	1732		$1732.6 \pm 6.5$	$1742.1 \pm 2.8$	$1729.6 \pm 7.1$	$1708.2 \pm 2.6$
	866		$864.7 \pm 4.6$	$857.1 \pm 2.0$	$826.2 \pm 11.4$	$880.2 \pm 15.6$
	433		$397.5 \pm 7.9$	$413.5 \pm 18.7$	$425.0 \pm 3.7$	$421.2 \pm 3.4$
	216.5		$157.6 \pm 32.3$	$180.8 \pm 5.6$	$163.5 \pm 23.7$	$154.7 \pm 17.2$
	108.25		NaN $\pm$ NaN	NaN $\pm$ NaN	NaN $\pm$ NaN	NaN $\pm$ NaN